creative commons
COMMONS DEED

저작자표시-비영리-변경금지 2.0 대한민국

이용자는 아래의 조건을 따르는 경우에 한하여 자유롭게

- 이 저작물을 복제, 배포, 전송, 전시, 공연 및 방송할 수 있습니다.

다음과 같은 조건을 따라야 합니다:

저작자표시. 귀하는 원저작자를 표시하여야 합니다.

비영리. 귀하는 이 저작물을 영리 목적으로 이용할 수 없습니다.

변경금지. 귀하는 이 저작물을 개작, 변형 또는 가공할 수 없습니다.

- 귀하는, 이 저작물의 재이용이나 배포의 경우, 이 저작물에 적용된 이용허락조건을 명확하게 나타내어야 합니다.
- 저작권자로부터 별도의 허가를 받으면 이러한 조건들은 적용되지 않습니다.

저작권법에 따른 이용자의 권리는 위의 내용에 의하여 영향을 받지 않습니다.

이것은 이용허락규약(Legal Code)을 이해하기 쉽게 요약한 것입니다.

Disclaimer

dCollection

Ph.D Thesis

박사 학위논문

Characterization of voltage-sensing phosphatase regulation on membrane phosphoinositides and voltage-gated calcium channels

Dongil Keum (금 동 일 琴 棟 壹)

Department of Brain and Cognitive Sciences

DGIST

2016

Ph.D Thesis

박사 학위논문

Characterization of voltage-sensing phosphatase regulation on membrane phosphoinositides and voltage-gated calcium channels

Dongil Keum (금 동 일 琴 棟 壹)

Department of Brain and Cognitive Sciences

DGIST

2016

Characterization of voltage-sensing phosphatase actions on membrane phosphoinositides and voltage-gated calcium channels

Dongil Keum

Accepted in partial fulfillment of the requirements for the degree of
Doctor of Philosophy

5. 30. 2016

Head of Committee (Signature)
Prof. JaeHyung Koo

Committee Member (Signature)
Prof. Kyuhyung Kim

Committee Member (Signature)
Prof. Sung Bae Lee

Committee Member (Signature)
Prof. Deok-Jin Jang

Committee Member (Signature)
Prof. Byung-Chang Suh

Ph.D Thesis

박사 학위논문

Characterization of voltage-sensing phosphatase regulation on membrane phosphoinositides and voltage-gated calcium channels

Dongil Keum (금 동 일 琴 棟 壹)

Department of Brain and Cognitive Sciences

DGIST

2016

Ph.D Thesis

박사 학위논문

Characterization of voltage-sensing phosphatase regulation on membrane phosphoinositides and voltage-gated calcium channels

Dongil Keum (금 동 일 琴 棟 壹)

Department of Brain and Cognitive Sciences

DGIST

2016

Characterization of voltage-sensing phosphatase actions on membrane phosphoinositides and voltage-gated calcium channels

Advisor: Professor Byung-Chang Suh
Co-Advisor: Professor Deok-Jin Jang

by

Dongil Keum

Department of Brain and Cognitive Sciences

DGIST

A thesis submitted to the faculty of DGIST in partial fulfillment of the requirements for the degree of Doctor of Philosophy in the Department of Brain and Cognitive Sciences. The study was conducted in accordance with Code of Research Ethics1).

6. 29. 2016

Approved by

Professor (Advisor) Byung-Chang Suh (Signature)

Professor (Co-Advisor) Deok-Jin Jang (Signature)

---

1) Declaration of Ethical Conduct in Research: I, as a graduate student of DGIST, hereby declare that I have not committed any acts that may damage the credibility of my research. These include, but are not limited to: falsification, thesis written by someone else, distortion of research findings or plagiarism. I affirm that my thesis contains honest conclusions based on my own careful research under the guidance of my thesis advisor.

Ph.D Thesis

박사 학위논문

Characterization of voltage-sensing phosphatase regulation on membrane phosphoinositides and voltage-gated calcium channels

Dongil Keum (금 동 일 琴 棟 壹)

Department of Brain and Cognitive Sciences

DGIST

2016

Ph.D Thesis

박사 학위논문

Characterization of voltage-sensing phosphatase regulation on membrane phosphoinositides and voltage-gated calcium channels

Dongil Keum (금 동 일 琴 棟 壹)

Department of Brain and Cognitive Sciences

DGIST

2016

Ph.D/BS

201145002

금 동 일. Dongil Keum. Characterization of voltage-sensing phosphatase actions on membrane phosphoinositides and voltage-gated calcium channels. Department of Brain and Cognitive Sciences. 2016. 91p. Advisor Prof. Byung-Chang Suh. Co-Advisor Prof. Doek-Jin Jang.

ABSTRACT

After Luigi Galvani's first observation in 1789, it has been found that bioelectricity plays crucial roles in biological systems. Most vital activities including sensory reception, decision making, learning, memory, cognition, motion, and generation of cardiac impulse are electrically mediated in precise and works of many ion channels and their regulators in concert. For instance, in excitable cells, external stimulations such as light, pressure, temperature, pH change, and ligand can activate ion channels and evoke membrane depolarization. If the stimulations are sufficiently strong to overcome threshold, action potential is generated and propagates by sequential activation of voltage-gated sodium channel (Na_V) and voltage-gated potassium channel (K_V). Then, the action potential activates voltage-gated calcium channels (Ca_V) in pre-synaptic terminal and triggers secretion of neuro-transmitter, resulting in synaptic transmission to post synaptic neuron. Regulators of ion channels precisely control shape and strength of the signal at each step.

Phosphoinositides (PIs) are phosphorylated isomers of phosphoinositol (PI), which has inositol head group and fatty acid tail group, and are named after phosphorylation at 3, 4, or 5 position of the inositol ring. They are minor (<1%) lipid in cell membranes and dynamically and accurately maintained by working of phosphoinositide kinases and phosphatases. Also, they regulates important cellular and physiological events such as cell differentiation, migration, cell-shaping, axon-regeneration, cell death / survival, tumorigenesis, protein regulation, fertilization and so on. Additionally, discovery and development of

molecular probes attached with fluorescence proteins enables us to observe real-time concentration of PIs in live cells. Among these PIs, role of phosphatidylinositol 4,5-bisphosphate ($PI(4,5)P_2$) is relatively well established. Not only as precursor of IP_3 which induces release of Ca^{2+} from endoplasmic reticulum (ER), $PI(4,5)P_2$ is known to directly regulate various ion channels including Ca_V channels, one of our study targets.

Recently cloned voltage-sensing phosphatases (VSPs) extend the concept of bioelectrical signal and their application. VSPs are transmembrane proteins that have voltage-sensing domain mimicking that of voltage-gated ion channels, and cytosolic catalytic domain homologous to phosphatase and tensin homolog (PTEN), a phosphoinositide $PI(3,4)P_2$ and $PI(3,4,5)P_3$ 3-phosphatase. Thus, propagation of electricity can be transduced into catalytic activity. However, unlike PTEN, VSPs have a wider range of substrates, cleaving 3-phosphate from $PI(3,4)P_2$ and probably $PI(3,4,5)P_3$ and 5-phosphate from $PI(4,5)P_2$, and $PI(3,4,5)P_3$. Recent proposals say these reactions have differing voltage dependence. Using FRET probes specific for different phosphoinositides in living cells with zebrafish VSP, we quantitate both voltage-dependent 5- and 3-phosphatase subreactions against endogenous substrates. These activities become apparent with different voltage thresholds, voltage sensitivities, and catalytic rates. As an analytical tool, we refine a kinetic model that includes the endogenous pools of phosphoinositides, endogenous phosphatase and kinase reactions connecting them, and four exogenous voltage-dependent 5- and 3-phosphatase subreactions of VSP. We show that apparent voltage threshold differences for seeing effects of the 5- and 3-phosphatase activities in cells are not due to different intrinsic voltage dependence of these reactions. Rather the reactions have a common voltage dependence, and apparent differences arise only because each VSP subreaction has a different absolute catalytic rate that begins to surpass the respective endogenous enzyme activities at different voltages. For zebrafish VSP, our modeling also revealed clear 3-phosphatase activity against $PI(3,4,5)P_3$, but it is 55-fold slower than 5-phosphatase activity against $PI(4,5)P_2$, thus $PI(4,5)P_2$, generated more slowly from dephosphorylating $PI(3,4,5)P_3$, might never

accumulate. When 5-phosphatase activity was counteracted by coexpression of a phosphatidylinositol 4-phosphate 5-kinase, there was accumulation of $PI(4,5)P_2$ in parallel to $PI(3,4,5)P_3$ dephosphorylation, demonstrating that VSPs also cleave the 3-phosphate of $PI(3,4,5)P_3$.

Using these catalytic properties of Dr-VSP, role of Ca_V β subunits on determining portion of two inhibition pathways by G_q-protein coupled receptor (G_qPCR) activation was investigated. GPCRs signal through molecular messengers, such as Gβγ, Ca^{2+}, and $PI(4,5)P_2$, to modulate N-type $Ca_V2.2$ channels, playing a crucial role in regulating synaptic transmission. In our pervious studies, activation of Dr-VSP always showed weaker response than activation of M_1 muscarinic receptor in $Ca_V2.2$ current inhibition (10% and 40%, respectively) although either are known as $PI(4,5)P_2$ dependent pathways. In this study, we firstly identified that Gβγ dissociated from M_1 G_qPCR further inhibited Ca_V current beside $PI(4,5)P_2$ depletion. We also report that the location of Ca_V β subunits is key to determining the voltage dependence of $Ca_V2.2$ channel modulation by G_qPCRs. Application of the muscarinic agonist oxotremorine-M to tsA-201 cells expressing M_1 receptors, together with Ca_V N-type α1B, α2δ1, and membrane-localized β2a subunits, shifted the current-voltage relationship for $Ca_V2.2$ activation 5 mV to the right and slowed current activation. Muscarinic suppression of $Ca_V2.2$ activity was relieved by strong depolarizing prepulses. Moreover, when the C terminus of β-adrenergic receptor kinase (which binds Gβγ) was coexpressed with N-type channels, inhibition of $Ca_V2.2$ current after M_1 receptor activation was markedly reduced and delayed, whereas the delay between PIP_2 hydrolysis and inhibition of $Ca_V2.2$ current was decreased. When the Gβγ-insensitive $Ca_V2.2$ α1C-1B chimera was expressed, voltage-dependent inhibition of calcium current was virtually abolished, suggesting that M_1 receptors act through Gβγ to inhibit $Ca_V2.2$ channels bearing membrane-localized Ca_V β2a subunits. Expression of cytosolic β subunits such as β2b and β3, as well as the palmitoylationnegative mutant β2a(C3,4S), reduced the voltage dependence of M_1 muscarinic inhibition of $Ca_V2.2$ channels, whereas it increased inhibition mediated by PIP_2 depletion. Together, our results indicate that, with membrane-localized Ca_V β subunits, $Ca_V2.2$ channels are subject to Gβγ-mediated voltage-dependent inhibition, whereas cytosol-localized β subunits confer more effective PIP_2-mediated voltage-independent regulation. Thus, the voltage dependence of G_qPCR regulation of calcium channels can be determined by the location of isotype-specific Ca_V β subunits.

These results suggest novel physiological roles of VSPs and Ca_V channels. Since VSPs also dephosphorylate 3-phosphate of $PI(3,4,5)P_3$ as PTEN does, VSPs may participate in axon re-generation, spermato-genesis or stem cell differentiation which might even be triggered and regulated by electro-chemical signals. VSPs also can compensate defect of PTEN activity in neural development or tumor suppression. Different temporal property of voltage-dependent and -independent inhibitions on Ca_V channels may be resposible for formation of M_1R induced long term potentialtion and depression.

Keywords: bioelectricity, voltage-gated calcium channel, voltage-sensing phosphatase, phosphoinositides, PTEN

CONTENTS

ABSTRACT ………...i
CONTENTS ……………………………………………………………………………v
TABLES ………………………………………………………………………………vii
FIGURES ………………………………………………………………..............viii

I. INTRODUCTION ……………………………………………………………………..1
1-1. Voltage-sensing phosphatase (VSP) is a unique voltage-activated enzyme ……………….……….......1
1-2. Structure of VSP ……………………………………………………………………........4
1-3. Phosphoinositide phosphatase activity of VSP ....………………………………….........6
1-4. G-protein coupled receptor (GPCR) regulation on N-type voltage-gated Ca^{2+} (Ca_V) channels .....…………8

II. MATERIALS AND METHODS ….…………………………………………………12
2-1. Cell Culture and transfection ………………………………………………………12
2-2. Electrophysiology ……………………………………………………………………13
2-3. Förster Resonance Energy Transfer (FRET) ………………………………………15
2-4. Normalization and fitting of traces ……………………………………………...16
2-5. Confocal microscopy ……………………………………………………………...17
2-6. Mathematical modeling ………………………………………………………...17
2-7. Analysis and statistics ……………………………………………………………..18
2-8. Materials ……………………………………………………………………………..19

III. VOLTAGE-SENSING PHOSPHATASE (VSP) REGULATION OF PHOSPHOINOSITIDES …...20
3-1. Voltage-dependet PI 3- and 5-phosphatase activities ……………………………...20
3-2. Perturbations with wortmannin ……………………………………………………31
3-3. Voltage-dependent PI(3,4,5)P_3 3-phosphatase activity of Ci-VSPTEN …………………..34
3-4. Phosphatidylinositol 4-phosphate 5-kinase type Iγ (PIPKIγ) nullifies 5-phosphatase effects of Dr-VSP ………………...……………………………………...…..37
3-5. Step response of Dr-VSP in PIPKIγ co-expressing cells …………………………..43

IV. VOLTAGE-SENSING PHOSPHATASE (VSP) REGULATION OF VOLTAGE-GATED CALCIUM CHANNELS ………………………………….....…..45

4-1. Activation of Dr-VSP inhibits $Ca_V2.2$ current ……………………………………………………………..45
4-2. M_1 muscarinic recptors may suppress N-type $Ca_V2.2$ through two pathways ……………………………...47
4-3. Gβγ scavenger attenuates M_1 muscarinic receptor-inducuced $Ca_V2.2$. current inhibition …………………50
4-4. Single-cell assay reveals separation of fast and slow pathways in M_1R-induced current modulation ……………………………..……………………………………...54
4-5. Gβγ-dependent, but not PIP_2-dependent, modulation is absent in a chimeric N-type channel ……………………………………………………………………………58

V. DISCUSSION ……………………………………………………………………………………...64

VI. REFERENCES …………………………………………………………………………………...81

VII. SUMMARY IN KOREAN ………………………………………………………………………91

TABLES

Table 1. VSP homologues and their expression patterns ……………………………………………..……...…..3

Table 2. Subunit variation of voltage-gated Ca^{2+} (Ca_V) channels …………………………………………….....10

Table 3. Genetically encoded PI probes ……………………………………………………………………..…25

Table 4. Rate constants and parameters for modeling at 22℃ ……………………………………………………….26

Table 5. Rate constants and parameters for Ci-VSP models ………………………………………………...…76

FIGURES

Figure 1. Structural characteristics of VSP ………………………………………………………….………………..5

Figure 2. Phosphoinositide 3- and 5-phosphatase activity of VSP …………………………………..……………..7

Figure 3. Subunit association and topology of voltage-gated Ca^{2+} (Ca_V) channel ……………………...…………11

Figure 4. A patch clamp setup for simultaneous FRET acquisotion in Current Lab, DGIST …………………..……14

Figure 5. Measuring voltage-dependent changes of PIs using FRET probes in living cells …………….……...…27

Figure 6. Dynamic changes of FRET probes during ramp activation of Dr-VSP ………………………….........28

Figure 7. Evaluating endogenous voltage-dependent phosphatase activity on $PI(3,4)P_2$ in tsA201 ………..………..30

Figure 8. Effect of PI3K inhibition on PI dynamics after Dr-VSP activation ……………………………….........32

Figure 9. Voltage-dependent effects of Ci-VSPTEN 3-phosphatase on PI dynaamics ……………………………...36

Figure 10. Expression of PIPKIγ unmasks innate 3-phosphatase activity toward $PI(3,4,5)P_3$ ………………………39

Figure 11. $PI(4,5)P_2$ is differentially regulated by Dr-VSP and M1R in PIPKIγ expressing cells ………………..…41

Figure 12. Step response of Dr-VSP in the absene and presence of PIPKIγ …………………………………………44

Figure 13. Simultaneous measurement of FRET and Ca$_V$ current in a live cell 46

Figure 14. Differential modulation of Ca$_V$2.2 channels by muscarinic receptors depends on the Ca$_V$ β subunit 49

Figure 15. βARK-ct attenuates M$_1$ muscarinic receptor-induced inhibition of Ca$_V$2.2(β2a) currents 52

Figure 16. Differential effects of βARK-ct on M$_1$R- and Dr-VSP-induced inhibition of Ca$_V$2.2(β2a) currents 53

Figure 17. Simultaneous measurement of current inhibition and PIP$_2$ hydrolysis in single cells 56

Figure 18. Kinetics assay reveal participation of Gβγ in M$_1$ receptor-induced Ca$_V$2.2(β2a) current inhibition 57

Figure 19. Voltage-dependent muscarinic modulation disappears in Gβγ-insensitive chimeric Ca$_V$2.2(α1C-1B) channels 61

Figure 20. Cytosolic β subunit decreases the Gβγ-mediated, voltage dependent suppression of Ca$_V$2.2 currents 62

Figure 21. Cytosolic β subunit increases the PIP$_2$ depletion-mediated suppression of Ca$_V$2.2 currents 63

Figure 22. Simulation of FRETr responses to activation of Ci-VSP in oocytes of *X. laevis* 77

Figure 23. Simulation of activation of mutant variants of Ci-VSP 79

Figure 24. M$_1$R suppresses Ca$_V$2.2 currents through two separate pathways 80

I. INTRODUCTION

1-1. Voltage-sensing phosphatase (VSP) is a unique voltage-activated enzyme

Bioelectricity, caused by difference of ion concentration between inside and outside of plasma membrane, is a means that regulates important biological activities, such as generation, propagation and processing of neuronal signals, muscle contraction, and secretion of hormones and humors. Voltage-gated ion channels were the first identified protein family that possess bioelectric sensing properties and play crucial roles in such biological activities. Many ion channels have well conserved 6 transmembrane segments (S1 – S6), where S1 – S4 segments forming a voltage-sensing domain (VSD) transfer the membrane depolarizing signals to the other S5 – S6 segments, a pore domain for ion fluxes.

Recently, a quite unanticipated voltage-sensing enzyme with voltage-sensing domain was cloned from *Ciona intestinalis*, sea squirt (Murata et al., 2005). Biochemical and electrophysiological examination revealed a voltage-dependent phosphatase activity toward phosphoinositides that was given the name *C. intestinalis* voltage-sensing phosphatase (Ci-VSP). Since then, its homologues have been discovered in other species, e.g. zebrafish (Dr-VSP, Hossain et al., 2008), African frog (Xl- and Xt-VSP, Ratzan et al., 2011), chicken (Gg-VSP, Yamaguchi et al., 2014), and salamander (Hn- and Cp-VSP, Mutua et al., 2014). In addition, voltage-sensing properties of mammalian VSP homologues including transmembrane phosphatases with tensin homology (TPTE) and TPTE and PTEN homologous inositol lipid phosphatase (TPIP) were re-examined (Wu et al., 2001; Walker et al., 2001; Halaszovich et al., 2012; Rosasco et al., 2015). Although VSPs have been found in the testis of mice (Wu et al., 2001), the testis, brain and stomach of human (Walker et al., 2001), the testis and neuronal complex of the ascidian (Murata et al., 2005), neuron of mouse (Rosasco et al., 2015) and the testis, ovary, kidney and liver of the African frog (Ratzan et al., 2011), their physiological functions are still unclear (Table 1). Instead, due to fast and strong phosphatase activity of VSPs on PI(4,5)P_2, they had been used as electrophysiological tool for studying PI(4,5)P_2 regulation of voltage-gated ion channels (Suh et al., 2010, 2012; Keum et al., 2014; Kim et al., 2015).

Table 1. VSP homologues and their expression patterns

Nomenclature	Species	Literature	Gene expression pattern	Amino Acid Sequence near Active Site (aligned)	Remarks
Ci-VSP	*Ciona intestinalis*	Murata et al., 2005	Neuronal complex, Testis, Juvenile tissue	HCKGGKGRTGTLV	
Dr-VSP	*Dario rario*	Hossain et al., 2008		HCKGGKGRTGTMV	
Gg-VSP	*Gallus gallus*	Kurokawa et al., 2012		HCKGGKGRTGTMV	
Xl-VSP1	*Xenopus leavis*	Ratzan et al., 2011	Testis, Liver, Ovary,	HCKGGKGRTGTMV	
Xl-VSP2	*Xenopus leavis*	Ratzan et al., 2011	Testis, Heart, Kidney, Brain, Ovary	HCKGGKGRTGTMV	
Xt-VSP	*Xenopus tropicalis*	Ratzan et al., 2011	Testis, Kidney, Liver, Ovary	HCKGGKGRTGTMV	
Hn-VSP	*Hynobius nebulosus*	Mutua et al., 2014	Kidney, Spleen, Testis	HCKGGKGRTGTMV	Truncated C2 domain
Cp-VSP	*Cynops pyrrhogaster*	Mutua et al., 2014	Heart, Lung, Testis	HCKGGKGRTGTMV	
Hs-VSP1 (TPIP)	*Homo sapience*	Walker et al., 2001	Brain, Testis	HCKGGKGRTGTMV	Golgi targeting
Hs-VSP2 (TPTE)	*Homo sapience*	Chen et al., 1999	Brain, Testis, Lung cancer	HCKGGTDRTGTMV	
Mm-VSP (mTPTE)	*Mus musculus*	Wu et al., 2001	Testis, neuron	HCKGGKGRTGTMV	Golgi targeting
Hs-PTEN	*Homo sapience*	Li et al., 1997 Steck et al., 1997	Ubiquitous	HCKAGKGRTGVMI	Tumor suppressor

1-2. Structure of VSP

As in voltage-gated ion channels, VSD of VSPs also consists of 4 transmembrane segments, S1 – S4, where the voltage sensor, S4 segment, moves by intense electric fields across the plasma membrane during depolarization. On the other hands, VSPs have a cytosolic enzyme domain instead of the pore-forming domain (S5 – S6) of voltage-gated ion channels (Fig. 1*A* and *B*). This enzyme domain is analogous to tumor suppressor phosphatase and tensin homolog (PTEN), a PI 3-phosphatase working on both PI(3,4)P_2 and PI(3,4,5)P_3 (Murata et al., 2005) and shows structural similarity to PTEN (Fig. 1*C*). PTEN has three distinctive regions, N-terminus phospholipid binding motif (PBM) that anchors the protein to the plasma membrane (Campbell et al., 2003; Iijima et al., 2004), phosphatase domain (PD) that has active dephosphorylation site and C-terminus lipid-interacting C2 domain. These three regions are also sequentially and structurally well conserved in VSPs (Matsuda et al., 2011; Okamura and Dixon, 2011; Hobiger et al., 2012; Liu et al., 2012). In VSPs, it is reported that the PBM links between membrane VSD and cytosolic PD but also that a part of PBM overhangs the PD (Liu et al., 2012). Crystal structure studies revealed that the active site in which PI dephosphorylation takes place is located inner leaflet facing side of PD and surrounded by an active pocket, a cleft formed between PBM, PD and C2 domain of VSPs (Matsuda et al., 2011; Liu et al., 2012). Interestingly, the cytosolic enzyme domain of VSPs peculiarly has a glutamate switch on C2 domain that adjusts internal size of the active pocket and replacement of amino acid on the switch altered substrate specificity of the PD (Liu et al., 2012). However, functional mechanism of the glutamate switch (Fig. 1*A*) on voltage-dependence of VSP activity is still unrevealed.

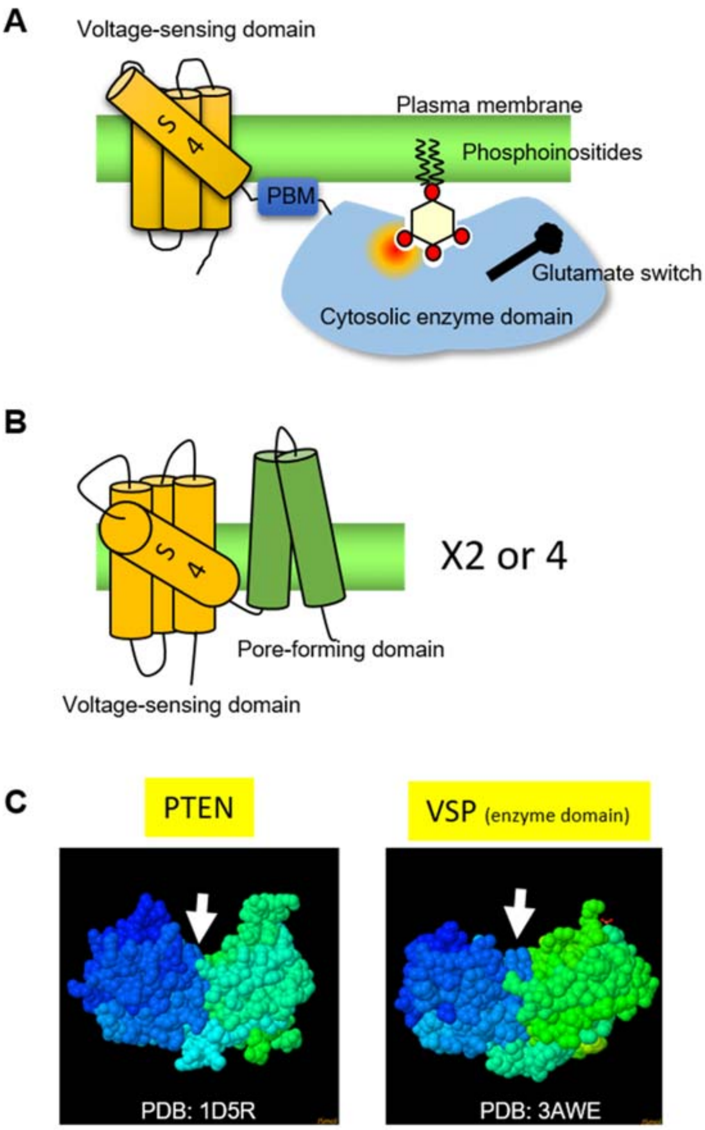
A
Voltage-sensing domain
S4
Plasma membrane
Phosphoinositides
PBM
Glutamate switch
Cytosolic enzyme domain
B
S4
X2 or 4
Pore-forming domain
Voltage-sensing domain
C
PTEN
VSP (enzyme domain)
PDB: 1D5R
PDB: 3AWE

Figure 1. Structural characteristics of VSP

(A) VSPs consist of transmembrane voltage-sensing domain, cytosolic enzyme domain and linker (PBM) between them. *(B)* Simplified structure of voltage-gated ion channels. *(C)* Structural comparison between PTEN and cytosolic enzyme domain of VSPs. White arrows indicate location of active site. 3D images are from Protein Data Bank (http://rcsb.org/pdb/home/home.do) and IDs are indicated in figures.

1-3. Phosphoinositide phosphatase activity of VSP

Propagation of depolarization-induced conformational changes in VSD to the cytosolic enzyme domain through PBM triggers a unique voltage-activated PI phosphatase activity (Matsuda et al., 2011; Liu et al., 2012; Villalba-Galea, 2012). PIs are phosphorylated isomers of phosphoinositol (PI), which has inositol head group and fatty acid tail group, and are named after phosphorylation at 3, 4, or 5 position of the inositol ring (Fig. 2*A*). They are minor (< 1%) lipid in cell membranes and dynamically and accurately maintained by working of phosphoinositide kinases and phosphatases. Also, they regulates important cellular events such as cell differentiation, migration, shaping, axon-regeneration, cell death / survival, tumorigenesis, protein regulation, fertilization and so on. Unlike its analogue PTEN which has only cleaves 3-phosphate activity (Campbell et al., 2003; McCrea and Camilli, 2009), VSPs were firstly known to cleave 5-phosphate from PI(4,5)P_2 and PI(3,4,5)P_3 in response to membrane depolarization and consequently generate PI(4)P and PI(3,4)P_2, respectively (Murata et al., 2005; Murata and Okamura, 2007; Iwasaki et al., 2008; Halaszovich et al., 2009). Recently, it was further reported that VSPs can cleave 3-phosphate from PI(3,4)P_2 and generate PI(4)P at relatively higher membrane potential (Kurokawa et al., 2012). However, whether the VSPs can cleave 3-phosphate from PI(3,4,5)P_3 is still controversial (Wu et al., 2001; Walker et al., 2001; Murata et al., 2005; Murata and Okamura, 2007; Iwasaki et al., 2008; Okamura et al., 2009; Castle et al., 2015; Grimm and Isacoff, 2016) (Fig. 2*B*). The amino acid sequence of active site of VSPs is well conserved among species (Matsuda et al., 2011), as shown in table 1, and shows a single amino acid difference from that of PTEN (Murata et al., 2005). When the amino acid was mutated to the same amino acid of PTEN active site, however, the mutated Ci-VSP still showed both 5- and 3-

phosphatase activities towards PIs (Liu et al., 2012). Therefore, it was suggested that such complicated substrate specificity and voltage-dependent dual phosphatase activities of VSPs might be determined by the active pocket surrounding active site, rather than the active site itself (Liu et al., 2012).

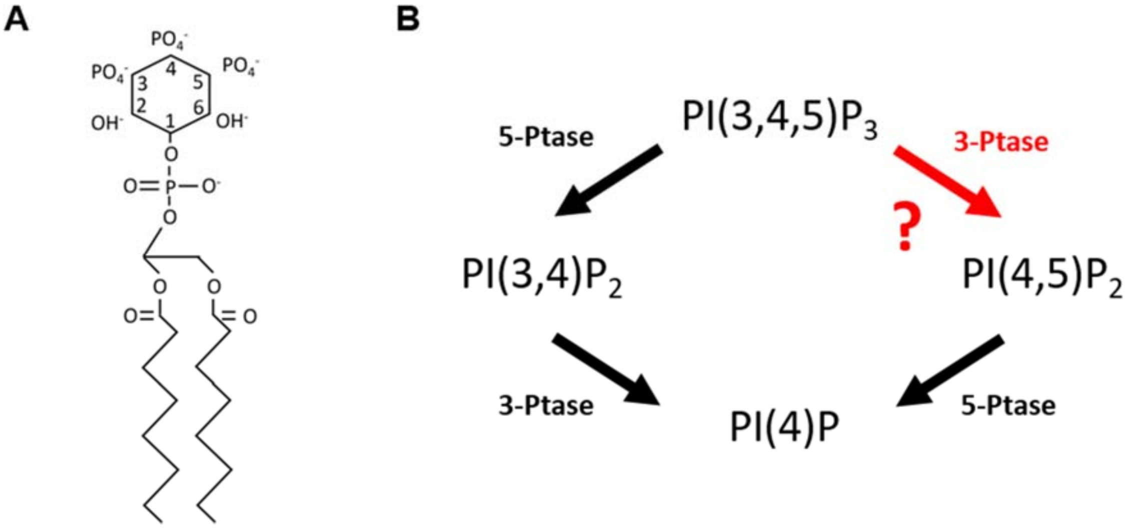
A
PO4-
PO4-
PO4-
3
4
5
2
1
6
OH-
OH-
O
O=P—O-
O
O
O
O=
=O
B
PI(3,4,5)P3
5-Ptase
3-Ptase
?
PI(3,4)P2
PI(4,5)P2
3-Ptase
5-Ptase
PI(4)P

Figure 2. Phosphoinositide 3- and 5-phosphatase activity of VSP

(A) Chemical structure of phosphatidylinositol 3,4,5-triphosphate (PI(3,4,5)P_3). Phosphorylation at 3, 4 or 5 position of inositol ring determines chemical and physiological characteristic and name of PIs. *(B)* Characterized PI phosphatase activity of VSP. However, whether VSPs can dephosphorylate 3-phosphate of PI(3,4,5)P_3 (red question mark) had been controversial until quite recently.

1-4. G-protein coupled receptor (GPCR) regulation of N-type voltage-gated Ca^{2+} (Ca_V) channels

The biophysical and pharmacological properties of voltage-gated Ca^{2+} (Ca_V) channels are determined by diverse combinations of α1, α2δ and/or β subunits (Table 2 and Fig. 3). Transmembrane Ca_V α1 subunits are responsible for forming the voltage-sensitive pore of the channel while Ca_V α2δ subunits are responsible for promoting Ca_V α1 subunit stabilization at the plasma membrane (Yasuda et al., 2004). Ca_V β subunits are intracellular components that play an essential role in regulating the gating properties and receptor modulation of Ca_V channels. β subunits bind to the I-II linker of the α1 subunit and finely tune the trafficking of α1 channel proteins to the plasma membrane, current density, channel inactivation and channel regulation by phospholipids (Hofmann et al., 1999; Catterall, 2000; Hurley et al., 2000; Suh et al., 2012).

N-type Ca_V ($Ca_V2.2$) channels are widely expressed throughout the brain (Westenbroek et al., 1992) and spinal cord (Westenbroek et al., 1998). They are central to synaptic transmission in response to the propagation of electrical stimulations and to the processes it underlies, such as learning and memory (Normann et al., 2000) and gene transcription (Wheeler et al., 2012). $Ca_V2.2$ gene knockout mice show cardiovascular impairment (Mori et al., 2002), hyperactivity (Beuckmann et al., 2003), reduced alcohol consumption (Newton et al., 2004), and hyper-aggressive behavior (Kim et al., 2009).

G-protein coupled receptors (GPCRs) precisely regulate Ca^{2+} ion influx through Ca_V channels (Hille, 1994; Zamponi and Currie, 2013). GPCRs coupled to $G\alpha_{i/o}$ ($G_{i/o}$PCRs) and $G\alpha_{q/11}$ (G_qPCRs) are known to suppress $Ca_V2.1$ or $Ca_V2.2$ current through two distinct pathways. The first operates via Gβγ heterodimer dissociation from $G_{i/o}$PCR. The Gβγ heterodimer then directly binds to the I-II linker of these Cav α1 subunits, which partially overlaps with the binding site of the Cav β subunit, and triggers fast current inhibition (Agler et al., 2005). Since the Gβγ binding to Cav α1 subunit slows channel activation and shifts the voltage dependence of the channel opening towards a positive charge, a stronger depolarization of the plasma membrane is needed for the channels to open. This inhibition can be relieved by supplying a large depolarizing pulse (Bean, 1989; Elmslie et al., 1990) and is thus referred to as "voltage-dependent (VD)" (Hille, 1994). The second pathway, for G_qPCRs, depends on phosphatidylinositol 4,5-bisphosphate (PI(4,5)P_2) hydrolysis by phospholipase C (PLC) (Gamper et al., 2004; Suh et al., 2010; Wu et al., 2002) and/or arachidonic acid (AA) generation by phospholipase A_2 (PLA_2) activation (Liu and Rittenhouse, 2003) following $G\alpha_{q/11}$ subunit activation. This pathway is responsible for relatively slow and voltage-independent (VI) Cav channel inhibition.

However, though fast and voltage-dependent inhibition of Cav2.2 current was frequently observed during M_1 G_qPCR activation (Gamper et al., 2004; Kammermeier et al., 2000; Melliti et al., 2001; Suh et al., 2010; Vivas et al., 2013), this phenomenon could not be identified due to complex downstream of $G_{q/11}$PCR such as Ca^{2+} release from the endoplasmic reticulum or PKC activation via diacylglycerol generation. In this study, we verified involvement of Gβγ subunit dissociated from M_1 G_qPCR in N-type Cav2.2 current inhibition with the aid of voltage-sensing phosphatase and other useful tools. We also identified that subcellular location of Cav β subunit is important to determine proportions of VI and VD inhibitions during M_1R activation.

Table 2. Subunit variation of voltage-gated Ca^{2+} (Ca_V) channels

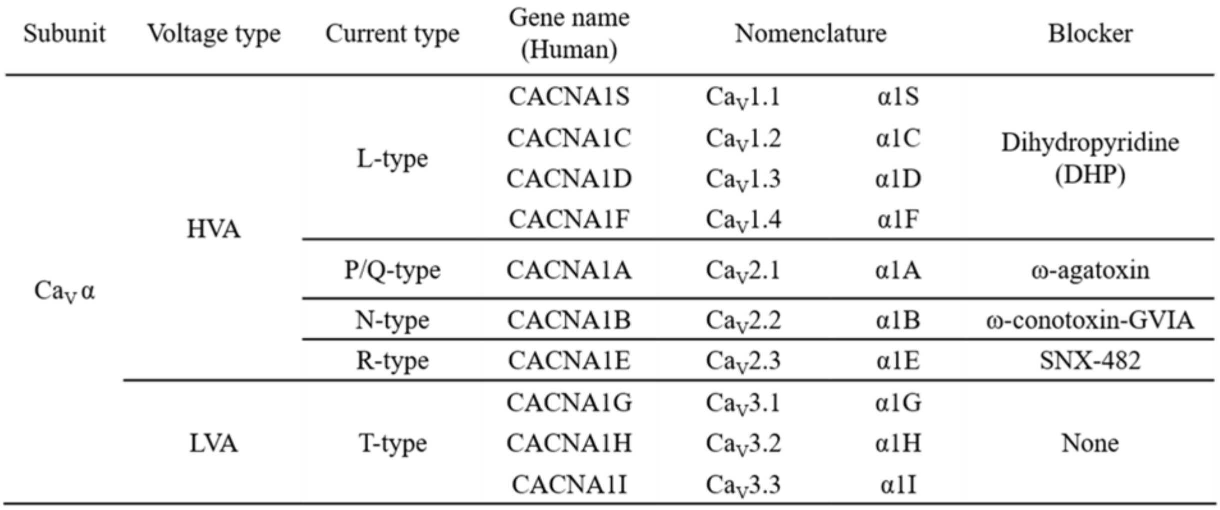

Subunit	Voltage type	Current type	Gene name (Human)	Nomenclature		Blocker
Ca_V α	HVA	L-type	CACNA1S	$Ca_V1.1$	α1S	Dihydropyridine (DHP)
			CACNA1C	$Ca_V1.2$	α1C	
			CACNA1D	$Ca_V1.3$	α1D	
			CACNA1F	$Ca_V1.4$	α1F	
		P/Q-type	CACNA1A	$Ca_V2.1$	α1A	ω-agatoxin
		N-type	CACNA1B	$Ca_V2.2$	α1B	ω-conotoxin-GVIA
		R-type	CACNA1E	$Ca_V2.3$	α1E	SNX-482
	LVA	T-type	CACNA1G	$Ca_V3.1$	α1G	None
			CACNA1H	$Ca_V3.2$	α1H	
			CACNA1I	$Ca_V3.3$	α1I	

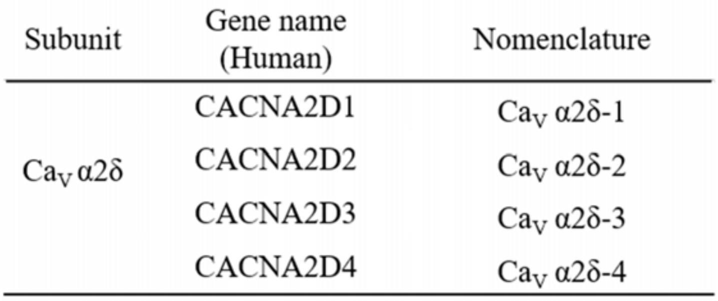

Subunit	Gene name (Human)	Nomenclature
Ca_V α2δ	CACNA2D1	Ca_V α2δ-1
	CACNA2D2	Ca_V α2δ-2
	CACNA2D3	Ca_V α2δ-3
	CACNA2D4	Ca_V α2δ-4

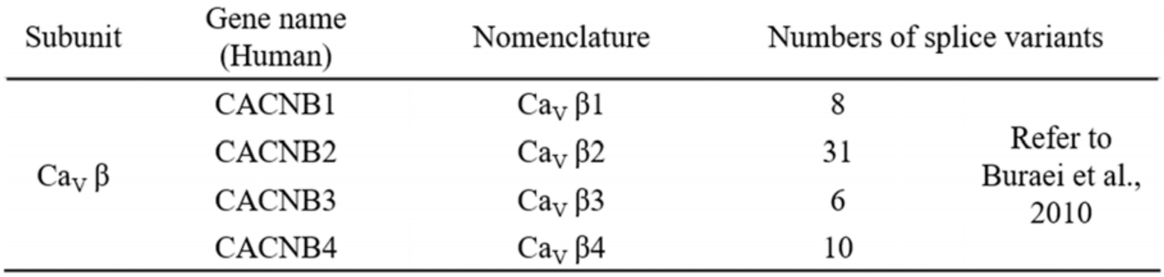

Subunit	Gene name (Human)	Nomenclature	Numbers of splice variants	
Ca_V β	CACNB1	Ca_V β1	8	Refer to Buraei et al., 2010
	CACNB2	Ca_V β2	31	
	CACNB3	Ca_V β3	6	
	CACNB4	Ca_V β4	10	

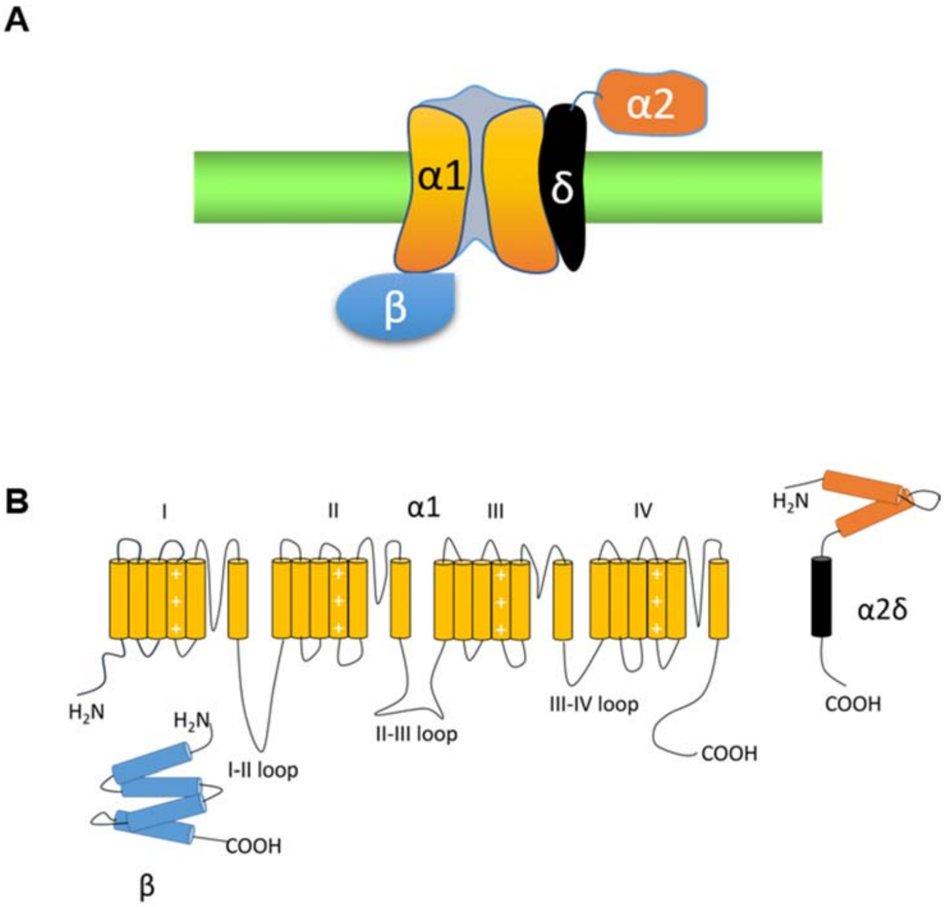

Figure 3. Subunit association and topology of voltage-gated Ca^{2+} (Ca_V) channel

(A) Ca_V channels consist of pore-forming α1 and auxiliary α2δ and β subunits. α1 and α2δ subunits are transmembrane where β subunit is cytosolic or membrane anchored. *(B)* Ca_V α1 subunit consists of 4 homologous transmembrane domains which contains 6 segments for voltage sensing (S1-S4) and Ca^{2+} selective pore-forming (S5-S6). N-, C-terminus and inter domain loops have regulatory functions. α2 and δ subunits are encoded by same gene and post-translationally distinguished. Extracellular α2 and transmembrane δ subunits are connected by disulfide bond. β subunit is basically cytosolic, but some splice variants are membrane anchoring due to palmitoylation (β2a) or electrostatic interaction with lipids (β2e).

II. MATERIANLS AND METHODS

2-1. Cell culture and transfection

HEK293-derived tsA201 cells were grown in DMEM supplemented with 10% fetal bovine serum and 0.2% penicillin/streptomycin. They were subcultured every 6 or 7 days (70 to 80% confluence), transfected 1 to 4 days after subculture using Lipofectamine2000 (Invitrogen, Carlsbad, US) following the manufacturer's instruction, and then plated on a poly-L-lysine-coated coverslip 12 to 24 hours after transfection using trypsin. Experiments were carried out 24 to 36 hours after transfection. The following cDNAs were generously given to us: Voltage sensitive phosphatase derived from *Danio rerio* (Dr-VSP) with IRES EGFP (from Y. Okamura, Osaka University, Osaka, Japan) and without fluorescence protein (from Björn Falkenburger, University of Aachen, Germany), human PTEN conjugated with the voltage sensing-domain of Ci-VSP (Ci-VSPTEN16) (from Christian Halaszovich, University of Marburg, Marburg, Germany), ECFP and EYFP tagged Pleckstrin Homology domains derived from phospholipase C-δ1 (PH-PLCδ1) (from Kees Jalink, The Netherlands Cancer Institute, Netherland), AKT/protein kinase B (PH-AKT) (from Tamas Balla, NIH, Bethesda, MD, USA), Bruton's tyrosine kinase (PH-Btk) and tandem PH domain-containing protein 1 (PH-TAPP1) (originated from Tamas Balla then sub-cloned into pECFP-C1 and pEYFP-C1 vector (Clontech, Mountain View, CA) by the authors), the P4M domain of PI(4)P binding domain of SidM (P4M-SidM) (from Tamas Balla), and PIPKIγ (from Thomas F. J. Martin, University of Wisconsin, WI, USA), α1B of rat Cav2.2e[37b], rat β3, and rat α2δ1 (from D. Lipscombe, Brown University, Providence, RI), rat β2a(from W.A. Catterall, University of Washington, Seattle, WA), chimeric rat β2a(C3,4S) (from J. Hurley, Indiana University, Bloomington, IN), rat β2a(C3,4S)-GFP (subcloned by D. Kim), chimeric Cav2.2(α1C-

1B) (from D. Yue, Johns Hopkins University, Baltimore, MD), M_1 muscarinic receptor (from N. Nathanson, University of Washington), human M_2 muscarinic receptor (from Guthrie Resource Center, Rolla, MO), and C terminus of β-adrenergic receptor kinase (βARK-ct; from R. Lefkowitz, Duke University, Durham, NC).

2-2. Electrophysiology

The whole-cell configuration of the patch-clamp method was used to depolarize the membrane and record ion currents using an EPC-10 patch-clamp amplifier (HEKA Elektronik, Lambrecht, Germany) at room temperature. Pipette resistance was 1.3 – 4.0 MΩ and series resistance was between 3.4 to 6.0 MΩ with 60% compensation. The bath solution contained 160 mM NaCl, 2.5 mM KCl, 2 mM $CaCl_2$-$2H_2O$, 1 mM $MgCl_2$, 10 mM HEPES and 8 mM glucose. The pipette solution contained 175 mM KCl, 5 mM $MgCl_2$, 5 mM HEPES, 0.1 mM BAPTA-K_4, 3 mM Na_2ATP and 0.1 mM Na_3GTP, titrated to pH 7.4 with NaOH. For Ca_V current recording, Ba^{2+} was used as charge carrier, thus, bath solution contained 150 mM NaCl, 10 mM $BaCl_2$-$2H_2O$, 1 mM $MgCl_2$, 10 mM HEPES, and 8 mM glucose and was titrated to pH 7.4 with NaOH. The pipette solution contained 160 mM CsCl, 5 mM $MgCl_2$, 5 mM HEPES, 0.1 mM 1,2-bis(2-aminophenoxy)ethane *N*,*N*,*N*'*N*'-tetraacetic acid (BAPTA), 3 mM Na_2ATP, and 0.1 mM Na_3GTP and was also titrated to pH 7.4 with CsOH. The holding potential in all experiments was -80 mV, and depolarizing electrical stimulation patterns were either voltage ramps or voltage steps. We mainly used ramp protocols to study the voltage dependence of the 3- and 5-phosphatase activities of Dr-VSP. In most cases, voltage ramps started at 0 mV and rose to 120 mV over 20 s (dV/dt = 6 mV/s) with a final 2 s hold at 120 mV. For Ca_V study, 10 mV step depolarization with 10-ms duration pulsed every 2 or 4 s for recording currents with p/5 subtraction. Application of step depolarization to 120 mV for 1 s induced full activation of Dr-VSP. A conditioning depolarizing prepulse was used to test the involvement of Gβγ. A picture of patch clamp setup used for these experiments is shown in Fig. 4.

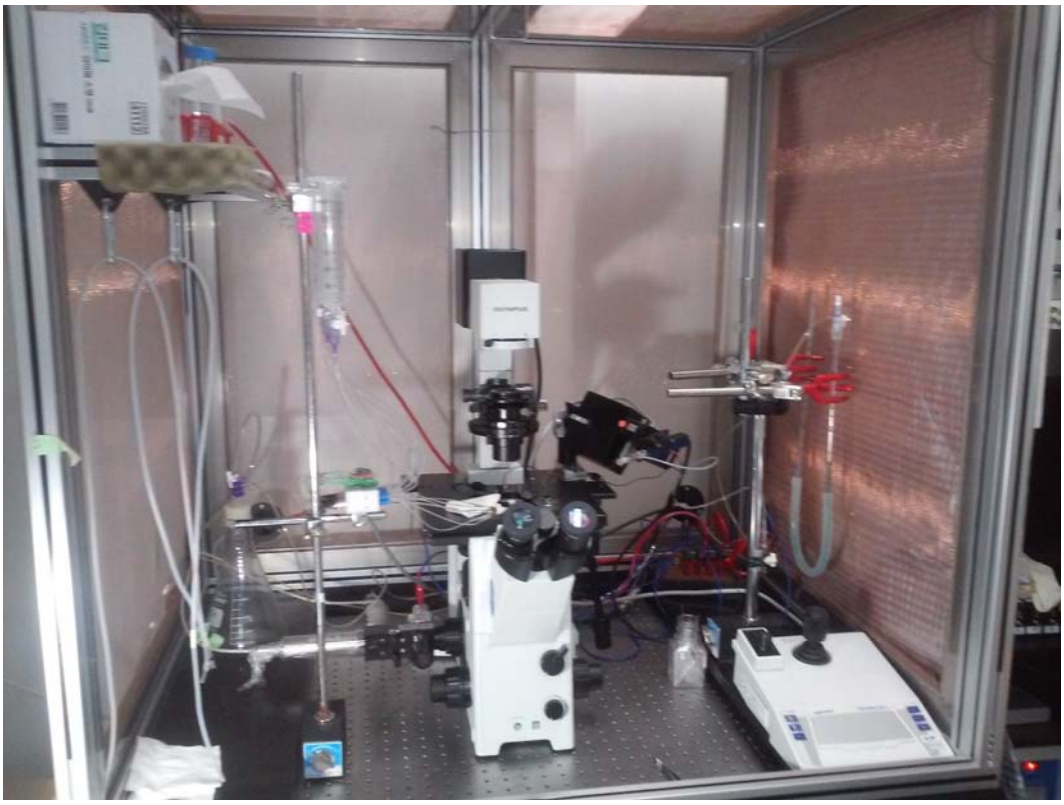

Figure 4. A patch clamp setup for simultaneous FRET acquisition in Current Lab, DGIST

In this patch clamp setup, my first current data were recorded and, from here, my abilities for scientific instrumentation started. I can remember the first detection of reliable FRET signal at the end of 2 years in uncertainty.

2-3. Förster Resonance Energy Transfer (FRET)

FRET between ECFP and EYFP fused to PH-domains was measured by a photomultiplier tube (PMT)-based photometry system (Till Photonics GmbH, Grafelfing, Germany). Indigo exciting light (438 ± 12 nm) from a PolychromeV monochrometer (Till Photonics GmbH) was applied for 45 ms every 500 ms. Simultaneously, the emission was split into short (480 ± 40 nm) and long (535 ± 15 nm) wavelengths by a dichroic mirror (505DCLP) and band-pass filters (D480-40 for short and ET535-30 for long wavelengths, Chroma Technology, Bellows Falls, Vermont, US) and detected by two PMTs connected with an FDU-2 fluorescence detection unit (Till Photonics). The analog outputs were digitized by the data acquisition board (PCI-6221, National Instruments, Austin, TX, USA) at a sampling rate of 10 kHz and averaged. Then, FRETr was calculated by the equation: $FRETr = (YFP_C - cFactor \times CFP_C) / CFP_C$ (Jensen et al., 2009). The numerator is the voltage output of the long-wavelength PMT minus calculated bleed-through from the donor, indicating excitation of acceptor by FRET, and the denominator is the voltage output of the short-wavelength PMT indicating direct donor excitation by the light source. The bleed through from CFP to the long band PMT was 0.55 and from YFP to short, 0.02, which was ignored. Timing control, data acquisition and real-time calculation of FRETr including background compensation were performed using an in-house program that also controlled the monochromator and patch clamp amplifier through the data acquisition interface. Photobleaching of donor and acceptor were compensated during post-processing.

Changes of the membrane density of each lipid were monitored by FRET between ECFP- and EYFP-tagged versions of the same lipid probe. Since probe density at the plasma membrane is dependent on the abundance of the lipid in the cytoplasmic leaflet of the plasma membrane the FRETr falls as the density falls (Itsuki et al., 2014; Jensen et al., 2009; van der Wal et al., 2001).

2-4. Normalization and fitting of traces

The FRETr traces were normalized to their minima and maxima as follows: The point at $t = 0$ s was set to the initial minimum (0.0) or maximum (1.0) value depending on the direction of subsequent changes and the trace maximum or minimum during depolarization was set to the opposite extremum. For empirical characterization of the FRETr responses to applied voltage ramps in the presence of Dr-VSP, FRETr traces were fitted to a sigmoid curve against voltage:

$$FRETr(V) = \mathrm{FRETr}_{V0} + \frac{\Delta FRETr_{peak}}{1 + \exp\left(r_{max}\left(V - V_{half}\right)\right)}$$

Here V is voltage during the ramp, $FRETr_{V0}$ is the FRETr value at $t = 0$ s, $\Delta FRETr_{peak}$ is the peak amplitude of the change during depolarization, V_{half} is the voltage for half maximal change and r_{max} is maximum steepness of the change (V^{-1}). In the text and figures, r_{max} is converted to a rate of change (s^{-1}) by multiplying by dV/dt. We also used an empirical parameter that we call voltage threshold (V_{th}) to denote the voltage at which the effects of the VSP phosphatase first became apparent. It was determined as follows: A sequential sliding t-test was performed between two groups of points each containing 10 samples around the target point. V_{th} is defined as the first point that shows statistically significant deviation in the transition region.

2-5. Confocal microscopy

Confocal microscope (LSM700, Carl Zeiss, Munich, Germany) was used for time-lapse images. The interval between images was 1 min for wortmannin-mediated PI 3-kinase (PI3K) blocking experiments and was 5 s for Cav study. Successive pairs of 512 x 512 pixel images were averaged, and the fluorescence intensity was obtained with Image J (NIH, Bethesda, MD, USA) and plotted by using IGOR Pro 6.0 (WaveMetrics).

2-6. Mathematical modeling

The Virtual Cell software environment (University of Connecticut Health Center, available at http://www.nrcam.uchc.edu) was used to develop a kinetic description of modulation of phosphoinositide levels in tsA201 cells by the voltage-sensitive lipid phosphatases in situ. This allowed extraction of all reaction rates from the recordings from this complex system. For comparison with experimental results, such a description must include the endogenous phosphoinositide metabolism of the cell, the effects of exogenous enzymes that we transfect into the cells, the properties of the lipid-binding probes that are used to measure the dynamic changes of phosphoinositides, and most interesting for this paper, the deduced voltage dependence and catalytic rates of the VSPs. As a starting point we used a compartmental model(Dickson et al., 2013; Falkenburger et al., 2013) that had been developed to describe phosphoinositide metabolism upon modulation by muscarinic receptors and Dr-VSP in the tsA201 cell line. Final conditions used to simulate the results obtained from FRET recordings are shown in Table 4 including the dissociation constants for each of the fluorescent probes, taken from the literature. Rate constants were adjusted manually to fit experimental data. The modeled traces approximate changes in FRETr as a cooperative square law of the predicted membrane-bound fraction of FRET domains, as recently described (Itsuki et al., 2014). The voltage dependence of the enzymatic activities of VSP was described by a Boltzmann equation with no residual baseline activity at very negative voltages. Thus for each of the four enzymatic subreactions of VSP, the rate constants varied as a function of membrane voltage (*V*) as follows

$$\text{rate constant}(V) = \frac{\text{k\_VSP}}{1+\exp\left(\frac{z(V_{0.5}-V)}{25\ \text{mV}}\right)} \qquad \text{(Eq. 1)}$$

where the four subreaction-specific fully-activated rate constants k_VSP and the subreaction-independent half-activation voltage $V_{0.5}$ and equivalent valence z are listed in Table 1. For Dr-VSP, the midpoint potential; $V_{0.5}$ was +100 mV, and for Ci-VSP, +55 mV. The Virtual Cell model, "hillelab: KeumKruseKimHilleSuh_2016," is publicly available at http://www.vcell.org/.

2-7. Analysis and Statistics

All data were analyzed using Excel (Microsoft, Redmond, WA, USA), IGOR Pro 6.0 (WaveMetrics, Lake Osewgo, OR, USA), ImageJ (NIH, Bethesda, MA, USA) or GraphPad Prism 6.0 (GraphPad Software, La Jolla, CA, USA). Statistics in text or figures represent mean ± SEM (standard error of mean). Statistical comparisons were made by one-way ANOVA with or without Tukey's posthoc test depending on the number of experimental groups.

2-8. Materials

Wortmannin (Sigma-Aldrich) was dissolved in DMSO, stored in -20℃ with protection from light, and then diluted to 2 μM in Ringer's solution just before the experiments. Wortmannin was used for less than 1 month after unpacking.

III. VOLTAGE-SENSING PHOSPHATASE (VSP) REGULATION OF PHOSPHOINOSITIDES

3-1. Voltage-dependent PI 3- and 5-phosphatase activities

We tested the phosphatase activity of Dr-VSP on the phosphoinositides PI(3,4,5)P_3, PI(3,4)P_2, PI(4,5)P_2 and PI(4)P using the specific probes in Table 3. Each lipid was detected by FRET between diffusible ECFP and EYFP versions of the Pleckstrin homology (PH) domain probes. Separate tsA201 cell batches were cotransfected with Dr-VSP and individual FRET pairs of each PH domain. Unlike *Xenopus* oocytes in standard media used in previous studies (Lacroix et al., 2011; Murata et al., 2005; Villalba-Galea et al., 2008), tsA201 cells have enough PI(3,4,5)P_3 in the plasma membrane to localize the PI(3,4,5)P_3-specific PH-AKT and PH-Btk probes to the membrane without additional treatment (Suh et al., 2006). On the other hand, we did not detect any basal PI(3,4)P_2. A slow depolarizing ramp voltage stimulus (Fig. 5*C*) progressively activated Dr-VSP, and the changing membrane lipid concentrations were measured by FRET (Fig. 5*C*). FRET is expressed as the FRET ratio FRETr defined approximately as long-wavelength light divided by short-wavelength (see Materials and Methods). Decreasing FRET signifies a loss of the monitored lipid at the plasma membrane. Fig. 5*A* diagrams the possible 5-phosphatase (red) and 3-phosphatase (purple) reactions of Dr-VSP on three of these lipids. During a strong depolarizing activation of Dr-VSP, the three lipids would be converted in one or two steps to PI(4)P. After Dr-VSP is turned off again, the endogenous 5-kinase (blue) and 3-kinase (black) enzymes of the cell (Fig. 5*B*) would restore the original status quo. Fig. 5*D* is an overview of the results for three probes. All probes start at the plasma membrane (high FRETr), go gradually to the cytoplasm during the depolarizing ramp, and return to the membrane after the ramp, reflecting lipid dephosphorylation by VSP followed by lipid rephosphorylation by endogenous kinases. It is clear from the time courses that the different phosphoinositides become depleted at different times during the ramp and are restored at different rates afterwards, properties that we will have to explain.

We turn to quantitative analysis of such experiments. The goal is to determine the substrate preferences and voltage dependence of the Dr-VSP phosphatase activities and the interactions with cellular lipid metabolism. In many of our figures we have included simulated traces like those of Fig. 5*E*. They come from a kinetic description of phosphoinositide metabolism that includes the phosphatase and kinase reactions of Fig. 5 *A* and *B* for endogenous cellular enzymes and for exogenous Dr-VSP as well as other enzymes that will be overexpressed and other endogenous enzymes that feed or deplete these lipid pools. The simulated traces serve as a qualitative and quantitative test of how well we understand the in-situ phosphatase subreactions of Dr-VSP. The derived rate constants are summarized in Table 4. Each experiment helped to inform the values of rate constants. For example, the recovery kinetics during long recordings like Fig. 5*D* were particularly helpful in setting the rate constants for the endogenous lipid kinases.

During the voltage ramp, each probe began to leave the plasma membrane as the membrane potential rose past some critical value. Qualitatively, we can consider this voltage a threshold (V_{th}) for seeing one of the enzymatic subreactions of Dr-VSP. At this potential the phosphatase activity of Dr-VSP has risen enough to noticeably perturb the dynamic steady-state set up by the endogenous metabolism for that lipid species. For example, one might anticipate that when the increasing VSP activity becomes equal to the endogenous activity so that the total phosphatase activity is twice as much as normal, the FRET probes should be reporting a noticeable perturbation of lipid pools. Our empirical definition for measuring V_{th} is given in Methods. It is helpful to understand this threshold first by considering the model. Fig. 6*A* plots phosphatase rate constants from the model against voltage. Three horizontal dashed lines represent the endogenous voltage-independent phosphatase activities of the cell, and the four rising solid curves represent the modeled four voltage-dependent phosphatase subreactions of the expressed Dr-VSP (note semi logarithmic axis). The VSP curves follow identical Boltzmann functions with a single voltage dependence taken from our earlier electrophysiological measurements of VSP sensing current (Falkenburger et al., 2010). They differ only by vertical scaling factors that reflect our derived conclusions for Dr-VSP (developed later) (i) that the 5-phosphatase subreactions are much faster than the 3-phosphatase subreactions and (ii) that PI(4,5)P_2 is a better substrate for the 5-phosphatase reaction than is PI(3,4,5)P_3. Two vertical lines mark the voltages where two of the voltage-dependent phosphatase subreactions become faster than their corresponding endogenous phosphatase reaction. They are very widely separated along the voltage axis. At the crossing point, the total phosphatase activity (endogenous plus VSP) has been approximately doubled. The separation of such crossings on the diagram illustrate one explanation for different apparent V_{th} values in our experiments. It is clear that each crossing point depends both on the rate constant of the VSP subreaction as well as the rate constant of the endogenous phosphatase. Now we can consider the experiments.

During a ramp, the FRETr trace for the PI(4,5)P_2-binding domain PH-PLCδ1 (Fig. 5*D* and 6*B*) began to show a fast decrease at 26 ± 5 mV (V_{th}) reflecting the canonical 5-phosphatase activity of VSPs depleting PI(4,5)P_2. Note that the x-axis of these traces is labeled in time, but it corresponds to the voltages on the ramp inset drawn above. The trace was fitted to a sigmoid function giving a half-maximal membrane potential (V_{half}) at 69 ± 5 mV and a maximum rate (r_{max}) of 1.0 ± 0.1 s^{-1} (Methods). The FRETr trace for the PI(4)P-reporter P4M-SidM was complementary (Fig. 6*B*, brown). It increased during the depolarization, reflecting the generation of PI(4)P from PI(4,5)P_2. As expected, the kinetics closely tracked those for PH-PLCδ1 (Fig. 6 *H-J*) but were opposite in direction (Fig. 6*B*). A small unexpected spike appeared consistently at the top of the P4M-SidM trace after the ramp-depolarization. A control experiment with VSP showed that the spike did not occur unless Dr-VSP was expressed. As an ad hoc explanation, the spike might be due to a final release of some trapped PI(4)P during deactivation of Dr-VSP including possible delivery of excess PI(4)P from the Golgi. The kinetic simulations (Fig. 6*E*) reproduce the PH-PLCδ1 and P4M-SidM traces including a final spike when making this latter empirical assumption.

Now we consider changes of PI(3,4,5)P_3 and PI(3,4)P_2, starting with the PH-AKT probe, which binds to these two species with similar affinity (Frech et al., 1997; James et al., 1996). The PH-AKT trace began a slow decrease only at 52 ± 3 mV (Fig. 5*D*, 6 *C* and *H*). When compared with PH-PLCδ1, the sigmoid fits gave a much more positive V_{half} (99 ± 1 mV) and a slower r_{max} (0.5 ± 0.02 s^{-1}) (Fig. 6 *I* and *J*). The FRETr trace for the PI(3,4,5)P_3-specific PH-Btk probe (Rameh et al., 1997) started to decrease from a low voltage (41 ± 5 mV), close to the V_{th} of PH-PLCδ1, but its slow kinetics and overall changes tracked those of PH-AKT ($V_{\mathrm{half}} = 93 \pm 5$ mV and $r_{\mathrm{max}} = 0.5 \pm 0.02$ s^{-1}) (Fig. 5*D*, 6 *C*, *H-J*, and Fig. 8*B*). Thus, the detectable effects of this mostly 5-phosphatase subreaction on PI(3,4,5)P_3 (red line in Fig. 6*A*) show quite different parameters from those for the 5-phosphatase subreaction on PI(4,5)P_2 (black line in Fig. 6*A*).

To confirm that the loss of PI(3,4,5)P_3 is primarily via a 5-phosphatase step, we looked for the expected product, PI(3,4)P_2, by constructing a pair of PH-TAPP1 FRET probes. The result was a bell-shaped curve (Fig. 6*D*, green) reporting at rest no $PI(3,4)P_2$, but at voltages between 30 and 90 mV the expected production of $PI(3,4)P_2$ (complementary to loss of $PI(3,4,5)P_3$), and then at high voltages a secondary loss of $PI(3,4)P_2$. We will be showing that this loss is a further dephosphorylation by a Dr-VSP 3-phosphatase subreaction of $PI(3,4)P_2$ to PI(4)P. The model curves (Fig. 6 *F* and *G*) predict the same result. The PH-AKT and PH-Btk traces were not identical (Fig. 6*C*, red and blue). The same graph shows a difference curve, AKT minus Btk (pink line). Since PH-AKT binds both $PI(3,4)P_2$ and $PI(3,4,5)P_3$ and PH-Btk is more specific for $PI(3,4,5)P_3$, the difference curve might represent the $PI(3,4)P_2$ pool. Indeed, as predicted, the AKT minus Btk difference curve (Fig. 6*D*, pink) is bell shaped, and it tracks the PH-TAPP1 FRET curve well (Fig. 6*D*, green) up to a membrane potential near 90 mV. Control experiments using the PH-TAPP1 FRET probes without expression of Dr-VSP showed that unlike *Xenopus* oocytes (14, 20), our cells had no endogenous voltage-dependent phosphatase activity in this kind of experiment (Fig. 7).

These observations begin to specify the 3- and 5-phosphatase subreactions of Dr-VSP as they become visible with different apparent voltage thresholds and different rates during a ramp. Our conclusions from the experiments are drawn through the kinetic model described in Methods and Table 4. The key findings are that (i) each of the Dr-VSP enzyme subreactions has the same voltage-dependent activation (Fig. 6*A*) given by the sensing charge movement measurements in Falkenburger et al. (2010) for Dr-VSP, and (ii) the four subreactions have very different fully-activated rates: 11.3, 2.0, 0.25, 0.2 s^{-1} for 5 phosphatase activity on $PI(4,5)P_2$ and $PI(3,4,5)P_3$ and for 3-phosphatase activity on $PI(3,4)P_2$ and $PI(3,4,5)P_3$, respectively. These numbers express the deduced substrate and catalytic selectivity of Dr-VSP. Even with identical catalytic voltage dependence, the predicted apparent voltage thresholds are quite different–as is observed. We continue with tests of this description.

Table 3. Genetically encoded PI probes

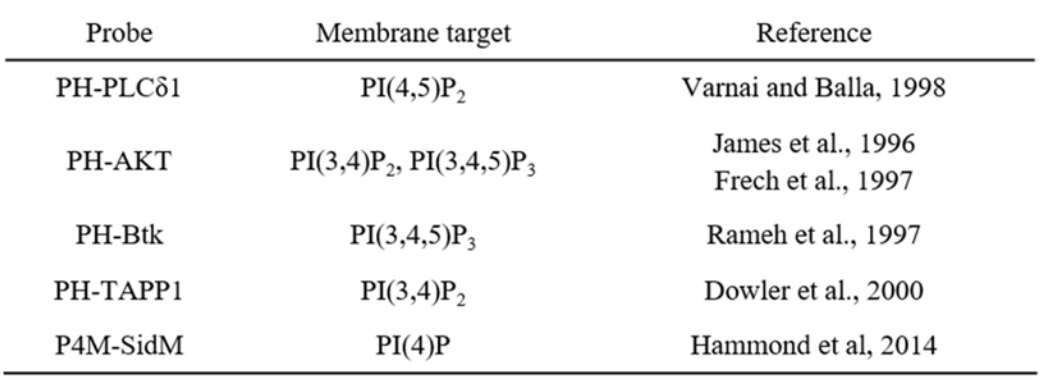

Probe	Membrane target	Reference
PH-PLCδ1	$PI(4,5)P_2$	Varnai and Balla, 1998
PH-AKT	$PI(3,4)P_2$, $PI(3,4,5)P_3$	James et al., 1996 Frech et al., 1997
PH-Btk	$PI(3,4,5)P_3$	Rameh et al., 1997
PH-TAPP1	$PI(3,4)P_2$	Dowler et al., 2000
P4M-SidM	PI(4)P	Hammond et al, 2014

Table 4. Rate constants and parameters for modeling at 22℃

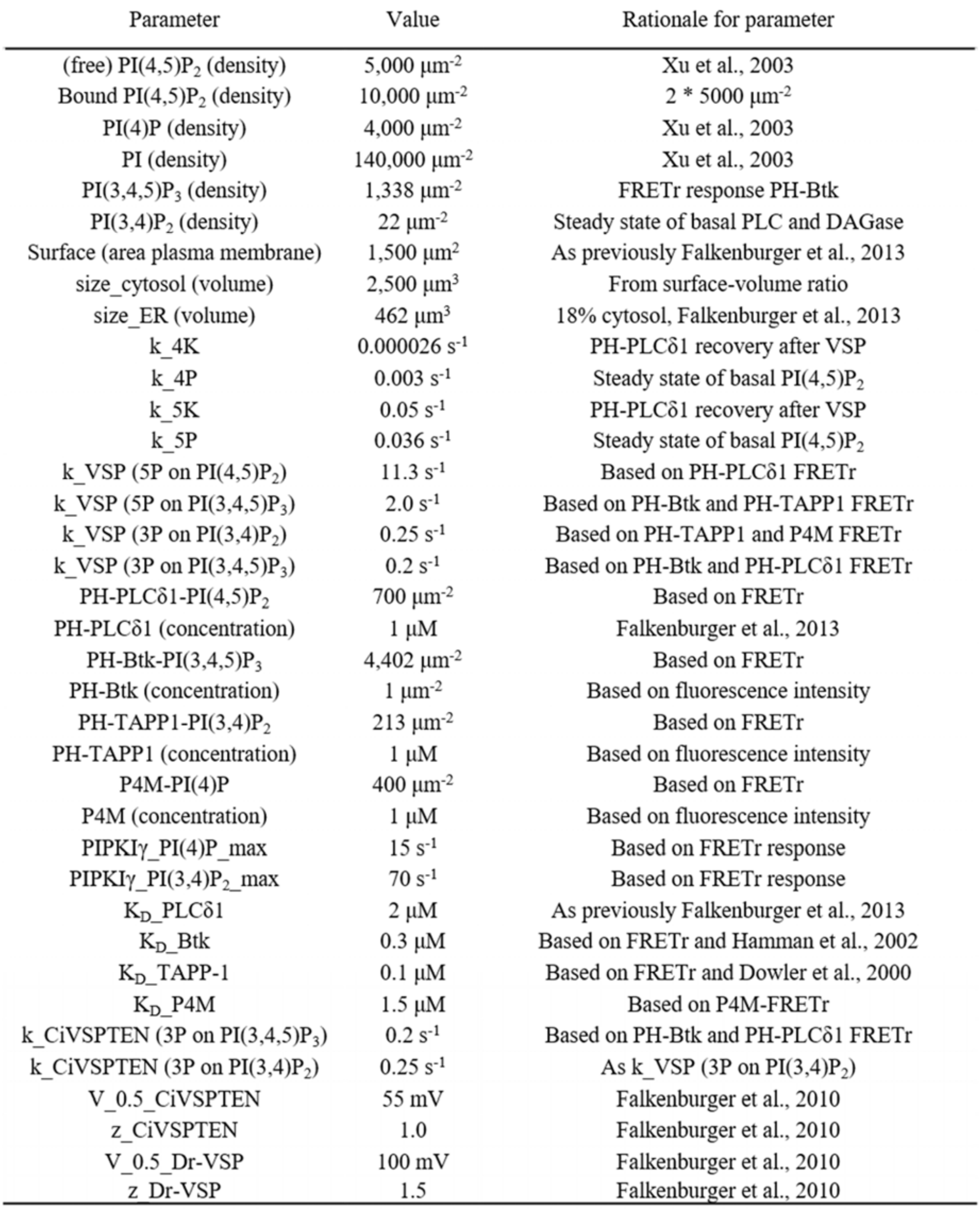

Parameter	Value	Rationale for parameter
(free) PI(4,5)P_2 (density)	5,000 μm^{-2}	Xu et al., 2003
Bound PI(4,5)P_2 (density)	10,000 μm^{-2}	2 * 5000 μm^{-2}
PI(4)P (density)	4,000 μm^{-2}	Xu et al., 2003
PI (density)	140,000 μm^{-2}	Xu et al., 2003
PI(3,4,5)P_3 (density)	1,338 μm^{-2}	FRETr response PH-Btk
PI(3,4)P_2 (density)	22 μm^{-2}	Steady state of basal PLC and DAGase
Surface (area plasma membrane)	1,500 μm^2	As previously Falkenburger et al., 2013
size_cytosol (volume)	2,500 μm^3	From surface-volume ratio
size_ER (volume)	462 μm^3	18% cytosol, Falkenburger et al., 2013
k_4K	0.000026 s^{-1}	PH-PLCδ1 recovery after VSP
k_4P	0.003 s^{-1}	Steady state of basal PI(4,5)P_2
k_5K	0.05 s^{-1}	PH-PLCδ1 recovery after VSP
k_5P	0.036 s^{-1}	Steady state of basal PI(4,5)P_2
k_VSP (5P on PI(4,5)P_2)	11.3 s^{-1}	Based on PH-PLCδ1 FRETr
k_VSP (5P on PI(3,4,5)P_3)	2.0 s^{-1}	Based on PH-Btk and PH-TAPP1 FRETr
k_VSP (3P on PI(3,4)P_2)	0.25 s^{-1}	Based on PH-TAPP1 and P4M FRETr
k_VSP (3P on PI(3,4,5)P_3)	0.2 s^{-1}	Based on PH-Btk and PH-PLCδ1 FRETr
PH-PLCδ1-PI(4,5)P_2	700 μm^{-2}	Based on FRETr
PH-PLCδ1 (concentration)	1 µM	Falkenburger et al., 2013
PH-Btk-PI(3,4,5)P_3	4,402 μm^{-2}	Based on FRETr
PH-Btk (concentration)	1 μm^{-2}	Based on fluorescence intensity
PH-TAPP1-PI(3,4)P_2	213 μm^{-2}	Based on FRETr
PH-TAPP1 (concentration)	1 µM	Based on fluorescence intensity
P4M-PI(4)P	400 μm^{-2}	Based on FRETr
P4M (concentration)	1 µM	Based on fluorescence intensity
PIPKIγ_PI(4)P_max	15 s^{-1}	Based on FRETr response
PIPKIγ_PI(3,4)P_2_max	70 s^{-1}	Based on FRETr response
K_D_PLCδ1	2 µM	As previously Falkenburger et al., 2013
K_D_Btk	0.3 µM	Based on FRETr and Hamman et al., 2002
K_D_TAPP-1	0.1 µM	Based on FRETr and Dowler et al., 2000
K_D_P4M	1.5 µM	Based on P4M-FRETr
k_CiVSPTEN (3P on PI(3,4,5)P_3)	0.2 s^{-1}	Based on PH-Btk and PH-PLCδ1 FRETr
k_CiVSPTEN (3P on PI(3,4)P_2)	0.25 s^{-1}	As k_VSP (3P on PI(3,4)P_2)
V_0.5_CiVSPTEN	55 mV	Falkenburger et al., 2010
z_CiVSPTEN	1.0	Falkenburger et al., 2010
V_0.5_Dr-VSP	100 mV	Falkenburger et al., 2010
z_Dr-VSP	1.5	Falkenburger et al., 2010

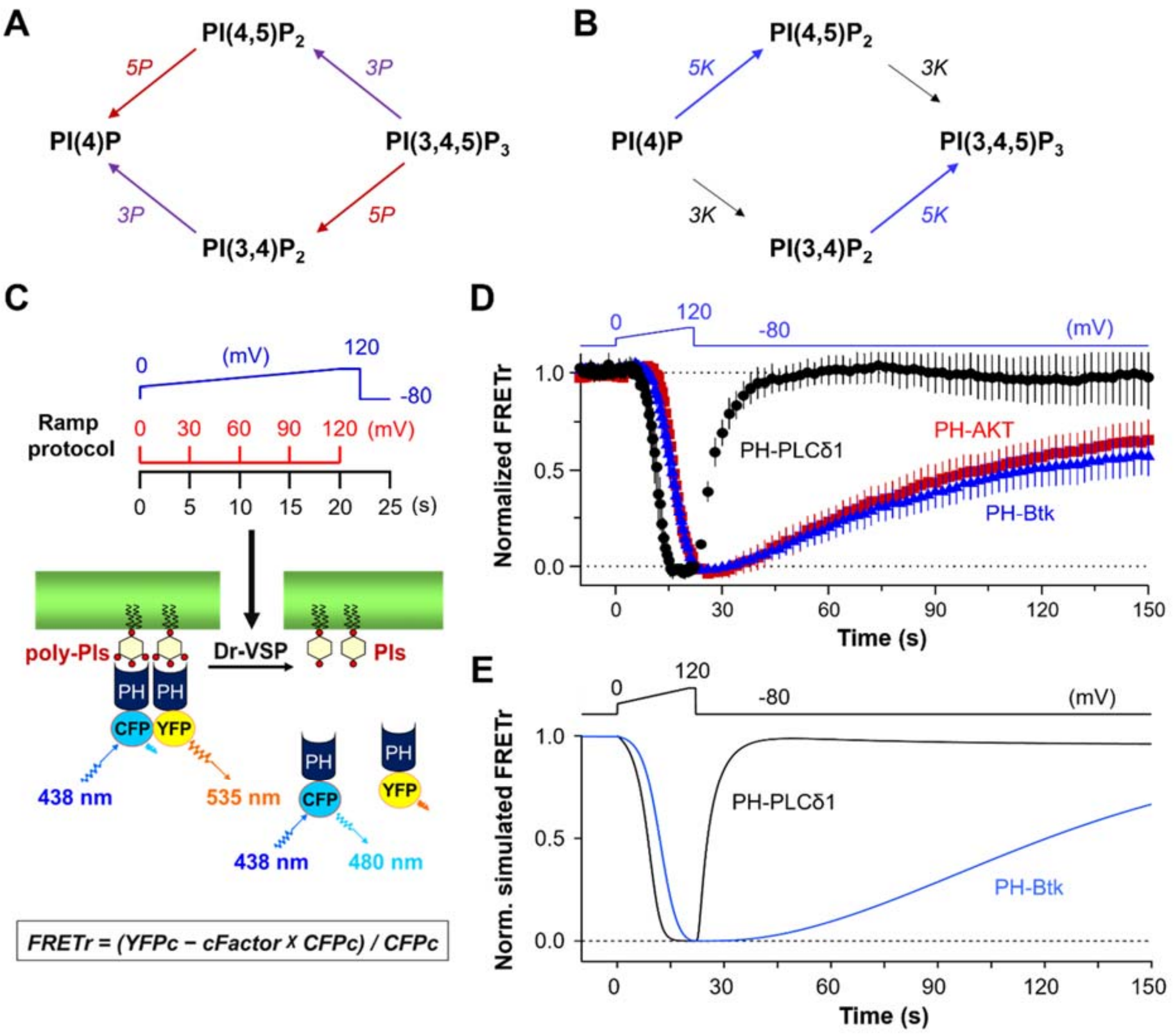

Figure 5. Measuring voltage-dependent changes of PIs using FRET probes in living cells

(*A*) Phosphoinositide dephosphorylation by 3-phosphatase (3P, purple) and 5-phosphatase (5P, red) activities of Dr-VSP. (*B*) Phosphoinositide re-synthesis by endogenous phosphoinositide 5-kinase (5K, blue) and 3-kinase (3K, black) enzymes after Dr-VSP activation. (*C*) Protocol for FRET measurements. A ramp depolarization (blue line) rising from 0 mV to 120 mV over 20 s (rising rate, dV/dt = 6 mV/s) followed by a 2 s hold at the apex is given to tsA201 cells expressing Dr-VSP and a CFP/YFP pair of phosphoinositide FRET indicators chosen from Table 1. Holding potential was -80 mV. (*D*) Normalized time-courses of FRETr responses of PH-PLCδ1 (black circles, n = 5), PH-AKT (red squares, *n* = 5) or PH-Btk (blue triangles, *n* = 6) during ramp Dr-VSP activation. Four points were averaged during repolarization (after 22 s) for better visibility. (*E*) Normalized simulated FRETr responses from the model of PH-PLCδ1 and PH-Btk domains for the experimental conditions in *D*.

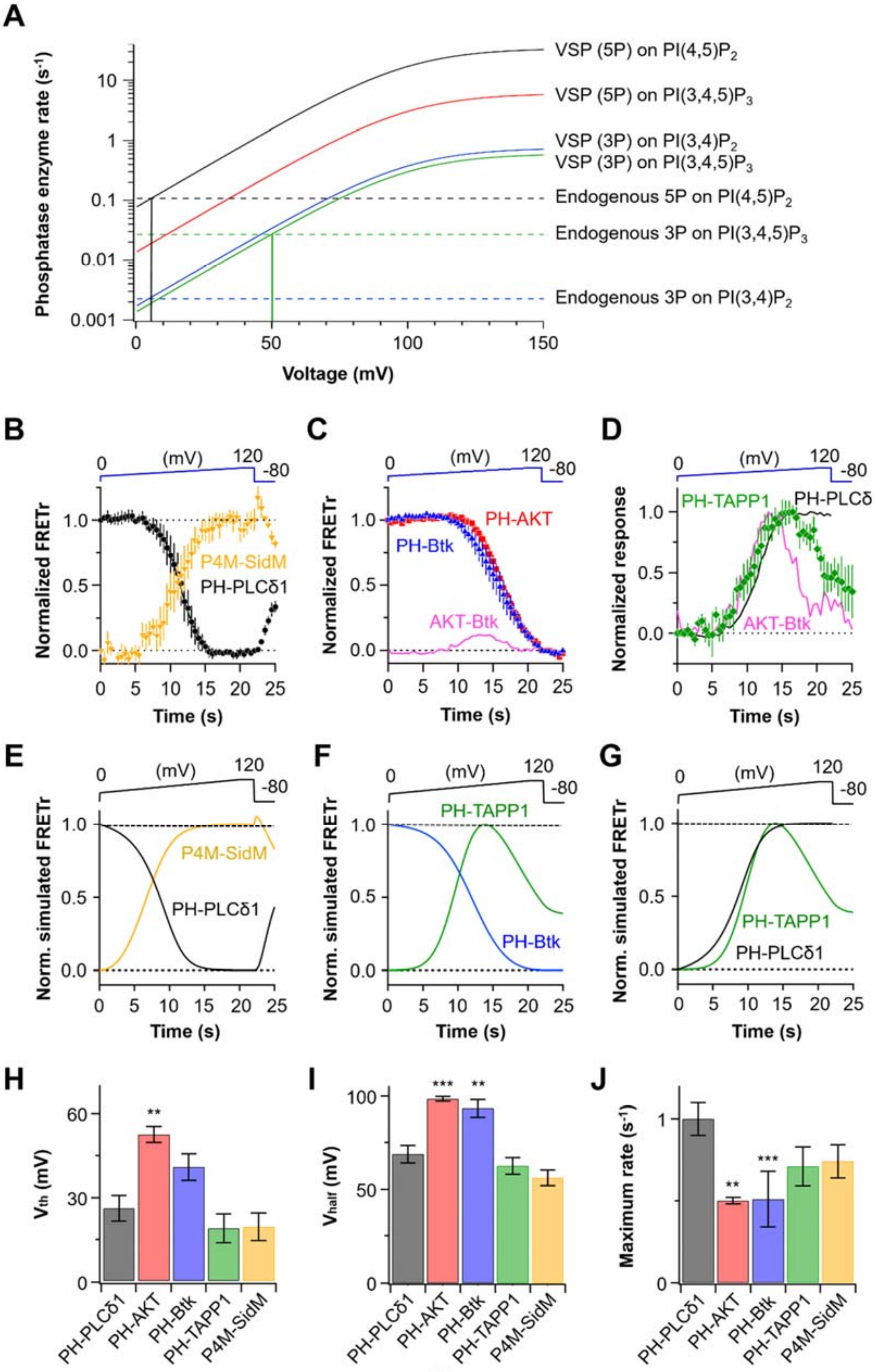
A
Phosphatase enzyme rate (s-1)
10
1
0.1
0.01
0.001
0
50
100
150
Voltage (mV)
VSP (5P) on PI(4,5)P2
VSP (5P) on PI(3,4,5)P3
VSP (3P) on PI(3,4)P2
VSP (3P) on PI(3,4,5)P3
Endogenous 5P on PI(4,5)P2
Endogenous 3P on PI(3,4,5)P3
Endogenous 3P on PI(3,4)P2
B
0
(mV)
120
-80
Normalized FRETr
P4M-SidM
PH-PLCδ1
Time (s)
C
PH-AKT
PH-Btk
AKT-Btk
D
Normalized response
PH-TAPP1
PH-PLCδ1
AKT-Btk
E
Norm. simulated FRETr
P4M-SidM
PH-PLCδ1
F
PH-TAPP1
PH-Btk
G
PH-TAPP1
PH-PLCδ1
1.0
0.5
0.0
0
5
10
15
20
25
H
Vth (mV)
60
30
0
**
I
Vhalf (mV)
100
50
0
***
**
J
Maximum rate (s-1)
1
0
**
***
PH-PLCδ1
PH-AKT
PH-Btk
PH-TAPP1
P4M-SidM

Figure 6. Dynamic changes of FRET probes during ramp activation of Dr-VSP

(*A*) Postulated voltage dependence of phosphatase enzyme rate constants of Dr-VSP (colored curves) and of endogenous phosphatases (dashed lines) in the model. (*B*) Comparison of FRETr responses for PH-PLCδ1 (black) and P4M-SidM (brown, $n = 5$) during ramp depolarization. (*C*) Magnified view of PH-AKT (red squares) and PH-Btk (blue triangles) FRETr changes during the ramp depolarization from Fig. 5*D*. Pink line shows FRETr difference between PH-AKT and PH-Btk, obtained by subtracting the PH-Btk trace from PH-AKT. (*D*) Superposition of PH-TAPP1 (green diamond, n =5), PH-PLCδ1 (black trace), and the subtracted difference between PH-AKT and BH-Btk signals from *C* (pink trace). (*E*-*G*) Normalized simulated FRETr changes of P4M-SidM, PH-PLCδ1, PH-TAPP1 and PH-Btk domains for experimental conditions shown in *B*-*D*. (*H*) Membrane potential at which FRETr of each probe starts to change (voltage threshold). Time at the beginning of descent was converted to voltage threshold by $V_{th} = (t_{\text{threshold}} \times 6)$. (*I* and *J*) Analyzed membrane potential of half-maximal change (V_{half}) (*I*) and maximum rate (*J*) obtained from fitted traces of FRETr data (*B*-*D*) with a sigmoid function. $^{**}p < 0.01$ and $^{***}p < 0.001$, compared to values of PH-PLCδ1. All data are mean ± SEM.

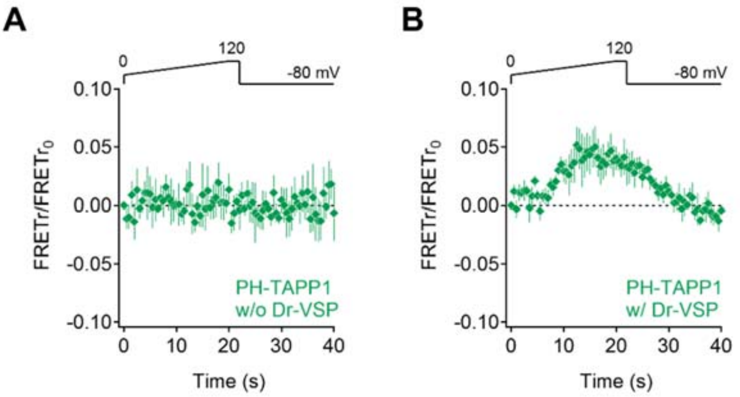

Figure 7. Evaluating endogenous voltage-dependent phosphatase activity on PI(3,4)P_2 in tsA201
PH-TAPP1 FRET traces during ramp depolarization in control *(A)* and Dr-VSP co-expressing cells *(B)* (*n* = 5). Data are mean ± SEM. This work was done as a response to reviewer to Professor Yasushi Okamura at Osaka University.

3-2. Perturbations with wortmannin

In order to characterize the 3-phosphatase activities of Dr-VSP more directly, we first need to examine the opposing endogenous cellular 3-kinase enzyme activity. We used the PI kinase inhibitor wortmannin. When cells were incubated with 2 μM of wortmannin to inhibit PI3 kinases preferentially, both the AKT probes and the Btk probes gradually translocated away from the plasma membrane (Fig. 8*A*) reflecting a slow spontaneous loss of PI(3,4,5)P_3. In experiments with Dr-VSP and voltage ramps, wortmannin did not affect the recovery of PI(4,5)P_2 as reported by PH-PLCδ1, but it abrogated recovery of PI(3,4,5)P_3 as reported by PH-AKT and PH-Btk (Fig. 8*B*). Even without wortmannin, the recovery was quite slow. Such observations guide our choice of 3-kinase rate for the model (Fig. 8*C*). They mean that in normal cells an endogenous background PI3K synthesizes PI(3,4,5)P_3 continuously, filling pools slowly with a time course of more than a minute. That would also tell us the turnover time of PI(3,4,5)P_3 molecules in resting cells. As we saw in Fig. 6, with low voltage depolarizations this constitutive 3-kinase activity is able to counteract and mask the slow 3-phosphatase activity of Dr-VSP against PI(3,4,5)P_3. Wortmannin had some effects on the dynamic dephosphorylation parameters during the ramp (Fig. 8 *D* and *E*). The principal change was that V_{th} and V_{half} for PH-Btk reporting PI(3,4,5)P_3 were shifted by 12 and 26 mV to the left, implying that the 3-phosphatase activity of Dr-VSP became more effective. This result is expected when the masking endogenous 3-kinase activity is reduced by wortmannin. As could be anticipated, there was no change in the V_{th} and V_{half} for PH-PLCδ1 reporting PI(4,5)P_2, i.e., 3-kinases do not affect PI(4,5)P_2 production. The kinetic modeling describes these results well (Fig. 8 *C* and *F*).

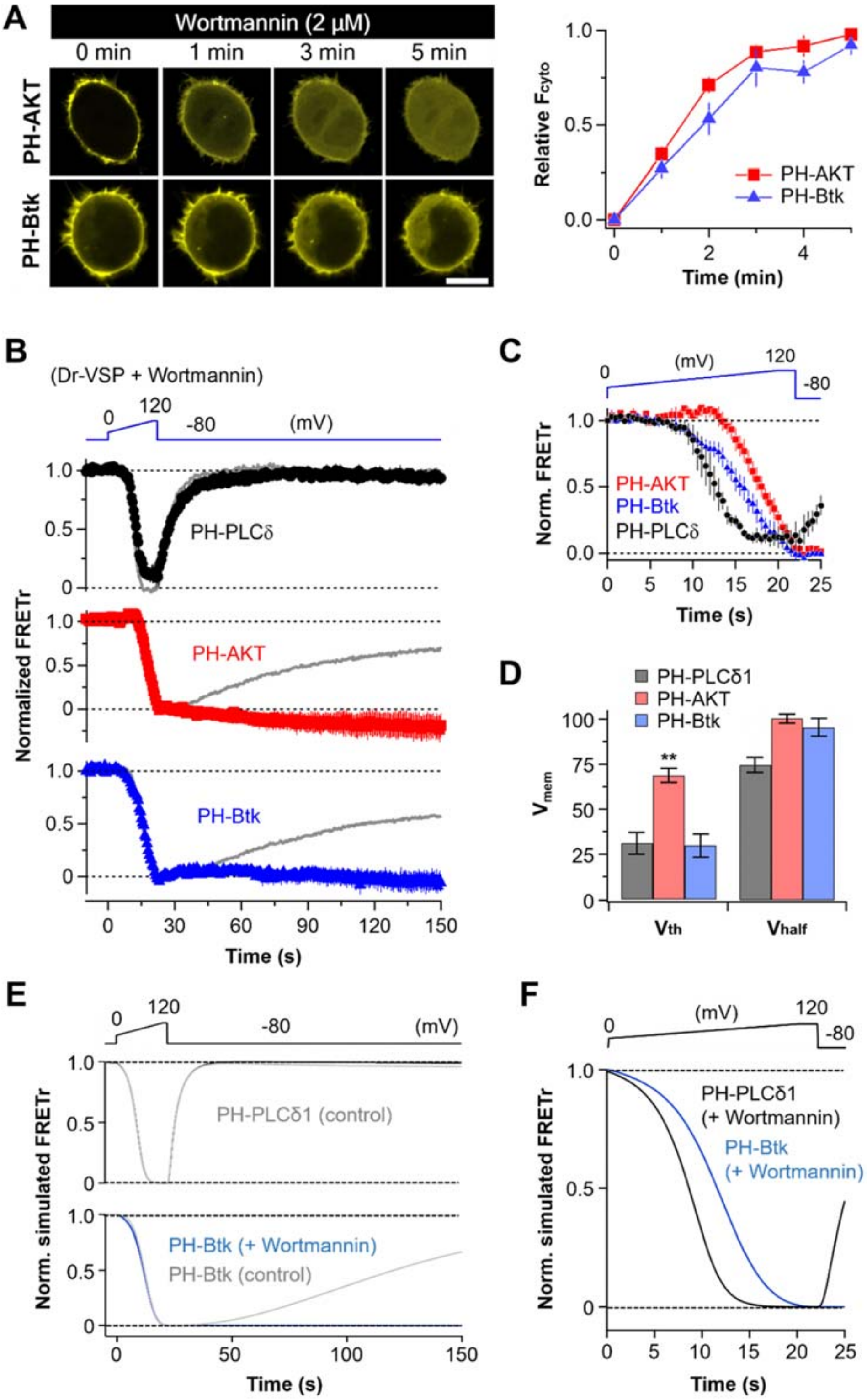
A
Wortmannin (2 µM)
0 min
1 min
3 min
5 min
PH-AKT
PH-Btk
Relative F$_{cyto}$
1.0
0.5
0.0
0
2
4
Time (min)
PH-AKT
PH-Btk
B
(Dr-VSP + Wortmannin)
0
120
-80
(mV)
Normalized FRETr
1.0
0.5
0
PH-PLCδ
PH-AKT
PH-Btk
0
30
60
90
120
150
Time (s)
C
0
(mV)
120
-80
Norm. FRETr
1.0
0.5
0.0
PH-AKT
PH-Btk
PH-PLCδ
0
5
10
15
20
25
Time (s)
D
PH-PLCδ1
PH-AKT
PH-Btk
V$_{mem}$
100
75
50
25
0
**
V$_{th}$
V$_{half}$
E
0
120
-80
(mV)
Norm. simulated FRETr
1.0
0.5
0
PH-PLCδ1 (control)
PH-Btk (+ Wortmannin)
PH-Btk (control)
0
50
100
150
Time (s)
F
0
(mV)
120
-80
Norm. simulated FRETr
1.0
0.5
0
PH-PLCδ1
(+ Wortmannin)
PH-Btk
(+ Wortmannin)
0
5
10
15
20
25
Time (s)

Figure 8. Effect of PI3K inhibition on PI dynamics after Dr-VSP activation

(A) Time lapse confocal images of cells expressing YFP-tagged PH-AKT (top) or PH-Btk (bottom) after application of wortmannin (left) and their relative response of cytosolic fluorescence intensity (right). Scale bar indicates 10 μm. Data are mean ± SEM (*n* = 6). *(B)* Dr-VSP-induced FRETr responses of PH-PLCδ1 (top, black circles), PH-AKT (middle, red squares) or PH-Btk (bottom, blue triangles) were plotted in the presence of wortmannin (2 μM). Wortmannin was perfused 40 s to 60 s before the ramp depolarization. Cells held at -80 mV were depolarized from 0 mV to 120 mV for 20 s and then sustained additional 2 s. Grey lines indicate averaged control traces shown in Fig. 5*D*. Data are mean ± SEM (*n* = 4-5). *(C)* Normalized simulated FRETr responses of experiment shown in *(B)*. *(D)* Horizontal magnification of FRETr signals *(B)* between 0 and 25 s. Note that the FRETr traces decrease with different kinetics depending on the PI probes. *(E)* Voltage threshold (V_{th}) and half-maximal effective voltage (V_{half}) of PH-PLCδ1 (black), PH-AKT (red) and PH-Btk (blue) FRETr traces. Data are mean ± SEM. *(F)* Normalized simulated FRETr responses of PH-PLCδ1 and PH-Btk domains in the presence of wortmannin as shown in *(C)*.

3-3. Voltage-dependent PI(3,4,5)P_3 3-phosphatase activity of Ci-VSPTEN

The 3-phosphatase activities of Dr-VSP are difficult to analyze in living cells because of the accompanying stronger 5-phosphatase activities. We decided to begin with the simpler chimeric enzyme construct Ci-VSPTEN (Lacroix et al., 2011) that combines the pure 3-phosphatase enzyme PTEN with the voltage sensor of Ci-VSP. With Ci-VSPTEN we could start to disentangle voltage-dependent effects of 3-phosphatase activities alone. This PTEN enzyme dephosphorylates PI(3,4,5)P_3 to PI(4,5)P_2. Since the chimera is based on Ci-VSP, which has a more negative mid-point voltage for activation $V_{0.5}$ than Dr-VSP, the activation does not require as strong depolarizations (Falkenburger et al., 2010; Hossain et al., 2008). Note, for example, the 45 mV shift in the modeling parameters between V_0.5_Dr-VSP and V_0.5_Ci-VSPTEN in Table 4. The modified ramp depolarization started from -80 mV to 120 mV for 25 s (dV/dt = 8 mV/s) with a 2-s final hold (Fig. 9*A*). As anticipated, PI(3,4,5)P_3 was dephosphorylated relatively slowly and at relatively positive voltages for the Ci-based voltage sensor (V_{half} = 53 ± 9 mV, r_{max} = 0.44 ± 0.06 s^{-1} for PH-AKT and V_{half} = 62 ± 4 mV, r_{max} = 0.41 ± 0.02 s^{-1} for PH-Btk). In a complementary manner, the expected product PI(4,5)P_2 increased as seen by FRETr of PH-PLCδ1 (Lacroix et al., 2011). The FRETr changes of all PH-pairs initiated around -20 mV (Fig. 9 *B* and *E*), and there was no longer any difference between PH-AKT and PH-Btk kinetics (Fig. 9*C*). No PI(3,4)P_2 generation was detected by PH-TAPP1 (Fig. 9*D*). After the repolarization, the recovery of PH-PLCδ1 FRETr was fast ($t_{1/2}$ = 3.6 ± 1.1 s), whereas the recovery of PH-Btk and PH-AKT FRETr was quite slow ($t_{1/2}$ = 50 ± 5 s and 41 ± 8 s, respectively) (Fig. 9*F*). Unlike for Dr-VSP-induced responses, the FRETr of PH-Btk and PH-AKT recovered fully after Ci-VSPTEN activation (Fig. 9*G*). Remarkably all these effects of Ci-VSPTEN could be reproduced in the Dr-

VSP model by making only two changes: (i) that the only voltage-dependent enzyme activity to consider is the PI(3,4,5)P_3 3-phosphatase, and (ii) that the maximum 3-phosphatase activity is the same as it was for Dr-VSP but with a 45 mV shifted voltage dependence given by our previous measurements of sensing currents of wild-type Ci-VSP (Falkenburger et al., 2010). Thus, here the VSPTEN chimera copies just one subreaction of intact VSP remarkably precisely.

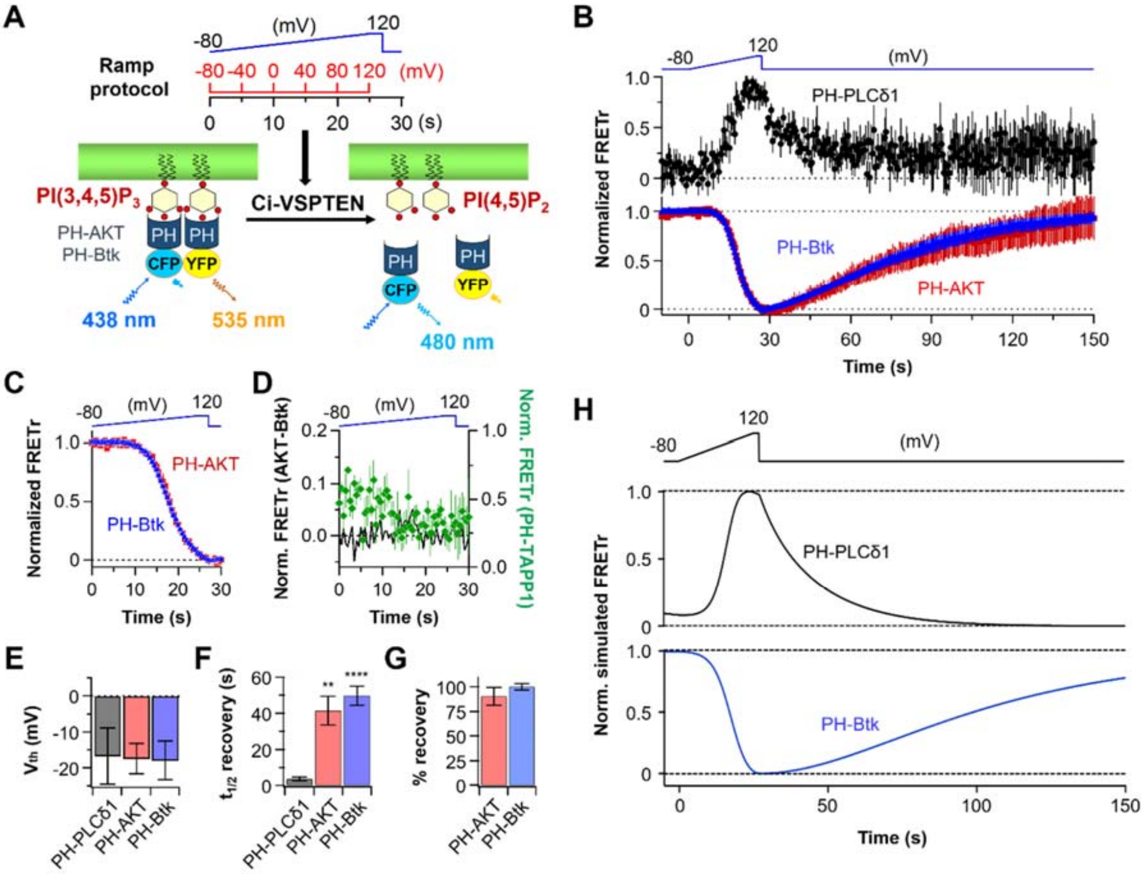

Figure 9. Voltage-dependent effects of Ci-VSPTEN 3-phosphatase on PI dynamics

(*A*) Ramp protocol for Ci-VSPTEN. Cells cotransfected with Ci-VSPTEN and PH-PLCδ1, PH-AKT, PH-Btk or PH-TAPP1, labeled with CFP or YFP, are held at -80 mV and gradually depolarized to 120 mV over 25 s (dV/dt = 8 mV/s) then held for another 2 s. (*B*) Normalized FRETr responses to depolarization of PH-PLCδ1 (black circles, *n* = 5), PH-AKT (red squares, *n* = 4) and PH-Btk (blue triangles, *n* = 7). Traces of PH-PLCδ1 FRETr were normalized using 0 s as minimum and a point between 25 and 32 s as maximum. PH-AKT and PH-Btk traces were normalized between 0 s (maximum) and 27 s (minimum). Data are mean ± SEM. *(C)* Magnified view of PH-AKT and PH-Btk FRETr signals between 0 s and 30 s. (*D*) Difference between PH-AKT and PH-Btk FRETr traces (black line) of *C* compared to normalized FRETr response of PH-TAPP1 (green diamonds, *n* = 3). The difference trace is scaled to match the signal-to-noise ratio for PH-TAPP1. (*E*) Threshold voltages for change of probe signals. One-way ANOVA showed no significant difference in V_{th} among probes. (*F*) Time to half-maximal ($t_{1/2}$) recovery of each PH-probe. $^{**}p < 0.01$ and $^{****}p < 0.0001$, compared to the value for PH-PLCδ1. (*G*) Relative amplitude of recovery compared to whole FRETr decrease. The signal-to-noise ratio was too small to fit the recovery of PH-PLCδ1 FRETr. Data are mean ± SEM. (*H*) Simulated FRETr responses of PH-PLCδ1 (black trace) and PH-Btk (blue trace) upon Ci-VSPTEN activation with the voltage protocol shown.

3-4. Phosphatidylinositol 4-phosphate 5-kinase type Iγ (PIPKIγ) nullifies 5-phosphatase effects of Dr-VSP

We next returned to Dr-VSP and tried to mask its 5-phosphatase reactions by countering them with a coexpressed 5-kinase. This would allow us to study the voltage-dependent 3-phosphatase subreactions in isolation. PIPKIγ is a PI 5-kinase that can phosphorylate PI(4)P to PI(4,5)P_2 and PI(3,4)P_2 to PI(3,4,5)P_3 (Fig. 10*A*). Its activity would elevate the standing levels of PI(4,5)P_2 (Wenk et al., 2001) and potentially PI(3,4,5)P_3 in the plasma membrane and would counteract Dr-VSP 5-phosphatase activity (Halstead et al., 2001; Rudge and Wakelam, 2013). As soon as a lipid species lost its 5-phosphate, the 5-kinase would put it back on again. Cells were co-transfected with Dr-VSP and PIPKIγ in a 1:1 plasmid ratio together with FRET probes. When a ramp-depolarization was given, PH-Btk FRETr, reporting PI(3,4,5)P_3, fell (V_{th} = 53 ± 6 mV), whereas PH-PLCδ1 FRETr, reporting PI(4,5)P_2, began to rise above control (V_{th} = 52 ± 3 mV) in a fully complementary manner (Fig. 10*B*; *n* = 5-9). These responses resembled those just described with Ci-VSPTEN as if now the 5-phosphatase activities of Dr-VSP indeed had been totally masked. The results are well described by simulations using the kinetic model with a boosted 5-kinase activity (Fig. 10*C*). The observed changes of the two FRET probes occurred at the same high, right-shifted voltage compared to the normal cells as if the PI(4,5)P_2 increase was mediated by Dr-VSP 3-phosphatase acting on PI(3,4,5)P_3. Apparently under normal conditions with no exogenous 5-kinase, any PI(4,5)P_2 generated from PI(3,4,5)P_3 by the VSP 3-phosphatase activity at high voltage is immediately dephosphorylated to PI(4)P by the high 5-phospatase activity of Dr-VSP, but here, PI(4,5)P_2 is continually restored. Further, consistent with highly elevated 5-kinase activity, there was no detectable buildup of PI(3,4)P_2 (PH-TAPP1, Fig. 10*D*) or of PI(4)P (P4M-

SidM, Fig. 10*E*), again much as we saw with Ci-VSPTEN. Those results are well described in the kinetic model simply by boosting the basal 5-kinase activity (Fig. 10 *F* and *G*).

For further analyze 3- and 5-phosphatase activity of Dr-VSP toward PI(3,4,5)P_3, dephosphorylation by Dr-VSP and hydrolysis by G_qPCR-PLC pathway upon PI(4,5)P_2 were compared in single cells (Fig. 11*A*). In confocal microscopy, cells transfected with PIPKIγ, M_1 muscarinic acetylcholine receptor (M_1R) and EYFP-tagged PH-PLCδ showed significant increase in cytosolic YFP intensity after the treatment with M_1 receptor agonist oxotremorine methiodide (Oxo-M, 10 μM) with relatively smaller and slower compared to that of control (Fig. 11 *B* and *C*). This indicates that the activation of M_1R can decrease the PI(4,5)P_2 level in the plasma membrane even though the PI(4,5)P_2 resynthesis by PIPKIγ is still strong. The M_1R-induced PI(4,5)P_2 decrease was also found in FRETr signals in cells expressing PIPKIγ (Fig. 11 *D* and *E*). The effect was also weaker and slower compared to that of control. However, in the cells expressing PIPKIγ the activation of Dr-VSP rather enhanced the PI(4,5)P_2 level (Fig. 11 *D*, bottom). The results may be due to that M_1R not only hydrolyze PI(4,5)P_2 to diacylglycerol (DAG) and inositol 1,4,5-trisphosphate (IP_3) but also cleave PI(4)P to DAG and inositol 1,4-bisphosphate (IP_2) (Wilson et al., 1984; Falkenburger et al., 2013) (Fig. 11*A*), thus block PI(4,5)P_2 resynthesis pathway by reducing the substrate PI(4)P level in the plasma membrane. In the case of Dr-VSP activation in the presence of PIPKIγ, the PI(4)P is not degraded but rapidly phosphorylated by PIPKIγ for resynthesis of PI(4,5)P_2, resulting in the increase of PH-PLCδ FRETr signals. These results strongly support our hypothesis that PIPKIγ expression can selectively antagonize the 5-phosphatase activity of Dr-VSP without affecting 3-phosphatase activity and that Dr-VSP directly cleaves 3-phosphate from PI(3,4,5)P_3 through its 3-phosphatase activity.

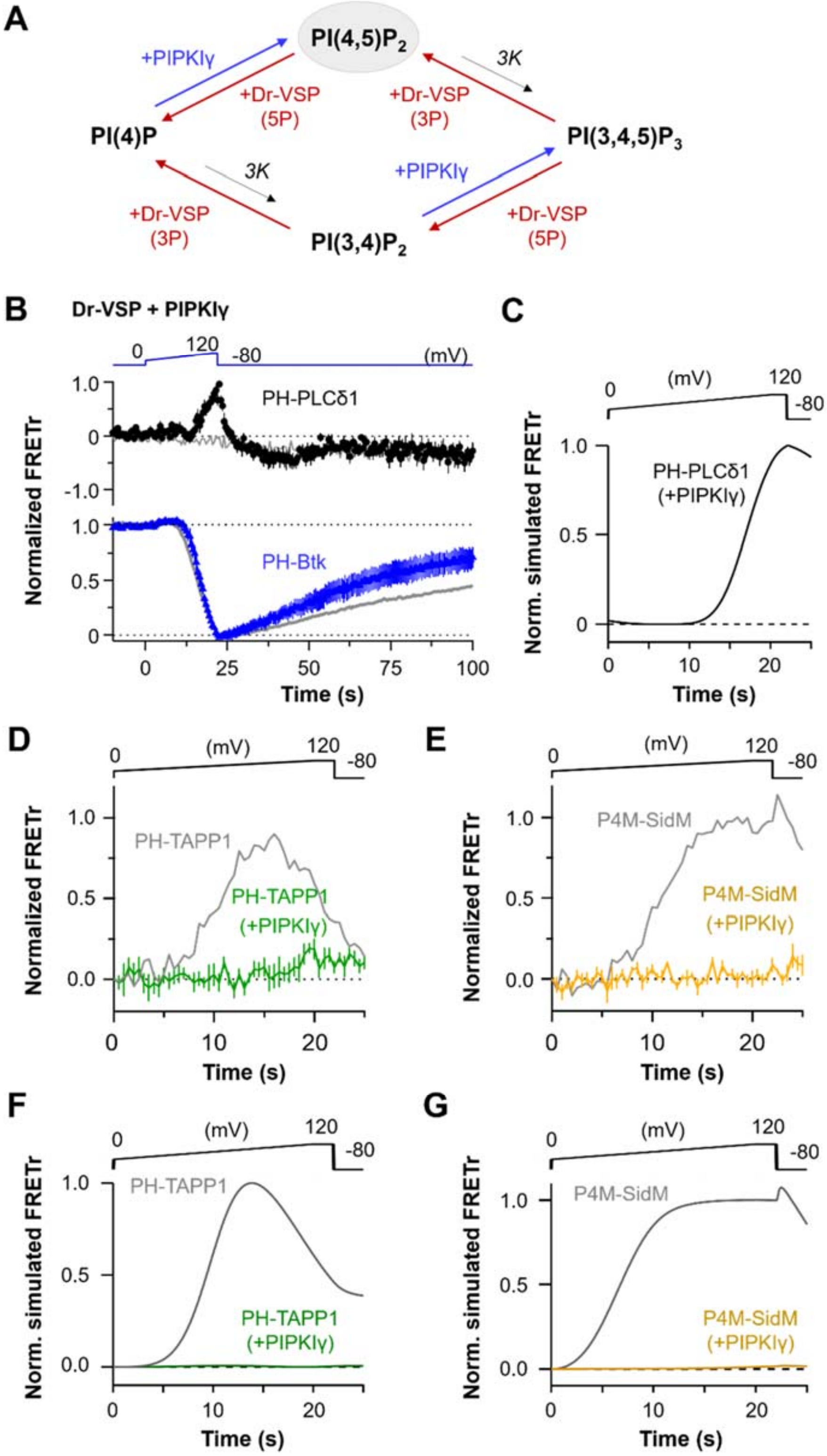
A
PI(4,5)P$_2$
+PIPKIγ
+Dr-VSP (5P)
3K
+Dr-VSP (3P)
PI(4)P
PI(3,4,5)P$_3$
3K
+PIPKIγ
+Dr-VSP (3P)
PI(3,4)P$_2$
+Dr-VSP (5P)
B
Dr-VSP + PIPKIγ
0
120
-80
(mV)
PH-PLCδ1
PH-Btk
Normalized FRETr
1.0
0
-1.0
1.0
0.5
0
0
25
50
75
100
Time (s)
C
0
(mV)
120
-80
PH-PLCδ1 (+PIPKIγ)
Norm. simulated FRETr
1.0
0.5
0
0
10
20
Time (s)
D
0
(mV)
120
-80
PH-TAPP1
PH-TAPP1 (+PIPKIγ)
Normalized FRETr
1.0
0.5
0.0
0
10
20
Time (s)
E
0
(mV)
120
-80
P4M-SidM
P4M-SidM (+PIPKIγ)
Normalized FRETr
1.0
0.5
0.0
0
10
20
Time (s)
F
0
(mV)
120
-80
PH-TAPP1
PH-TAPP1 (+PIPKIγ)
Norm. simulated FRETr
1.0
0.5
0.0
0
10
20
Time (s)
G
0
(mV)
120
-80
P4M-SidM
P4M-SidM (+PIPKIγ)
Norm. simulated FRETr
1.0
0.5
0.0
0
10
20
Time (s)

Figure 10. Expression of PIPKIγ unmasks innate 3-phosphatase activity toward PI(3,4,5)P_3

(*A*) Relationship between Dr-VSP 3- and 5-phosphatase activities (red), endogenous phosphatidylinositol 3-kinase (3K, black), and phosphatidylinositol 4-phosphate 5-kinase Iγ (PIPKIγ, blue). (*B*) Cells held at -80 mV were depolarized from 0 mV to 120 mV for 20 s (dV/dt = 6 mV/s) followed by a hold at 120 mV for 2 s. FRETr of PI(4,5)P_2 and PI(3,4,5)P_3 probes during the ramp depolarization and repolarization in cells expressing Dr-VSP and PIPKIγ in a plasmid ratio of 1:1. PH-PLCδ1 FRETr increased (black, *n* = 6) whereas PH-Btk FRETr decreased (blue, *n* = 5) during ramp depolarization. Grey lines indicate PH-PLCδ1 FRETr response without Dr-VSP (upper) and PH-Btk FRETr response in control cells without PIPKIγ (bottom, from Fig. 5*D*). Points were averaged in groups of 4 after 22 s for better visibility. (*C*) Normalized simulated FRETr of PH-PLCδ1 domains in the presence of PIPKIγ. Simulated Dr-VSP was activated by the voltage protocol shown. (*D* and *E*) FRETr response of PH-TAPP1 (*D*, *n* = 6) and P4M-SidM (*E*, *n* = 5) probes in cells expressing Dr-VSP and PIPKIγ. Grey lines indicate FRETr responses in control cells without PIPKIγ (from Fig. 2 *D* and *B*, respectively). Unresponsive traces were scaled down to match the signal-to-noise ratio of normal traces. Data are mean ± SEM. (*F* and *G*) Normalized simulated FRETr of PH-TAPP1 (*F*) and P4M-SidM (*G*) in the presence of PIPKIγ. Grey lines indicate FRETr responses in control cells without PIPKIγ (as shown in Fig. 2 *G* and *E*, respectively). Simulated Dr-VSP was activated by the voltage protocol shown.

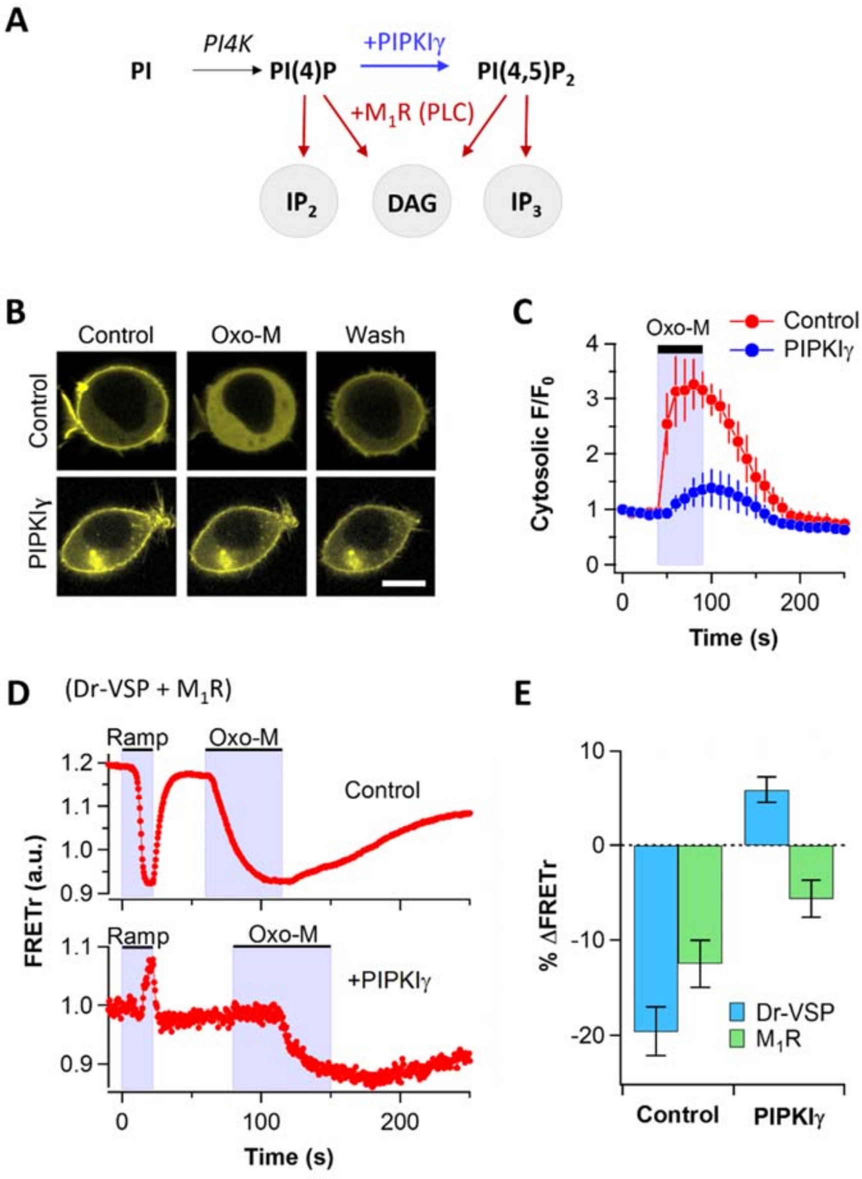

Figure 11. $PI(4,5)P_2$ is differentially regulated by Dr-VSP and M_1R in PIPKIγ expressing cells

(A) 3- and 5-phosphatase-mediated dephosphorylation of $PI(3,4,5)P_3$ and $PI(4,5)P_2$ by Dr-VSP (red) and PLC-mediated hydrolysis of $PI(4,5)P_2$ and PI(4)P by M_1R pathway (green). Through the activity of PIPKIγ, $PI(4,5)P_2$ will be accumulated when Dr-VSP is activated, while $PI(4,5)P_2$ will be decreased since M_1R-activated PLC hydrolyzed both PI(4)P and $PI(4,5)P_2$, resulting in the accumulation of intracellular messengers (oval circle). *(B)* Confocal images of $PI(4,5)P_2$ hydrolysis by M_1R in control *(upper)* or PIPKIγ expressing *(lower)* cells indicated by YFP-tagged

PH-PLCδ. Oxo-M (10 μM) was applied for 50 s. Scale bars indicate 10 μm. *(C)* Normalized cytosolic fluorescence intensity change by M_1R in control (red) and PIPKIγ-expressing (blue) cells. Data are mean ± SEM (n = 3 for control and n = 8 for PIPKIγ-expressing cells). *(D)* PH-PLCδ FRETr changes by Dr-VSP and M_1R activation. Representative single cell experiments in control (upper) and PIPKIγ-co-expressing (lower) condition. Ramp represents standardized protocol used in other experiments using Dr-VSP. *(E)* Percent change of PH-PLCδ FRETr by Dr-VSP (blue) and M_1R (green) was analyzed. Data are mean ± SEM (n = 5).

3-5. Step response of Dr-VSP in PIPKIγ co-expressing cells

So far, we have used depolarizing ramps. However, most VSP-related studies used step depolarizations, and during the process of fertilization, a possible arena for physiological action of VSPs, a steady egg depolarization develops within 3 s and lasts many minutes (Jaffe, 1976). Therefore, we wanted to extend our analysis to step-voltage stimuli. We gave 120-mV step depolarizations of various durations to cells coexpressing PH-PLCδ1 or PH-Btk with Dr-VSP. According to our heuristic diagram (Fig. 6*A*), at this high voltage both the 3-phosphatase and the 5-phosphatase activities should be well above the endogenous cellular activities. The experimental results showed that a 0.5-s step depolarization was enough for nearly complete PI(4,5)P_2 depletion (Fig. 12*A*) whereas the same step decreased PI(3,4,5)P_3 levels by only 15%, and a 20 s depolarization was needed for full depletion (Fig. 12*B*). The kinetic predictions are in full concordance (Fig. 12 *C* and *D*). Step voltages were also applied to cells cotransfected with a 5-kinase. Fig. 12*E* compares FRETr changes of PH-Btk (reporting PI(3,4,5)P_3) with (green) and without (blue) overexpression of PIPKIγ (1:1 ratio of Dr-VSP and PIPKIγ plasmids). The kinase, which as we have seen counteracts the 5-phosphatase activity of Dr-VSP, slows the depletion of PI(3,4,5)P_3 since now only the 3-phosphatase activity remains productive. At the same time there is accumulation of the product PI(4,5)P_2 (black) confirming the conversion of PI(3,4,5)P_3 to PI(4,5)P_2 at this high voltage. Our kinetic description duplicates this result (Fig. 12*F*). Thus we have confirmed our quantitative analysis of an enzyme with four subreactions tested by voltage ramps and by voltage steps yielding a single self-consistent description of all experiments.

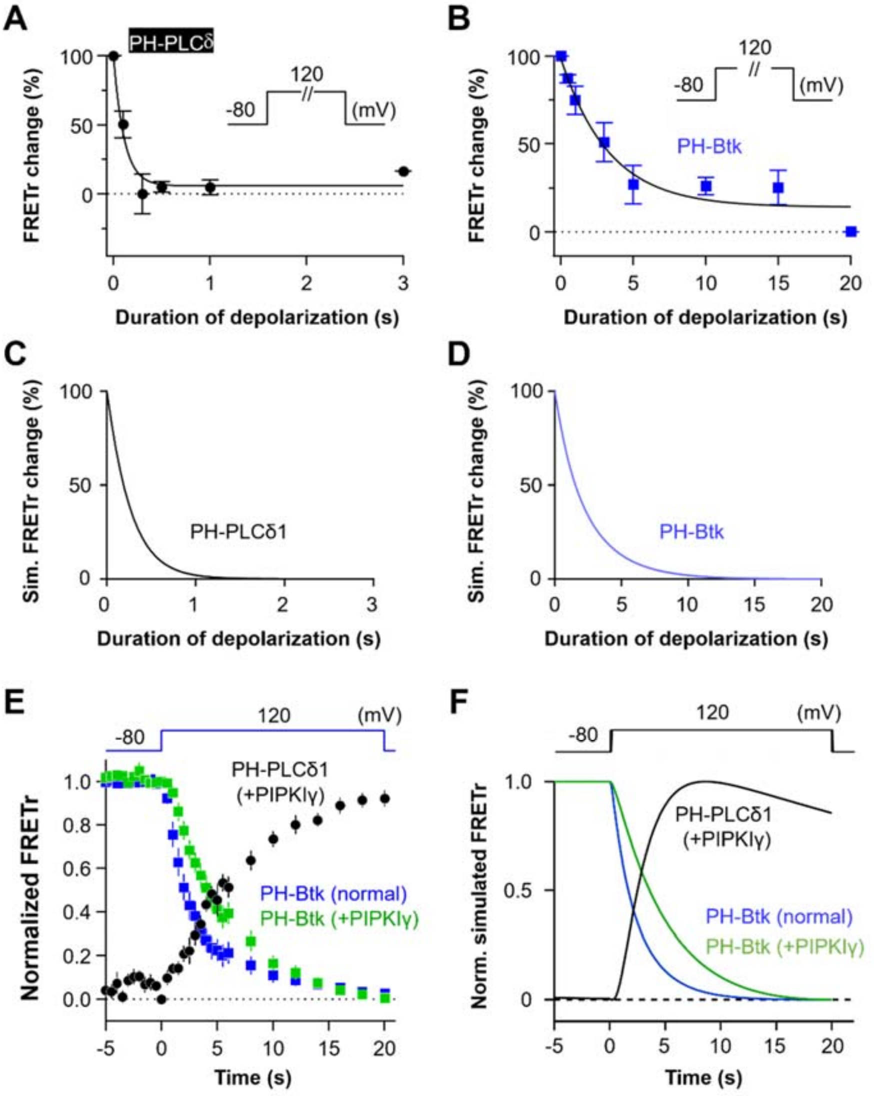

Figure 12. Step response of Dr-VSP in the absence and presence of PIPKIγ

(*A* and *B*) Dr-VSP step responses on the dephosphorylation of PI(4,5)P$_2$ (*A*, n = 5 at each point) and PI(3,4,5)P$_3$ (*B*, n = 2-5 at each point) against the duration of depolarization were measured by using FRETr probes PH-PLCδ1 and PH-Btk, respectively, in control cells. Cells were held at -80 mV and then depolarized to 120 mV for the time duration indicated in x-axis. (*C* and *D*) Simulated FRETr changes in percent of PH-PLCδ1 and PH-Btk domains upon step responses shown in *A* and *B*. (*E*) Dr-VSP step response upon PI(3,4,5)P$_3$ in normal (blue, n = 5) or PIPKIγ-co-expressing (green, n = 5) cells and upon PI(4,5)P$_2$ in PIPKIγ co-transfected cells (black, n = 5). (*F*) Normalized simulated FRETr of PH-PLCδ1 (black) and PH-Btk (green) domains in the presence of PIPKIγ or PH-Btk domains in the absence of PIPKIγ (blue) upon Dr-VSP step responses as shown in *E*.

IV. VOLTAGE-SENSING PHOSPHATASE (VSP) REGULATION OF VOLTAGE-GATED CALCIUM CHANNELS

4-1. Activation of Dr-VSP inhibits $Ca_V2.2$ current

As shown in previous chapter, Dr-VSP rapidly dephosphorylate 3- and 5-phosphate of PIs with same voltage dependence (Fig. 6). However, due to different substrate specificity, 1 sec-long strong depolarization was sufficient to deplete $PI(4,5)P_2$, while more than 20 sec was needed to induce full depletion of $PI(3,4,5)P_3$ in the plasma membrane. Thus, we can acutely manipulate plasma membrane $PI(4,5)P_2$ using this property of VSPs in ion channel studies. Fig. 13 shows simultaneous measurement of $PI(4,5)P_2$ change indicated by PH-PLCδ1 FRET probes and $Ca_V2.2$ (α1B, α2δ-1 and β2a) current measured by voltage clamp method in a living cell. Since repetitive gating pulses are just 10 mV high (see Materials and Methods) and not sufficient for Dr-VSP activation (Fig. 6), naive Ca_V currents can be measured. Inset figure shows shapes of raw $Ca_V2.2$ current. Averaged values of steady state region are taken from series of raw data and superpositioned as shown in black trace. Injection of 120 mV, 1 sec step depolarization (black arrows) induces complete depletion of $PI(4,5)P_2$ (green) and inhibited Ca_V current (inset, a and b indicate Ca_V current before and after Dr-VSP activation).

Although either M_1R and Dr-VSP induce channel inhibition through $PI(4,5)P_2$ depletion, previous studies (Suh et al., 2010, 2012) showed apparently different extent of inhibition: M_1R activation showed 40% while Dr-VSP activation showed 10% in $Ca_V2.2$ inhibition. As mentioned in Introduction, Gβγ activated during G_qPCR may be involved in this phenomenon (Gamper et al., 2004; Kammermeier et al., 2000; Melliti et al., 2001; Suh et al., 2010; Vivas et al., 2013). Serial experiments were conducted to solve this problem.

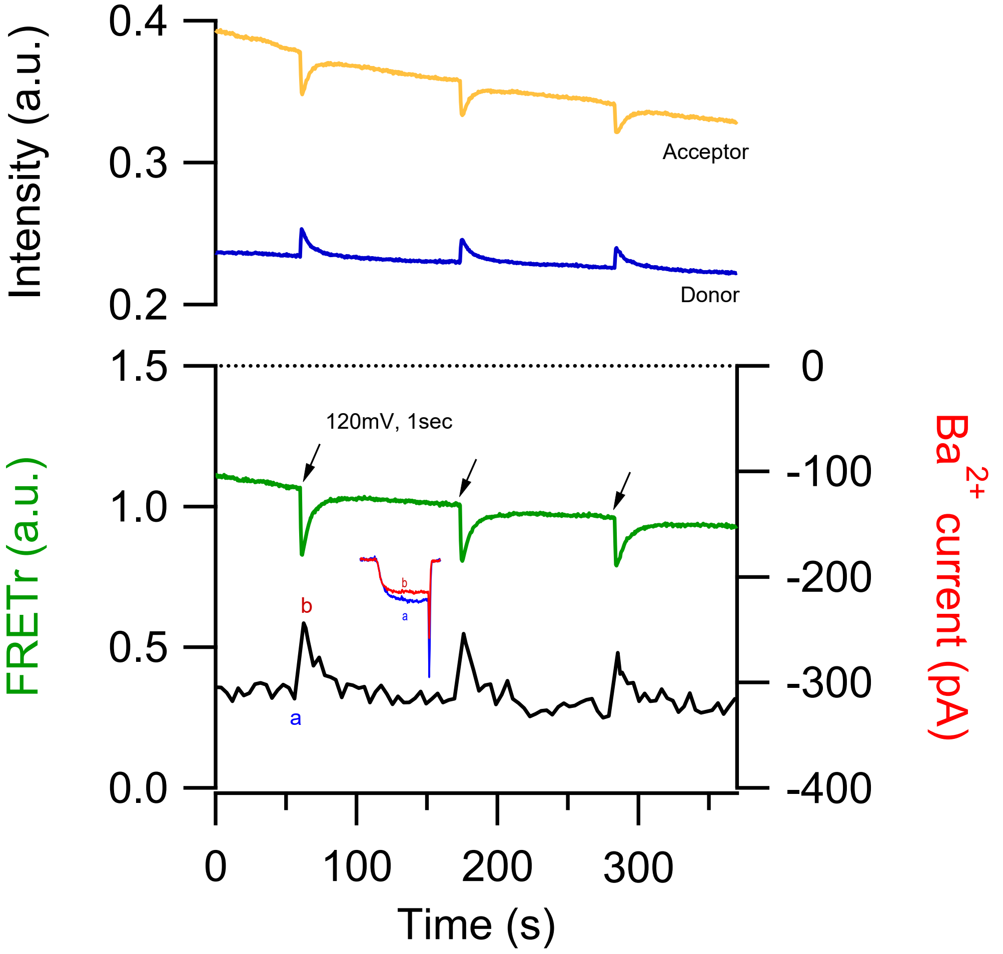

Figure 13. Simultaneous measurement of FRET and $\mathrm{Ca_V}$ current in a live cell

(*Upper*) Plasma membrane PI(4,5)P_2 concentration was measured by FRET. Orange and blue traces are intensity of acceptor (PH-PLCδ1-EYFP) and donor (PH-PLCδ1-ECFP). (*Lower*) FRETr (green) can be calculated from these values (see Methods). Coincident recording of Cav2.2 currents shows series of single raw trace (inset). Then, averaged values of steady state region of each raw trace are taken and super-positioned (black trace). Two traces (blue a and red b) in inset indicate Cav current before and after Dr-VSP activation.

4-2. M_1 muscarinic receptors may suppress N-type $Ca_V2.2$ through two pathways

Since M_1R downstream is quite complex and has many strong effects, we used several chemicals or heterogeneous expression systems to discriminate Gα-PLCδ pathway from Gβγ pathway. To dissect pathways by which Cav2.2 channels are modulated by muscarinic receptor activation, tsA-201 cells were transfected with Cav subunits α1B, α2δ1, and β3 and either M_1 or M_2 receptors. Barium currents were evoked by depolarizing voltage steps. Perfusion of the muscarinic agonist Oxo-M inhibited the current by 68 ± 3% for M_1R and by 72 ± 5% for M_2R (Fig. 14*A*). The differential modulatory pathways of these receptors were first isolated with the use of PTX, which inactivates $G_{i/o}$ by ADP ribosylation. As expected, preincubation in PTX (300 ng/ml, 12 h) strongly reduced Oxo-M–mediated current inhibition in cells expressing the $G_{i/o}$-coupled M_2R (9 ± 2%; Fig. 14*A*, right). Denatured PTX did not reduce the current. Furthermore, coexpressing βARK-ct, which chelates free Gβγ subunits, prevented Cav2.2 current inhibition in a manner similar to PTX (Koch et al., 1994). These experiments confirmed that the primary mechanism by which M_2R inhibits Cav2.2 is through Gβγ subunits released after activation of $G_{i/o}$ (Fig. 14*C*, bottom). In contrast, the G_qPCR M_1R is thought to inhibit Cav2.2 mainly via PLC and depletion of PIP_2 (Fig. 14*C*, top; Gamper et al., 2004; Suh et al., 2010; Vivas et al., 2013). Preincubation with PTX did not change the inhibition of current by M_1 muscarinic receptor stimulation (Fig. 14, *A* [left] and *B*). Thus M_1R function does not involve $G_{i/o}$. The PIP_2-dependent pathway can be studied in isolation using activation of the voltage-sensitive lipid phosphatase Dr-VSP, which can deplete PIP_2 from the plasma membrane quickly during a strong depolarizing pulse. The cotransfected Dr-VSP showed different extents of Cav2.2 current inhibition depending on the type of Ca$_V$ β subunit used, as reported in our previous study (Suh et al., 2012). Depolarization with the expressed Dr-VSP inhibited current more strongly in cells cotransfected with β3 subunits (Fig. 14*A*, left) than in those cotransfected with β2a subunits (Fig. 14*B*). A summary of the known signaling pathways is given in Fig. 14*C*, with a question mark designating this presumed additional pathway from M$_1$Rs.

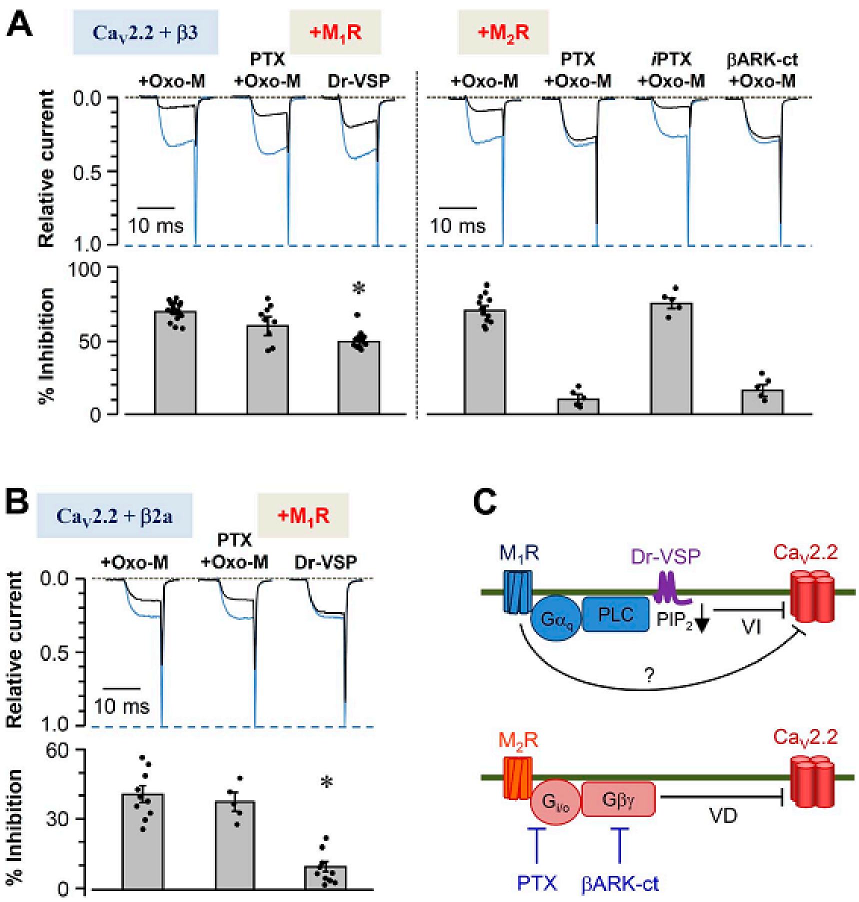

Figure 14. Differential modulation of Ca$_V$2.2 channels by muscarinic receptors depends on the Ca$_V$ β subunit.

(A and B) Cells transfected with α1B (Ca$_V$2.2), α2δ1, and β3 *(A)* or β2a *(B)* subunits were cultured in the presence or absence of PTX or heat-inactivated PTX (*i*PTX) for 12 h. The cells were stimulated with 10 μM Oxo-M to activate muscarinic receptors or depolarized to 120 mV for 1 s to activate the coexpressed Dr-VSP. *(A)* Ca$_V$2.2 currents before and after the stimulation of M$_1$ *(Left)* and M$_2$ *(Right)* muscarinic receptors or the activation of Dr-VSP were measured in cells expressing β3, and the currents were superimposed. Blue traces are the control, and black traces are after stimulation. Current regulation by M$_2$ receptor was also measured in cells cotransfected with βARK-ct. *(Bottom)* Summary of current inhibition by the activation of muscarinic receptors or Dr-VSP. Dots indicate the individual data points for each experiment (n = 5 – 15). Analysis was performed by one-way ANOVA followed by a post hoc test. *(B)* Ca$_V$2.2 currents were measured before and after the stimulation in cells expressing β2a. *(Bottom)* Summary of current inhibition by the activation of M$_1$R or Dr-VSP. *(A* and *B)* Mean ± SEM is shown. *, P < 0.01, compared with current inhibition by Oxo-M. *(C)* Diagram of inhibitory signaling to Ca$_V$2.2 channels by M$_1$ and M$_2$ muscarinic receptors. VD, voltage-dependent inhibition; VI, voltage-independent inhibition.

4-3. Gβγ scavenger attenuates M_1 muscarinic receptor–induced $Ca_V2.2$ current inhibition

A series of studies was performed to determine whether Gβγ subunits might play a role in Cav2.2 modulation by M_1 muscarinic receptor. Several results were consistent with this hypothesis, but as we eventually show, the outcomes depended on which Cav β subunit was used. Fig. 15*A* compares Cav2.2 (β2a) current inhibition in control cells with that in cells expressing the Gβγ scavenger βARK-ct. The scavenger attenuates inhibition strongly, as if Gβγ is needed for the M_1 muscarinic inhibition, when the Cav β2a channel subunit is present. There are additional hallmarks of inhibition by Gβγ subunits. The voltage-dependent activation curves showed a shift to the right by ~5 mV during the M_1 receptor activation (Fig. 15*B*). Furthermore, comparison of single traces of current recorded before and after Oxo-M treatment also revealed differences in the activation kinetics of control cells but not in cells expressing βARK-ct (Fig. 15*C*). The control cells transfected with α1B and β2a subunits displayed slowing of activation during Oxo-M (also see Fig. 15*D*, left), whereas cells cotransfected with βARK-ct showed little change of activation. This observation makes it seem as if the inhibition of Cav2.2 (β2a) by Oxo-M involves Gβγ. In contrast, for cells expressing β3 subunits, the Gβγ hallmark changes in current activation were much less prominent (Fig. 15*D*, right). We next tested the effects of Gβγ on channel inhibition by depleting PIP_2 by means of Dr-VSP (Okamura et al., 2009), which is appropriate for experimental designs involving reversible PIP_2 depletion after an activating depolarization. The standardized voltage protocol to deplete PIP_2 from the membrane by activating Dr-VSP was applied to cells expressing βARK-ct (Fig. 16*A*, top). Compared with control cells, the expression of βARK-ct did not diminish the current inhibition mediated by Dr-VSP (Fig. 16*A*). Thus, we conclude that βARK-ct does not impede the PIP_2-dependent pathway of Cav2.2 (β2a) inhibition, but it does block the Gβγ-dependent pathway. As is summarized in Fig. 16*B*, M_1 muscarinic current inhibition in β2a-expressing cells is significantly decreased by coexpressing βARK-ct, again as if Gβγ plays an important role in Cav2.2 (β2a) modulation. In contrast, the smaller current inhibition upon activation of Dr-VSP was not changed by coexpressing βARK-ct. This suggests that the M_1R-induced inhibition of Cav2.2 (β2a) could involve a direct action of Gβγ on the channel itself rather than an action through the phospholipid-sensitive pathway.

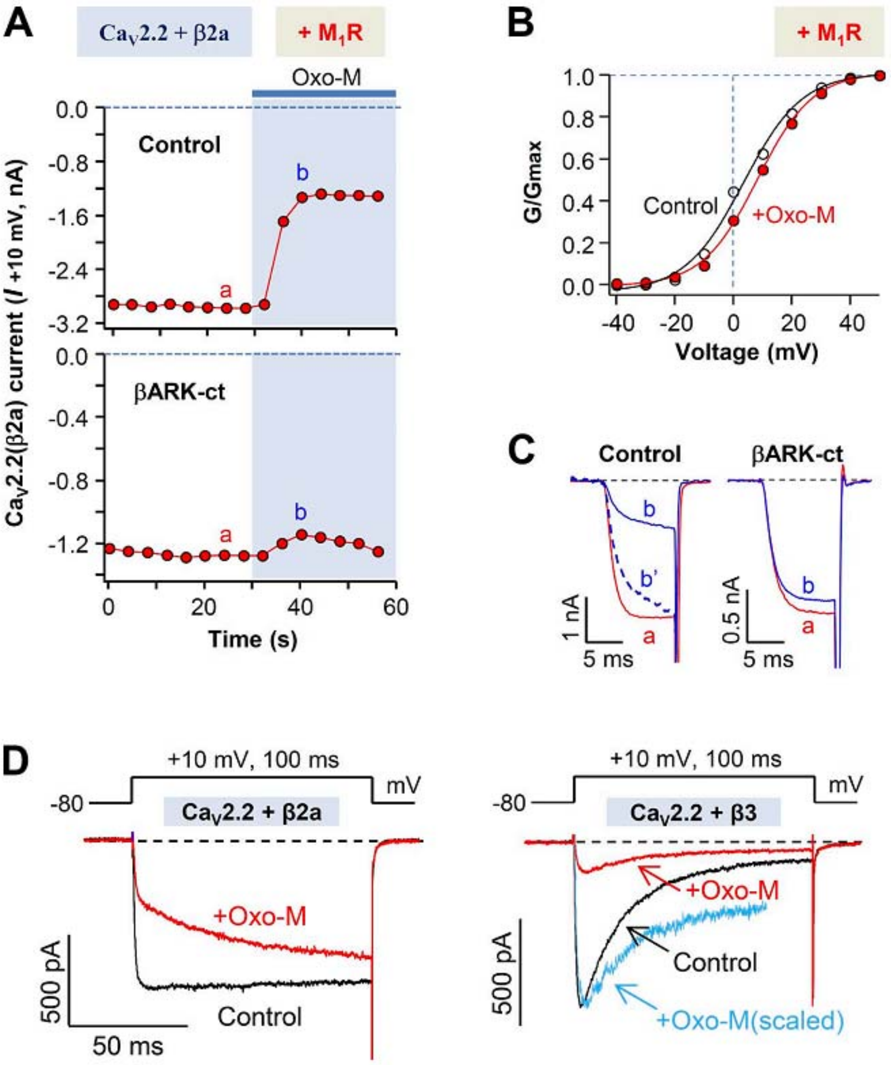

Figure 15. βARK-ct attenuates M_1 muscarinic receptor–induced inhibition of Ca$_V$2.2(β2a) currents

(A) Cells transfected with Cav2.2, α2δ1, and β2a in the presence and absence of βARK-ct were stimulated with Oxo-M, and the Cav2.2(β2a) current suppression was measured. *(B)* Voltage dependence of activation of the Cav2.2(β2a) channel before and during M_1 receptor stimulation with Oxo-M. Dashed line is the I-V relation during Oxo-M application, which is scaled to the peak amplitude of the control. *(C)* Superimposed Cav2.2(β2a)current traces a and b from *A*. In control, the b' dashed trace is a scaled version of b. *(D)* Superimposed Cav2.2(β2a) and Cav2.2(β3) current traces for control and during the stimulation of M_1 receptor. Blue line in right panel shows the scaled trace of Cav2.2(β3) current after Oxo-M application (red). Note that during the Oxo-M application, activation of Cav2.2(β2a) channels (left) but not Cav2.2(β3) channels (right) is dramatically slowed.

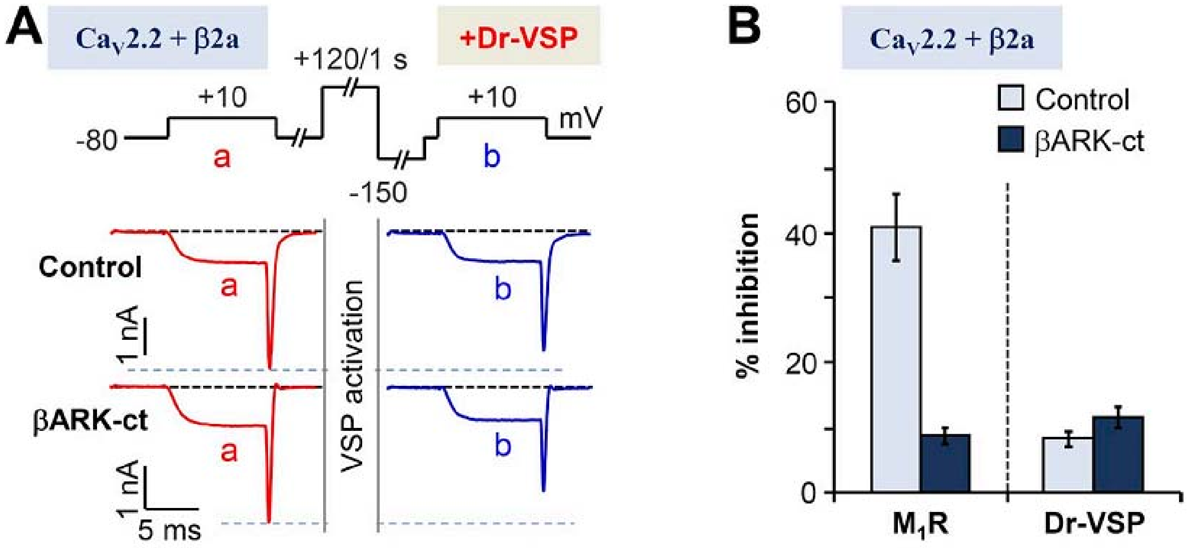

Figure 16. Differential effects of βARK-ct on M_1R- and Dr-VSP–induced inhibition of $Ca_V2.2$(β2a) currents.

(A) Cav2.2(β2a) current inhibition by Dr-VSP activation in control or cells expressing βARK-ct. Cells received a 10-ms test pulse (a) and then a1-s depolarization to 120 mV for activatingthe expressed VSP, followed by the second10-ms test pulse (b). Note that current inhibition by Dr-VSP activation was not significantly different between control and β ARK-ct–expressing cells. *(B)* Summary of the current inhibition after the activation of M_1 receptors (Fig. 15*A*) or Dr-VSP in control and βARK-ct–expressing cells. Data are mean ± SEM (*n* = 5 – 7).

4-4. Single-cell assay reveals separation of fast and slow pathways in M_1R-induced current modulation

We simultaneously measured the current modulation and PIP_2 hydrolysis in single control and βARK-ct–expressing cells. Plasma membrane PIP_2 was measured by FRET between CFP- and YFP-labeled probes that selectively bind to membrane PIP_2 (van der Wal et al., 2001; Jensen et al., 2009; Suh et al., 2010; Falkenburger et al., 2013). A decrease of their FRET interaction indicates depletion of PIP_2 that releases the probe from the membrane. Fig. 17*A* plots representative time courses of Cav2.2 current and the FRETr change in single control and βARK-ct–expressing cells. After perfusion of Oxo-M, the decrease of FRETr (blue trace) was comparable in the two cells, whereas the current inhibition (red trace) showed several differences. On average, current inhibition was 46 ± 4% in control cells ($n = 7$) and only 25 ± 5% in βARK-ct–expressing cells ($n = 6$; Fig. 17*C*). Furthermore, the latency for initiation of current inhibition was less than that for the FRETr decrease (Fig. 17, *A* [right] and *B*). The mean lag time between the initiation of Cav current inhibition and PIP_2 hydrolysis was 4.1 ± 0.6 s in control cells and 0.7 ± 0.3 s in βARK-ct–expressing cells (Fig. 17*D*). The variability of fluorescent protein expression was compensated by normalizing the FRET change between 0 and 1 and averaging the traces (Fig. 17*B*). As expected, the time constant of FRET change (PIP_2 hydrolysis) was not affected by βARK-ct (Fig. 17*E*, $\tau = 8.7 \pm 1.5$ s for control and $\tau = 8.9 \pm 1.1$ s for βARK-ct–expressing cells). Fig. 18 summarizes the main results of Fig. 17. First, we estimated a putative component of current inhibition by G protein βγ subunits by subtracting the averaged current of the two groups (Fig. 18*A*, dashed green line). Then we mimicked the observed time courses with exponential curves Fig. 18*B*. This model showed that, as would be appropriate for direct G protein action, the difference component is fast with an exponential time constant of 1.6 s (Fig. 18*B*, dashed green line). The remaining component, attributed to PIP_2 signaling, has a slow time course like the FRETr change.

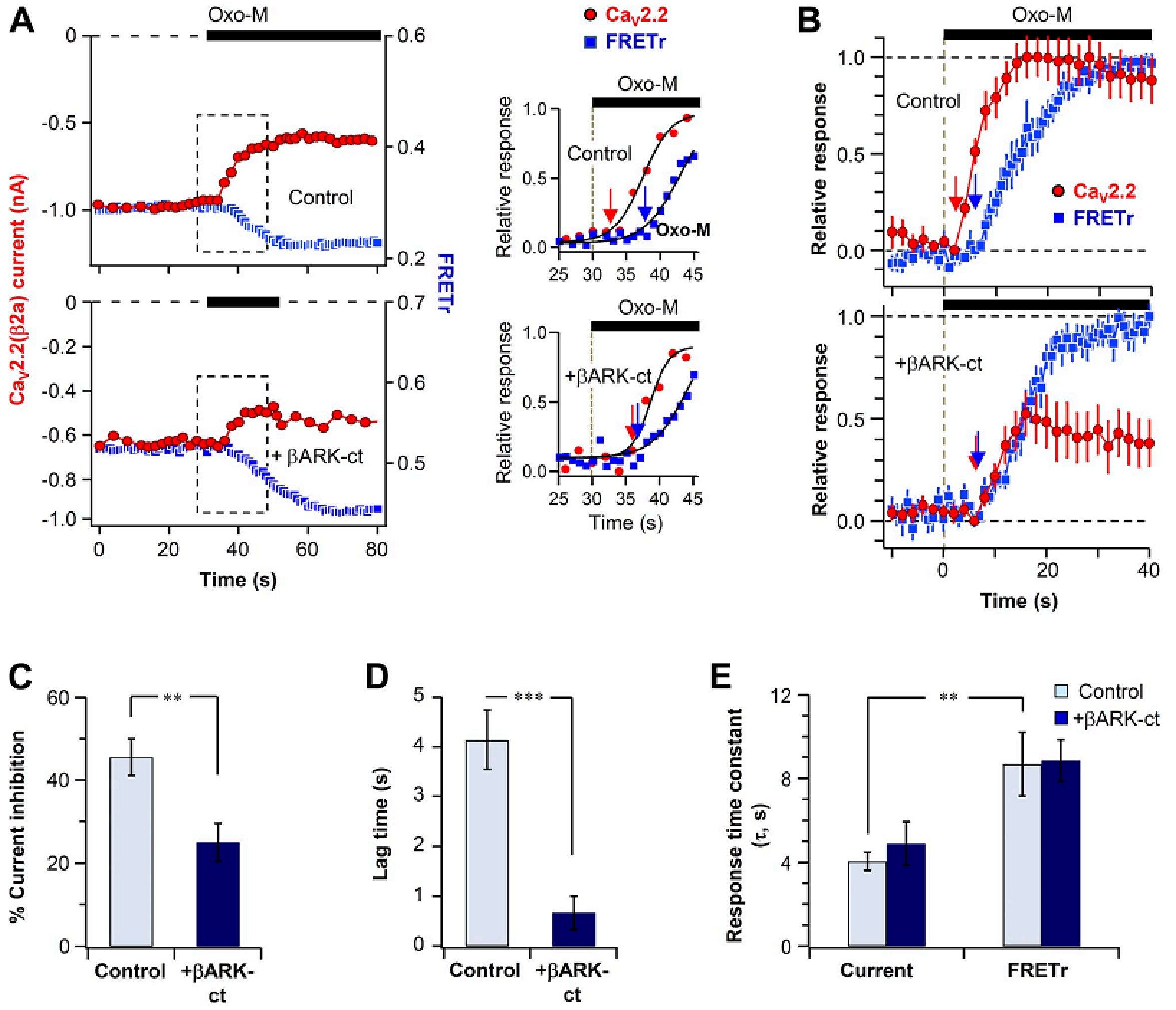

Figure 17. Simultaneous measurement of current inhibition and PIP$_2$ hydrolysis in single cells

All cells coexpressed Cav2.2(β2a) channel subunits, PH domain probes, and M$_1$ receptors. *(A)* Cav2.2(β2a) current and PIP$_2$ (FRETr) were measured simultaneously in single cells in the absence (top) or presence (bottom) of βARK-ct. 10 µM Oxo-M was applied during solid bars. *(right)* Scaled responses from the dashed boxes shown in the left panels. The initiation of the muscarinic response is indicated by arrows. *(B)* Normalized mean time courses of current suppression and PIP$_2$ hydrolysis (FRETr) from single cells without or with βARK-ct expression. *(C)* Summary of maximum current inhibition by Oxo-M in control and cells expressing βARK-ct. **, $P < 0.01$, compared with control. *(D)* Effect of βARK-ct on lag time between the initiation of current inhibition and the FRETr change. ***, $P < 0.001$. *(B–D)* Data are mean ± SEM. *(E)* Analysis of the onset time (τ) for current inhibition and PIP$_2$ hydrolysis (FRETr) in control and βARK-ct–expressing cells. Data are mean ± SEM (n = 6–7). **, $P < 0.01$.

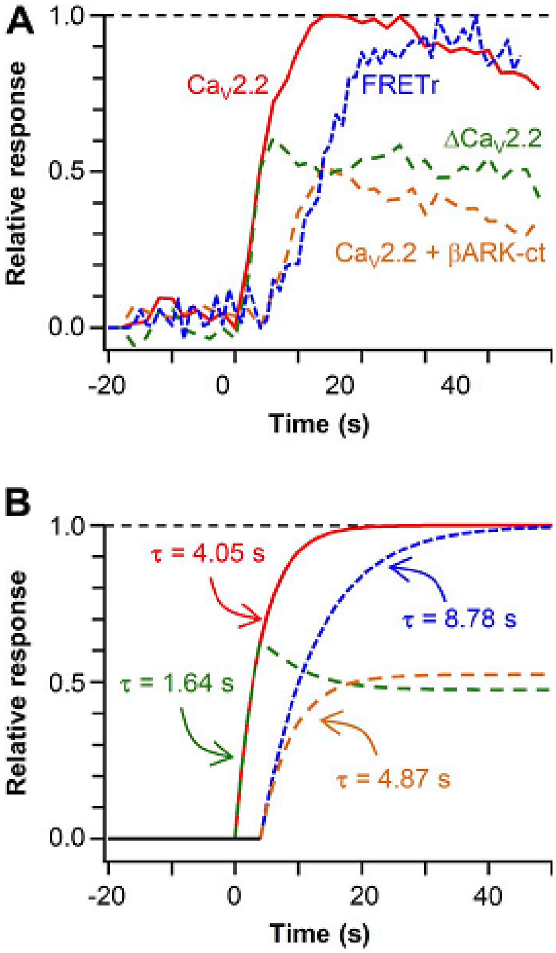

Figure 18. Kinetic assays reveal participation of Gβγ in M_1 receptor–induced Ca_V2.2(β2a) current inhibition

(A) Summary of Fig. 17*B*. The estimated effect of M_1R-mediated release of Gβγ on Ca_V2.2 current (ΔCa_V2.2, green) was calculated by subtracting the mean current of βARK-ct (orange) from that of control (red). Blue trace indicates M_1R-induced PIP_2 hydrolysis observed by FRET change. (B) Interpretation of the Ca_V2.2 current inhibition as a series of exponential curves in control and βARKct–expressing cells. $I_{control} = \exp(-t/4.05)$ $(t > 0$; red), $I_{\beta ARK\text{-}ct}=0.52*\exp(-(t - 4)/4.87)$ $(t > 4$; orange), FRETr $= \exp(-(t - 4)/8.78)$ $(t > 4$; blue). Predicted Gβγ-induced Ca_V current inhibition (dashed green) was calculated by subtracting the mean current of βARK-ct from that of control. The amplitude of $I_{\beta ARK\text{-}ct}$ is determined by obtaining the relative current amplitude between control and βARK-ct–expressing cells.

4-5. Gβγ-dependent, but not PIP$_2$-dependent, modulation is absent in a chimeric N-type channel

The effects of Gβγ on Cav2.2 regulation were investigated through a more direct approach. We used a mutated Cav2.2 α subunit that does not bind Gβγ subunits. In this chimera, called Cav2.2 α1C-1B, the N terminus of the Cav2.2(α1B) subunit was replaced by the N- terminus of the Cav1.2(α1C) subunit, which lacks the N-terminal Gβγ-binding site of α1B (Agler et al., 2005). Fig. 19*A* illustrates the modulation of N-type currents in cells expressing this α1 construct with β2a upon activation of either M$_2$R or M$_1$R receptors. The chimera shows a smaller response to either receptor, as is summarized in Fig. 19*C*. The M$_2$R, a G$_{i/o}$PCR, is anticipated to signal through the direct binding of Gβγ, so the chimera should lack modulation, exactly as seen. Inhibition dropped from 60 to 2%. However, now we find that signaling from the M$_1$R, a G$_q$PCR, is also decreased by the chimera, giving only ~10% inhibition of current instead of the > 40% seen in control cells (Fig. 14*B*), consistent with the concept that M$_1$Rs also can signal by the Gβγ pathway. Continuing on, as expected, Cav2.2(α1C-1B) (β2a) current inhibition by activation of Dr-VSP was not changed compared with control conditions (Fig. 19, *B* and *C*). We now consider whether switching from the Cav β2a subunit to the Cav β3 subunit alters the modulation of the Cav2.2(α1C-1B) chimera. Qualitatively, the modulation had similar features with either β subunit (Fig. 19*D*). As expected, activation of M$_2$R, which acts primarily through the Gβγ pathway, produced very little inhibition (Fig. 19*E*). However, interestingly, with the Cav β3 subunit, the inhibition upon activation of M$_1$ muscarinic receptors or upon PIP$_2$ depletion by VSP was much higher than with β2a-containing chimeric channels. Indeed it was more like the inhibition of wild-type Cav2.2 channels. This fits well with the concept that M$_1$ muscarinic inhibition of Cav2.2 channels with β3 is voltage-independent and does not need Gβγ subunits. M$_1$R-induced, voltage-dependent modulation of Cav2.2 currents is dependent on Cav β subtypes. Our results reveal that M$_1$Rs use two pathways to suppress Cav2.2 currents. We now examine further whether the choice between inhibitory pathways might depend on the Cav channel β subunit. Fig. 20*A* shows that different β subunits localize differently. Expressed by themselves, β2a subunits are membrane localized and β2b and β3 subunits are soluble in the cytosol (Fig. 20*A*). Palmitoylation on two consecutive N-terminal cysteines makes β2a subunits membrane resident (Chien et al., 1996; Hurley et al., 2000), and when the cysteines are substituted by serines, the mutant β2a(C3,4S) moves to the cytosol. Appending a membrane-targeting Lyn sequence to β3 makes the chimeric Lyn-β3 subunit localize at the plasma membrane (Suh et al., 2012). Using the Gβγ-resistant chimera Cav2.2(α1C-α1B), we saw that coexpression with β2a makes channels that are more sensitive to the Gβγ-dependent pathway and less sensitive to the PIP$_2$-dependent pathway, whereas coexpression with β3 makes channels more sensitive to the PIP$_2$-dependent pathway relative to the Gβγ-dependent pathway. The same switch applies to wild-type Cav2.2 channels. Using diverse β constructs, we further analyzed the voltage-dependent and -independent modulation of Cav2.2 currents by M$_1$ muscarinic receptors. By applying a prepulse of 130 mV (in the absence of VSP), the Gβγ-dependent portion of inhibition upon Oxo-M treatment could be estimated (Fig. 20*B*). M$_1$R activation before the prepulse gave rise to the expected inhibition percentage as in Fig. *14A*. However, after the prepulse, the inhibition percentage upon Oxo-M perfusion was much reduced in β2a expressing cells, ~40 to ~10%, and only slightly reduced in β2b-, β3-, and β2a(C3,4S)-expressing cells (Fig. 20*B*). Thus, the voltage-dependent inhibition of Cav2.2 depends on the subcellular location of the β subunits and is stronger in channels with membrane-binding β subunits. The voltage-independent inhibition is stronger in channels with cytosolic β subunits. The PIP$_2$-dependent portion of inhibition was tested in cells with different β subunits (Fig. 21*A*) using the potent PIP_2 5-phosphatase of Dr-VSP. Cells transfected with Cav2.2, various β subunits, and Dr-VSP were depolarized to 120 mV for 1 s. The PIP_2 depletion–dependent inhibition of current was low at 10% with β2a compared with 40–60% with cytosolic β2b, β3, and β2a(C3,4S). When membrane-targeted Lyn-β3 was expressed, the PIP_2 sensitivity decreased to ~20% (Fig. 21*B*). Fig. *21B* contrasts the inhibition percentages of PIP_2-dependent, voltage-independent and Gβγ-mediated, voltage-dependent pathways. Though M_1 receptor stimulation suppresses all combinations of Cav2.2 and β subunits, depending on the types of Cav β subunit, the modulatory mechanism by M_1 receptor is clearly different.

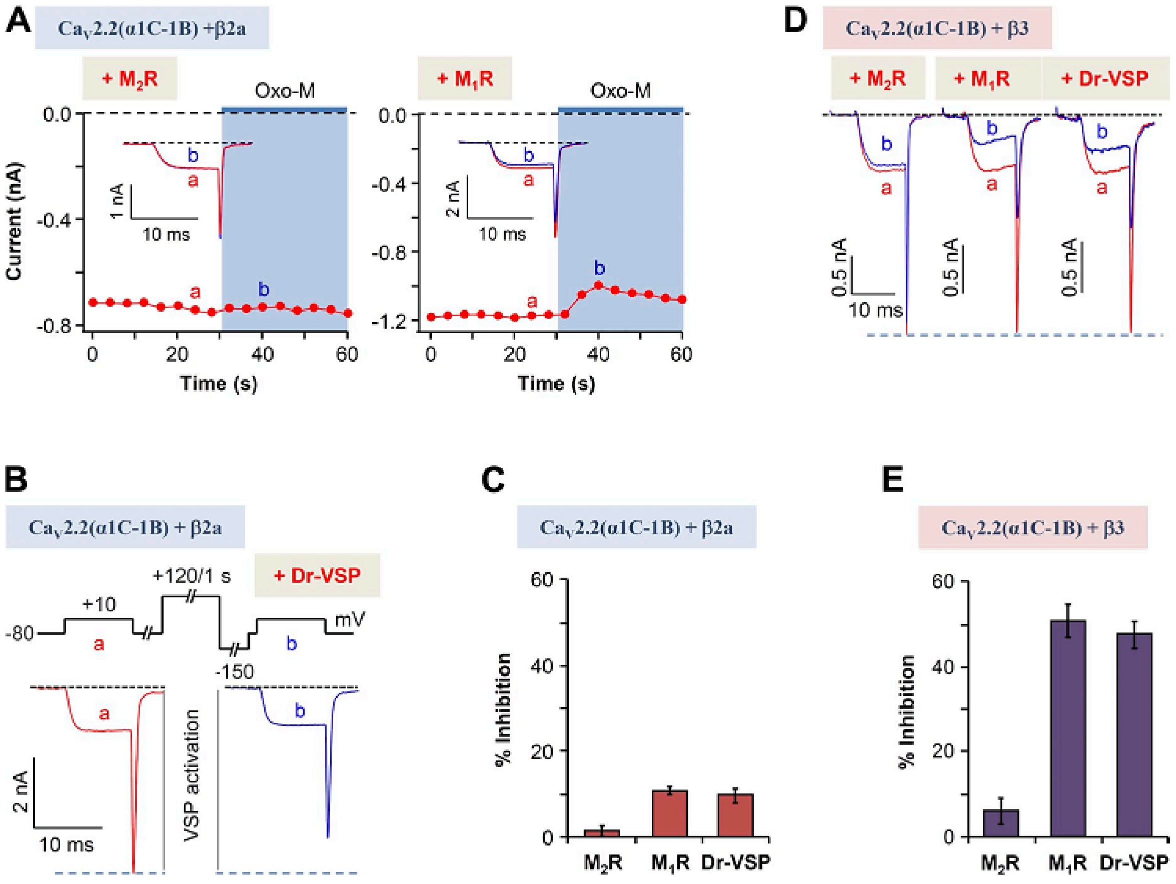

Figure 19. Voltage-dependent muscarinic modulation disappears in Gβγ-insensitive chimeric $Ca_V2.2$(α1C-1B) channels

(A) Effects on Cav2.2(α1C-1B) (β2a) currents of M_1 and M_2 muscarinic receptor stimulation. The current amplitude was measured at 10 mV every 4 s. Insets show currents a and b superimposed. *(B)* Inhibition by Dr-VSP activation of Cav2.2(α1C-1B) (β2a) currents. Cells received a test pulse (a) and then were depolarized to 120 mV for 1 s, followed by a second test pulse (b). Current traces before and after the Dr-VSP activation in cells expressing the α1C-1B and β3 subunits are shown. *(C)* Summary of current suppression by muscarinic stimulation or Dr-VSP activation. *(D)* Current traces before (a) and during (b) the Oxo-M application (left and middle) or Dr-VSP activation (right) in cells expressing the α1C-1B and β3 subunits. Effects on Cav2.2(α1C-1B) (β3) currents of M_1 and M_2 muscarinic receptor stimulation and Dr-VSP activation were traced as above. *(E)* Summary of current suppression by muscarinic stimulation or Dr-VSP activation. *(C and E)* Data are mean ± SEM (*n* = 5 for each bar).

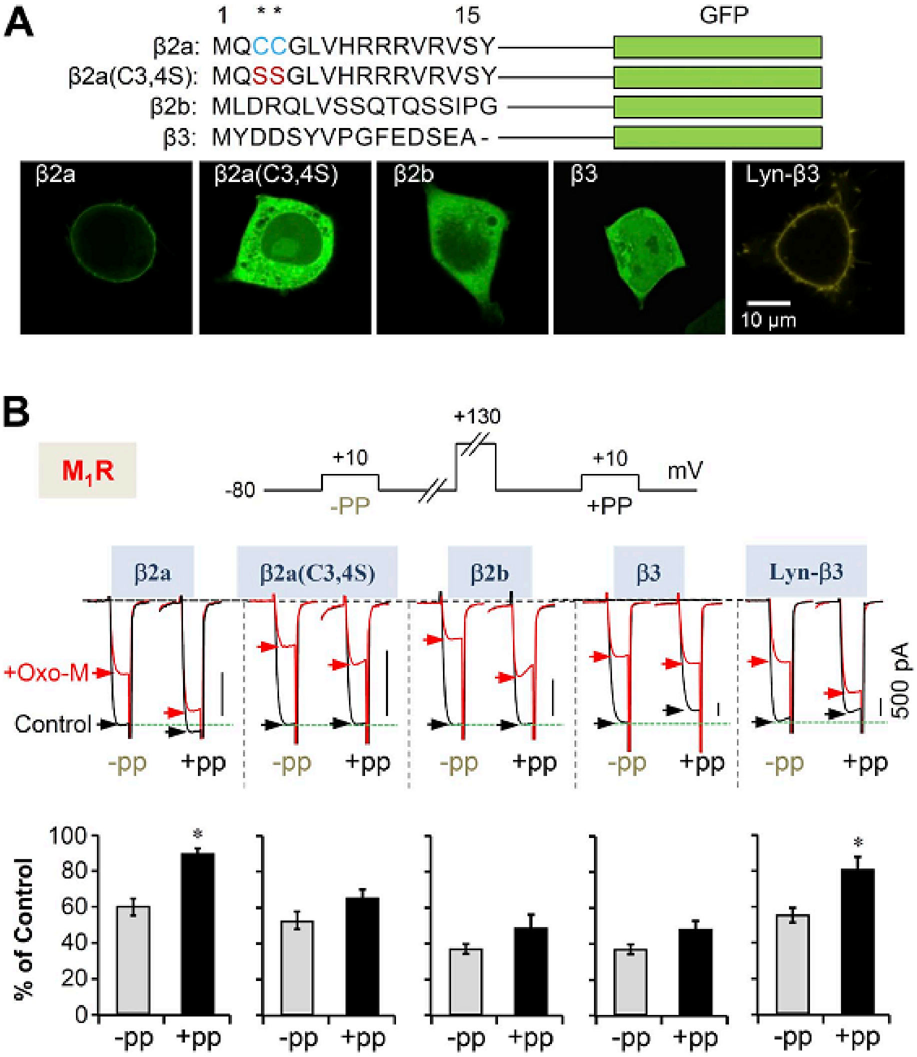

Figure 20. Cytosolic β subunit decreases the Gβγ-mediated, voltage dependent suppression of Ca$_V$2.2 currents

(A) N-terminal amino acid sequences of β2a, β2a(C3,4S), β2b, and β3 subunit with GFP as a fluorescent label. In the palmitoylation-resistant mutant β2a(C3,4S), both palmitoylated cysteine residues (*, blue) are replaced with serine (red). Lyn-β3 is labeled with YFP. *(bottom)* Confocal images of the β subunits expressed in tsA-201 cells. *(B)* Inhibition of Ca$_V$2.2 current by M$_1$ receptors is significantly relieved by a prepulse (+PP) in cells with membrane localized β subunits but not in cells with cytosolic β subunits. Cells were given a test pulse (+PP) and then depolarized to 130 mV for 20 ms, followed by the second test pulse after 20 ms (+PP). The experiments were performed before (control) and during the Oxo-M application (+Oxo-M). *(bottom)* Summary of the prepulse experiments in control and Oxo-M–perfused cells with different Cav β subunits. The current amplitude after Oxo-M application is given as percentage of the initial control. Data are mean ± SEM (*n* = 5–6). *, $P < 0.01$.

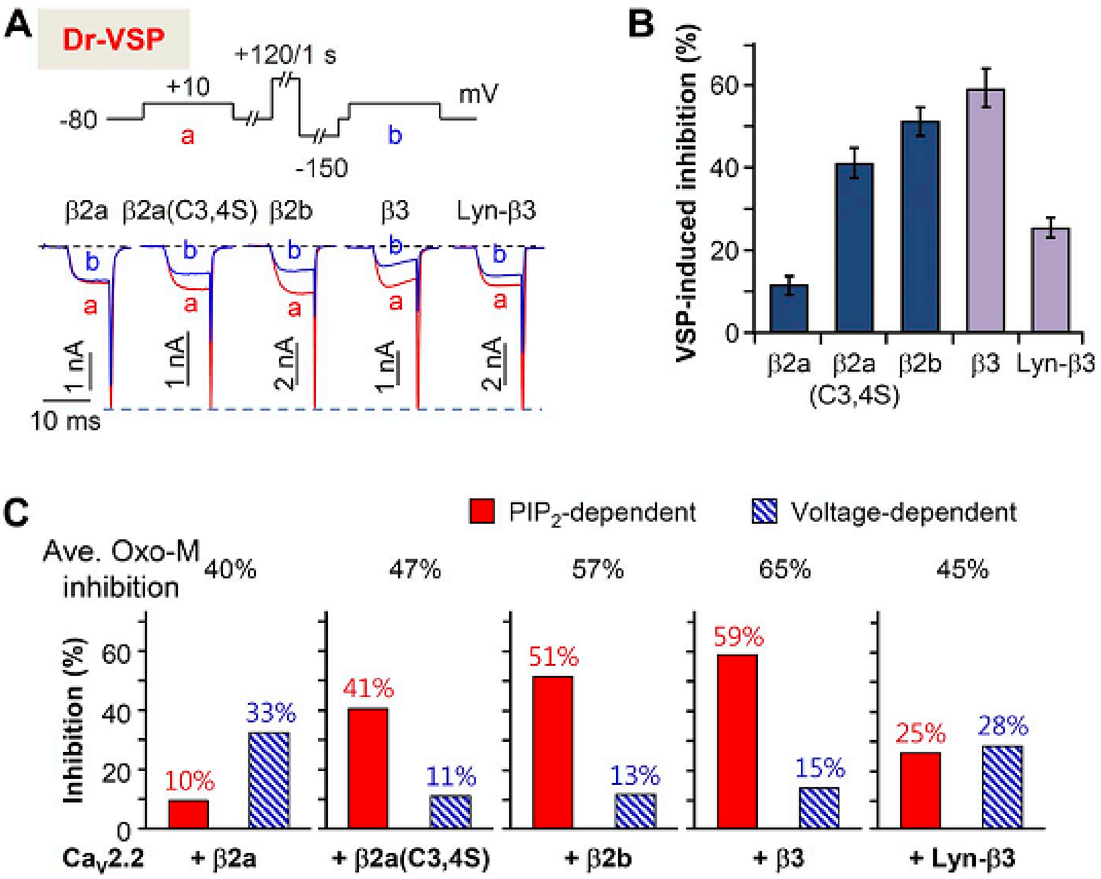

Figure 21. Cytosolic β subunit increases the PIP₂ depletion–mediated suppression of Cav2.2 currents

(A) Current inhibition by Dr-VSP activation in cells expressing different β subunits. Cells received a test pulse (a) and then were depolarized to 120 mV for 1 s, followed by the second test pulse (b). The a and b currents are superimposed. *(B)* Summary of the Dr-VSP–induced inhibition of Cav2.2 current. Data are mean ± SEM (*n* = 6–8). *(C)* Differential effects (mean percent inhibition) of Dr-VSP-induced, voltage-independent *(A)* and Gβγ-mediated, voltage-dependent (Fig. *20B*) pathways on the Oxo-M suppression of Cav2.2 channels with different Cav β subunits. Mean maximal inhibition by M_1 receptor activation is presented in the top.

V. DISCUSSION

We have measured voltage-dependent enzyme activity of Dr-VSP against PI(3,4,5)P_3, PI(4,5)P_2, and PI(3,4)P_2 in situ by expressed FRET indicators. Analysis with kinetic modeling allowed clear resolution and a full quantitative specification of each of four subreactions. Together they generate PI(4)P as a final product. Among them, the 5-phosphatase activities of Ci-VSP against PI(4,5)P_2 and PI(3,4,5)P_3 were previously well recognized (Halaszovich et al., 2009; Iwasaki et al., 2008; Kurokawa et al., 2012; Murata and Okamura, 2007), but the 3-phosphatase activities were less fully characterized. Previous work with Ci-VSP revealed PI(3,4)P_2 3-phosphatase activity at high voltages in addition to the PI(4,5)P_2 and PI(3,4,5)P_3 5-phosphatase activity at lower voltages (Kurokawa et al., 2012). Older, in-vitro studies with catalytic domains of mammalian VSP homologues also revealed a PI(3,4,5)P_3 3-phosphatase activity (Walker et al., 2001; Wu et al., 2001), and very recent live-cell experiments with Ci-VSP showed short-lived transient signals attributed to that activity as well (Castle et al., 2015; Grimm and Isacoff, 2016). Under appropriate conditions we could now show that Dr-VSP has the same 3-phosphatase activity against PI(3,4,5)P_3 as the chimeric Ci-VSPTEN enzyme, even with the same catalytic rate constant. Thus, when the 5-phosphatase activity of Dr-VSP was counteracted by overexpression of PIPKIγ, we could see generation of PI(4,5)P_2 from PI(3,4,5)P_3 during depolarization (Fig. 8*B*). In this way, we support catalytic pathways from PI(3,4,5)P_3 to PI(4)P through both PI(3,4)P_2 and PI(4,5)P_3 for Dr-VSP (Fig. 5*A*). Sequence similarity suggests that this feature is likely conserved in other VSP homologues.

Our quantitative approach now allows us to summarize the enzymology of Dr-VSP as follows: It is unnecessary to suppose that the several 5- and 3-phosphatase subreactions have different intrinsic voltage dependence even though the 3-phosphatase against PI(3,4)P_2 is slower and needs a larger depolarization to become evident in experiments with intact cells. It suffices to regard the enzyme as existing in only two principal catalytic states at the plasma membrane, one active and the other not active. Like a voltage-gated ion channel, the enzyme activity is switched between these states in a stochastic manner by transitions of the charged voltage sensor giving graded activity. The probability of being in the active state as a function of voltage follows the same Boltzmann distribution as the sensing charge movement that can be recorded electrophysiologically. The one active state can catalyze at least four subreactions. As described in Table 4 and Fig. 6*A*, the four catalytic rate constants of the active form of the Dr-VSP enzyme are: 11.3, 2.0, 0.25, and 0.2 s^{-1} for the 5-phosphatase activity against PI(4,5)P_2 and PI(3,4,5)P_3 and for the 3-phosphatase activity against PI(3,4)P_2 and PI(3,4,5)P_3, respectively. These are in the context of a living cell at room temperature and at the expression level we achieved. Possible additional VSP activity against PI(5)P and PI(3)P has not been assessed.

Our description of VSP as having only one active state contrasts with suggestions of multiple active states in the literature (Castle et al., 2015; Kurokawa et al., 2012) presented most explicitly in a new study published while our manuscript was under review (Grimm and Isacoff, 2016). There, Grimm and Isacoff (2016) analyzed the activity of Ci-VSP in oocytes of *Xenopus laevis* with PH domain probes and proposed an initial substrate preference for PI-trisphosphate (PI(3,4,5)P_3) at less depolarized membrane potentials followed by a preference for PI-bisphosphates (PI(4,5)P_2 and PI(3,4)P_2) at more depolarized potentials, with sequential transitions from "off" to "active state 1" and on to "active state 2." A key experiment used the PH-PLCδ1 probe to monitor PI(4,5)P_2 during the step depolarizations. The striking finding was an initial transient burst increase of the probe signal reflecting net $PI(4,5)P_2$ synthesis by rapid dephosphorylation of $PI(3,4,5)P_3$ followed by a slower profound decrease reflecting the dephosphorylation of $PI(4,5)P_2$ to PI(4)P. This effect was visible in the records of Liu et al. (2012) and clearly noted with some discussion in Castle et al. (2015), but by developing PH-domain probes that were prelocalized to the plasma membrane, Grimm and Isacoff (2016) could improve the time resolution, which was previously much slowed by diffusion in large oocytes. We found that all of the results in Fig. 3 of Grimm and Isacoff could be reproduced qualitatively with our model (see our Fig. 22 and its legend) and did not require the hypothesis of two active states. The model required three changes (see Table 5): (i) The sizes of some lipid pools had to be adjusted for *Xenopus laevis* oocytes based on published analyses (Liu et al., 1995). Notably, there was a modestly higher density of $PI(3,4,5)P_3$ in the oocytes (Table 5) since they had been treated with insulin to boost the endogenous lipid 3-kinase. (ii) The rate constants for some individual subreactions catalyzed by Ci-VSP were adjusted compared to Dr-VSP. In particular the 3-phosphatase activity against $PI(3,4,5)P_3$ was made more than 100-fold faster than for Dr-VSP. And (iii) the voltage dependence of the Boltzmann term was shifted and lowered in slope to match Ci-VSP (Falkenburger et al., 2010) as we had done for Ci-VSPTEN. With these changes, there is an initial rapid net production of $PI(4,5)P_2$ from $PI(3,4,5)P_3$ as the faster 3-kinase acts on the enlarged $PI(3,4,5)P_3$ pool. The production of $PI(4,5)P_2$ is transient, not because the enzyme changes to a new active state with different substrate preference, but because the $PI(3,4,5)P_3$ pool is rapidly consumed and all the time the 5-phosphatase activity is depleting $PI(4,5)P_2$.

Grimm and Isacoff (2016) also mutated the voltage sensor in the VSD of Ci-VSP, attempting to favor one or the other of their postulated voltage-sensitive active states (c.f. their Fig. 5). Fig.

S4 indicates that those results also are consistent with a one-active-state model. To mimic the results, it sufficed to shift the voltage dependence of all reactions equally or to slow all rate constants 20-fold without altering the ratios of the rates of the catalyzed subreactions (see legend). Our simulations show that a fixed substrate preference and a single Boltzmann voltage dependence suffice to describe a broad range of findings with Dr-VSP and Ci-VSP.

Taking a more critical view, although the qualitative experimental transitions of the FRET probes are nicely captured by our simplified model, the curves we present do not reproduce the experimental data precisely. Does that mean we should go to a two-active state model? First, we should remember that our simple model does reproduce all the qualitative phenomena that had inspired the proposed more complex models and that the alternative more complex concepts have not been given mathematical form by their proposers to allow an actual evaluation. Second, our model has not been optimized by some global fitting criterion, rather it was adjusted manually. Finally, our modeling omits several significant cell-biological complexities that would compromise a desire for more perfect fits. Our previous work and that of others shows that the four phosphoinositide species we have discussed actually have several dynamic pools on different membranes and organelles that exchange with each other by trafficking or lipid exchange in tens of seconds (Dickson et al., 2014, 2016). Further, we and others have shown that when phosphoinositide pools are depleted by activating phospholipase C, the cellular lipid kinases are accelerated considerably (Falkenburger et al., 2010; Xu et al., 2003). Is it possible that analogous rate changes of endogenous metabolic enzymes occur in response to the dynamic PI changes that follow activation of VSP? Our simple model did not include interchanging lipid compartments or changes of endogenous enzyme properties. Our kinetic description presumably lumps together dynamic pools to some degree. Some of our FRET probes might be reporting in part from intracellular membranes; however, the voltage activation of VSP would be confined to the plasma membrane and all the depolarization-stimulated 3- and 5-phosphatase subreactions we have described would be taking place there.

Our attempt to explain the results of Grimm and Isacoff led to the unexpected conclusion that Ci-VSP has a disproportionately faster 3-kinase activity against PI(3,4,5)P_3 in oocytes than either Dr-VSP or Ci-VSPTEN itself in tsA201 cells. Perhaps this is important in the physiology of *Ciona*. However, in selecting model parameters, the choice of the 3-kinase rate constant depends reciprocally on the postulated PI(3,4,5)P_3 pool size. If this pool were actually 5-fold larger in the insulin-treated oocytes than assumed here, the chosen 3-kinase rate constant for Ci-VSP would be 5-fold lower. Thus this parameter is not well determined by the available data, although in any version it is likely to be faster than for Dr-VSP. In the concept suggested by Grimm and Isacoff, the enzyme makes a transition probably quickly from a PI(3,4,5)P_3-preferring state to a PI-bisphosphate-preferring state. Since at that time the PI(3,4,5)P_3 is already depleted, we are not able to test whether the 3-phosphatase activity against PI(3,4,5)P_3 does change in time from the records available. It can be noted that fluorescence measurements with the VSD of VSP and functional measurements of other voltage-gated ion channels have suggested that voltage sensors do make more than one step on the way to the fully activated state (Bezanilla and Villalba-Galea, 2013).

Cells maintain a specific mix of phosphoinositide pools at the plasma membrane at rest. The lipids in turn regulate activities of many membrane proteins determining the physiological state of the cell. This status quo can be perturbed, by raising the expression or activity of enzymes like PIPKI or VSPs. VSPs would impart a membrane-potential dependence to the phosphoinositide mix. Small depolarizations might favor depletion of $PI(4,5)P_2$ and accumulation of $PI(3,4)P_2$, and higher depolarization can deplete $PI(3,4)P_2$ and favor accumulation of PI(4)P. Ci-VSP might favor depletion of $PI(3,4,5)P_3$. However, if a 5-kinase activity is also elevated, as we saw, the changes with VSP are again different and it is even possible to have an accumulation of $PI(4,5)P_2$ due to 3-phosphatase activity against $PI(3,4,5)P_3$. Previous studies report a range of $PI(3,4)P_2$ dynamics during Ci-VSP activation. Variously $PI(3,4)P_2$ may be increased (Halaszovich et al., 2009), or decreased (Kurokawa et al., 2012), or even decreased after an initial increase (Liu et al., 2012) by similar depolarizations. Based on our results, such a diversity of outcomes is possible depending on the other activities in the cells.

VSPs may be involved during the process of fertilization (Okamura, 2007; Walker et al., 2001; Wu et al., 2001; Ratzan et al., 2011). Considering that PIPKI isoforms may be highly activated during egg fertilization (Bates et al., 2014; Jarquin-Pardo et al., 2007; Sharma and Kinsey, 2006; Stith, 2015) we could envision why previous studies found $PI(4,5)P_2$ increases following the rapid membrane depolarization during fertilization (Ciapa et al., 1992; Halet et al., 2002; Kamel et al., 1985; Turner et al., 1984). Taken together, VSPs possibly regulate the spatial and temporal distribution of phosphoinositides in a cell membrane in response to voltage (Chang and Minc, 2014) or pH changes in the cell (Mavrantoni et al., 2015; Rosasco et al., 2015). If the distribution is localized and dynamic VSPs may determine binding of target proteins at specific regions and time resulting in for example cell migration or polarization (Comer and Parent, 2007; Fabian et al., 2010; Leslie et al., 2008).

PTEN is a well-characterized phosphoinositide 3-phosphatase acting on $PI(3,4,5)P_3$ and $PI(3,4)P_2$ (Campbell et al., 2003; McCrea and Camilli, 2009). Hence, as a negative regulator of the PI3K/AKT/mTOR pathway, PTEN enhances cell survival and suppresses tumorigenesis (Cantley and Neel, 1999; Luo et al., 2003). Two other mammalian enzymes, "transmembrane phosphatase with tensin homology" (TPTE) (Wu et al., 2001) and "TPTE and PTEN homologous inositol lipid phosphatase" (TPIP) (Walker et al., 2001), are PTEN homologs. The cytosolic enzyme domains of TPTE and TPIP have 35% and 37% sequence identity with PTEN and almost the same catalytic active site, suggesting that all may have similar substrate specificity. Unlike PTEN, TPTE and TPIP have N-terminal trans-membrane domains that resemble the voltage sensor of VSP and of voltage-gated ion channels (Kumánovics et al., 2002). Recently, a chimera of the voltage sensor of TPTE with the pore domain of bacterial voltage-gated potassium (K_V) channel was shown to reconstitute functional voltage-gated channel activity (Rosasco et al., 2015).

Despite the structural similarity between VSP and PTEN, the substrate selectivity and subreactions of VSP are broader than those of PTEN. The demonstration of a 3-phosphatase activity for VSP against $PI(3,4,5)P_3$ fills in an important connection between VSP and PTEN. We could speculate that VSP might participate in PTEN-related cellular signaling including balancing tumor suppression versus tumorigenesis (Cantley and Neel, 1999; Kuemmel et al., 2015; Luo et al., 2003), stem cell differentiation (Lachyankar et al., 2000; Sundelacruz et al., 2008; Zhang et al., 2006) and axon-regeneration (Ferreira et al., 2012; Liu et al., 2010; Park et al., 2008). Such processes might even be triggered and regulated by electro-chemical signals, giving VSPs important new roles in pathobiology and normal development.

We also have shown that with an appropriate choice of Ca_V β subunit, a G_qPCR can signal by Gβγ subunits to suppress N-type Ca^{2+} currents. This contrasts with the simpler view that PTX-insensitive, G_qPCRs modulate Ca^{2+} channels exclusively by actions downstream of PLC and that only PTX-sensitive $G_{i/o}$PCRs can modulate through Gβγ, and it extends earlier clear suggestions of Gβγ roles in M_1R signaling (Kammermeier et al., 2000; Melliti et al., 2001; Gamper et al., 2004; Suh et al., 2010; Vivas et al., 2013). Our adjusted working hypothesis is summarized as a flow chart in Fig. 24*A*. M_1Rs inhibit Cav2.2 not only through $G\alpha_q$ and PLC but also through the Gβγ pathway, whereas M_2Rs suppress principally through the Gβγ pathway. Furthermore, for M_1Rs, the choice between PLC and Gβγ pathways is biased by the subtype of Cav β subunit expressed. Channels with the membrane–lipid-interacting β subunit β2a were more sensitive to the Gβγ-dependent pathway and less to the PIP_2 depletion, whereas channels with cytosolic β subunits, including β2b, β3, and β2a(C3,4S), were more sensitive to PIP_2 depletion (Fig. 24*B*). Our data also showed that even though the maximum inhibition of N-type Cav current by M_1 receptors ranged from 40 to 65% for different cytosolic Cav β subunits, the relative proportion of the total inhibition mediated by PIP_2 and Gβγ was almost the same for each of the cytosolic β subtypes. For M_1 muscarinic inhibition with cytosolic β subunits, the fractional distribution between the Gβγ-dependent pathway and the PIP_2-dependent pathway was ~20 and ~80% of the total (Fig. 24*B*). In contrast, in cells expressing the membrane-localized β2a subunits, the fractional distribution was reversed, ~80 and ~20%, and in cells expressing the membrane-targeted form of β3, Lyn-β3, the distribution was equal, ~50 and 50%. This intermediate effect of Lyn-β3 is consistent with its weaker effects on current inactivation and on PIP_2 depletion–mediated suppression compared with control β3 (Suh et al., 2012). Several of our findings support Gβγ as one of the inhibitory signals in M_1 muscarinic suppression of Cav2.2 channels. (a) M_1 receptor activation shifts the voltage dependence of activation of channels rightward by ~5 mV and slows the activation kinetics, comparable with Gβγ-dependent regulation of N-type channels in sympathetic neurons (Elmslie et al., 1990; Beech et al., 1992; Boland and Bean, 1993). (b) Coexpression of the Gβγ chelator reduced inhibition of the Ca^{2+} currents by M_1R stimulation (Kammermeier et al., 2000; Melliti et al., 2001). (c) M_1 receptor activation induces a fast component of channel inhibition in addition to a slow one (Melliti et al., 2001). The fast, βARK-ct–sensitive component precedes the slow one by 3 s, about the time difference between G_q activation and PIP_2 depletion (Jensen et al., 2009). (d) A chimeric α1 calcium channel subunit unable to bind to Gβγ showed much less M_1 receptor–induced inhibition. Lastly (e), the suppression of Cav2.2 current by M_1Rs could be reversed partially by applying a strong positive prepulse. Thus, for M_1R signaling, a Gβγ-mediated, voltage-dependent pathway coexists with the well-known slow PLC and PIP_2-sensitive voltage-independent pathway that is not affected by the expression of βARK-ct, chimeric α1 subunits, or depolarizing prepulses (Fig. 19*A*; Melliti et al., 2001; Gamper et al., 2004; Suh et al., 2010). With M_1Rs, neither pathway is sensitive to PTX. Our single-cell experiments combining FRET and patch clamp confirmed that M_1 receptors can suppress the N-type current through the fast Gβγ-mediated signaling pathways and that the fast current inhibition is independent from and unable to be triggered by the slow PIP_2 depletion. Many previous studies suggested that N-type channel suppression by G_qPCRs occurs through both fast and slow pathways (Hille, 1994; Melliti et al., 2001; Mitra-Ganguli et al., 2009). Here, we clearly show that the M_1 receptor–mediated channel inhibition and the PIP_2 depletion are temporally separated (a lag time) in a live single cell. Current inhibition begins earlier than PIP_2 depletion, and the lag time was almost completely abolished by the Gβγ scavenger βARK-ct, resulting in almost the same time constants for the PIP_2 depletion and the current inhibition. This temporal separation can be interpreted as a Gβγ-dependent Cav current inhibition that occurs immediately after the receptor stimulation in synapse, followed by a PLC- and lipid-dependent slow current inhibition, if the receptor activation lasts longer than the lag time. Hence the lag time determines a threshold for diversity of signaling in synaptic transmission. For example, short (< 2 s) M_1 receptor stimulation may suppress the Ca_V currents only through the fast inhibitory pathway, whereas longer receptor stimulation may regulate slower signaling by PIP_2 depletion, PKC activation, Ca^{2+} release from the ER, and gene expression by activating the downstream PLC signaling. Thus, our new finding would provide clues to elucidate the role of M_1R and Ca_V channels in synaptic plasticity such as $G\alpha_q$-mediated long-term depression (Kamsler et al., 2010; Collingridge et al., 2010). Ca_V β subunit isoforms have profound effects on calcium channel trafficking, inactivation kinetics, and susceptibility to modulation. A key distinction governing the actions of isoforms is whether they are palmitoylated and membrane directed (β2a, Lyn-β3) or not (β2a(C3,4S), β2b, β3; Fig. 24; Chien et al., 1995; Hurley et al., 2000; Feng et al., 2001). Thus, Feng et al. (2001) showed that raising free Gβγ by transient expression of Gβ subunits induced kinetic slowing of activation in $Ca_V2.2$ channels expressed with lipidated β2a subunit, whereas it had little effect in channels with other types of Ca_V β subunit. Similarly, in our experiments, expression of β2a gave a stronger Gβγ-mediated, voltage-dependent inhibition, whereas expression of β3 gave a stronger PIP_2-mediated, voltage-independent regulation. The dependence on subcellular localization was confirmed by reversing the targeting of the β2a and β3 subunits. A cytosolic β subunit conferred reduced voltage dependency and increased voltage independency of the M_1 muscarinic inhibition of N-type calcium channels. So far, the mechanism of how the membrane-targeted Ca_V β subunit regulates the Gβγ signaling to $Ca_V2.2$ channel is not clear. However, it is well known that the intracellular I-II loop (as well as N and C termini) of the α1 subunit is the major target site for both Gβγ and Ca_V β subunits, and thus binding of Ca_V β2a to the I-II loop through the BID domain and the plasma membrane through N-terminal palmitoyl groups at the same time may affect the mobility of this region in an unfavorable way, making the Ca_V channel retain high Gβγ binding affinity and be more susceptible to Gβγ subunit–mediated inhibition (Zamponi and Currie, 2013). Our findings are important to understand regulation of Ca^{2+} channels by neurotransmitter receptors that couple to G_q in excitable cells. Previous studies reported that the lipidated β2a subunit is highly expressed in chromaffin cells, form non-inactivating N-type channel currents, and contribute to hormone release (Cahill et al., 2000). The β2a subunit is also expressed broadly in brain, heart, and aorta (Hullin et al., 1992; Pichler et al., 1997), though only a small proportion of endogenous Cav2.2 interacts with the β2a subunit (Scott et al., 1996). SCG neurons express mostly β2a subunits but also β3 and β4 (Heneghan et al., 2009)(Heneghan et al., 2009), accounting for relatively slow N-type current inactivation and less sensitivity to Dr-VSP–mediated PIP_2 depletion compared with expression systems with the β3 subunit alone (Suh et al., 2012). However, Gamper et al. (2004) and Vivas et al. (2013) clearly showed that the N-type Ca^{2+} current was still strongly suppressed by membrane PIP_2 depletion in neurons, suggesting that a disproportionate fraction of β3 subunits become bound to N-type α1B subunits. This is supported by previous studies showing that the modulation of N-type currents by M_1 receptors in SCG neurons appears as a mixture of voltage-dependent and –independent pathways (Kammermeier et al., 2000; Suh et al., 2010) and that β3 subunits are the predominant form associated with brain N-type Ca^{2+} channels (Vance et al., 1998). Furthermore, the temporal expression pattern of Cav β subunits varies across brain tissue and within a single cell type during the development (Vance et al., 1998; Wittemann et al., 2000). This implies that regulation of N-type channels in nerve might change with developmental stage. In conclusion, our study provides some insight into the possible mechanism of how G_qPCRs modulate the Ca^{2+} channel activity and thus regulate intracellular Ca^{2+} concentrations in excitable nerve terminals and tissues (Kubista et al., 2009). Our results showed that $G_{q/11}$PCRs can inhibit Cav2.2 channels through the Gβγ-mediated, voltage-dependent pathway and the PIP_2-sensitive, voltage-independent pathway and that this dual mode of inhibition after G_qPCR activation is tightly controlled by the type of Cav β subunit present. Considering the previous observations that Cav channels can be regulated by diverse intracellular signals, such as protein kinase C and SNARE proteins (Swartz, 1993; Zamponi et al., 1997; Hamid et al., 1999; Magga et al., 2000), our data provide further intricacy in the G protein modulatory mechanism of Ca^{2+} influx and therefore neurotransmitter release in the synaptic terminal.

Table 5. Rate constants and parameters for Ci-VSP-models

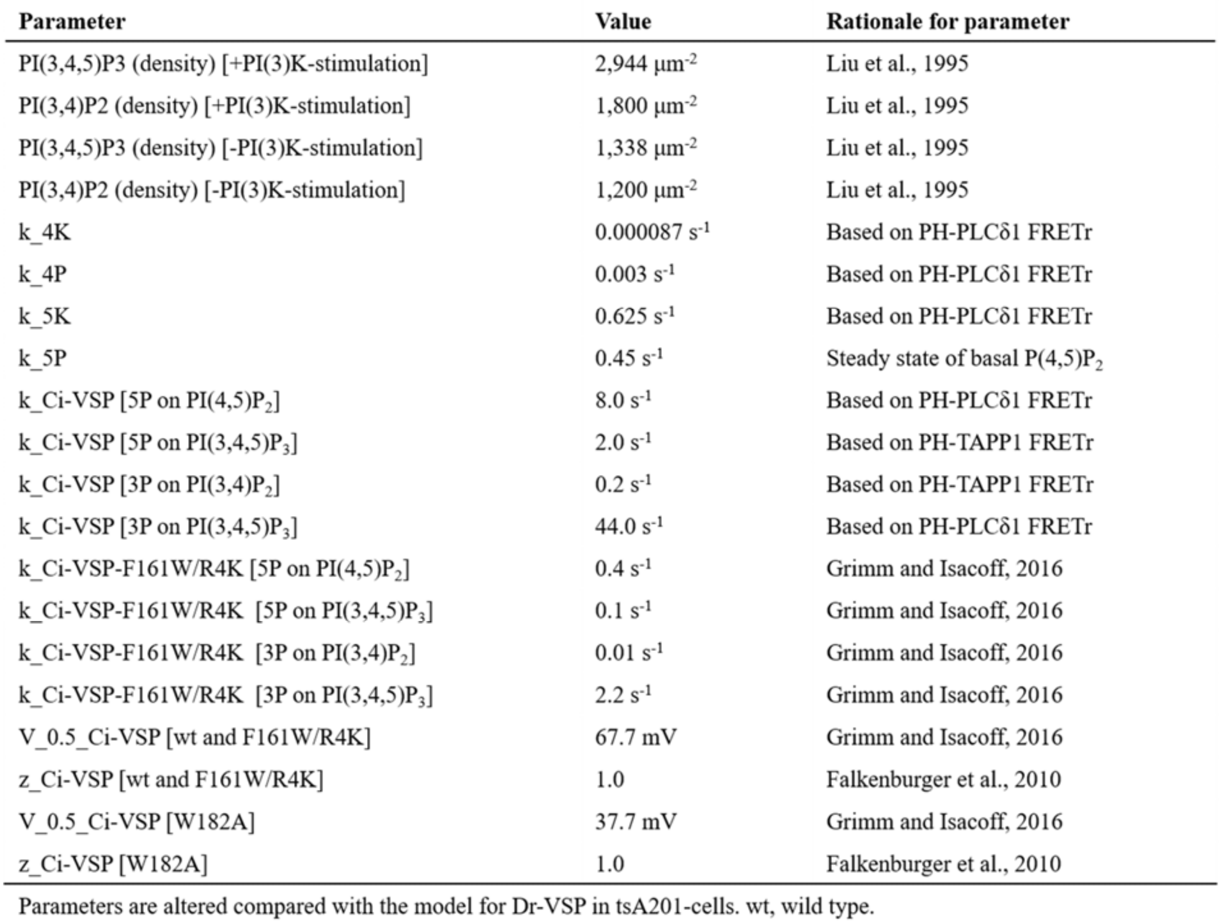

Parameter	Value	Rationale for parameter
PI(3,4,5)P3 (density) [+PI(3)K-stimulation]	2,944 μm^{-2}	Liu et al., 1995
PI(3,4)P2 (density) [+PI(3)K-stimulation]	1,800 μm^{-2}	Liu et al., 1995
PI(3,4,5)P3 (density) [-PI(3)K-stimulation]	1,338 μm^{-2}	Liu et al., 1995
PI(3,4)P2 (density) [-PI(3)K-stimulation]	1,200 μm^{-2}	Liu et al., 1995
k_4K	0.000087 s^{-1}	Based on PH-PLCδ1 FRETr
k_4P	0.003 s^{-1}	Based on PH-PLCδ1 FRETr
k_5K	0.625 s^{-1}	Based on PH-PLCδ1 FRETr
k_5P	0.45 s^{-1}	Steady state of basal $P(4,5)P_2$
k_Ci-VSP [5P on $PI(4,5)P_2$]	8.0 s^{-1}	Based on PH-PLCδ1 FRETr
k_Ci-VSP [5P on $PI(3,4,5)P_3$]	2.0 s^{-1}	Based on PH-TAPP1 FRETr
k_Ci-VSP [3P on $PI(3,4)P_2$]	0.2 s^{-1}	Based on PH-TAPP1 FRETr
k_Ci-VSP [3P on $PI(3,4,5)P_3$]	44.0 s^{-1}	Based on PH-PLCδ1 FRETr
k_Ci-VSP-F161W/R4K [5P on $PI(4,5)P_2$]	0.4 s^{-1}	Grimm and Isacoff, 2016
k_Ci-VSP-F161W/R4K [5P on $PI(3,4,5)P_3$]	0.1 s^{-1}	Grimm and Isacoff, 2016
k_Ci-VSP-F161W/R4K [3P on $PI(3,4)P_2$]	0.01 s^{-1}	Grimm and Isacoff, 2016
k_Ci-VSP-F161W/R4K [3P on $PI(3,4,5)P_3$]	2.2 s^{-1}	Grimm and Isacoff, 2016
V_0.5_Ci-VSP [wt and F161W/R4K]	67.7 mV	Grimm and Isacoff, 2016
z_Ci-VSP [wt and F161W/R4K]	1.0	Falkenburger et al., 2010
V_0.5_Ci-VSP [W182A]	37.7 mV	Grimm and Isacoff, 2016
z_Ci-VSP [W182A]	1.0	Falkenburger et al., 2010

Parameters are altered compared with the model for Dr-VSP in tsA201-cells. wt, wild type.

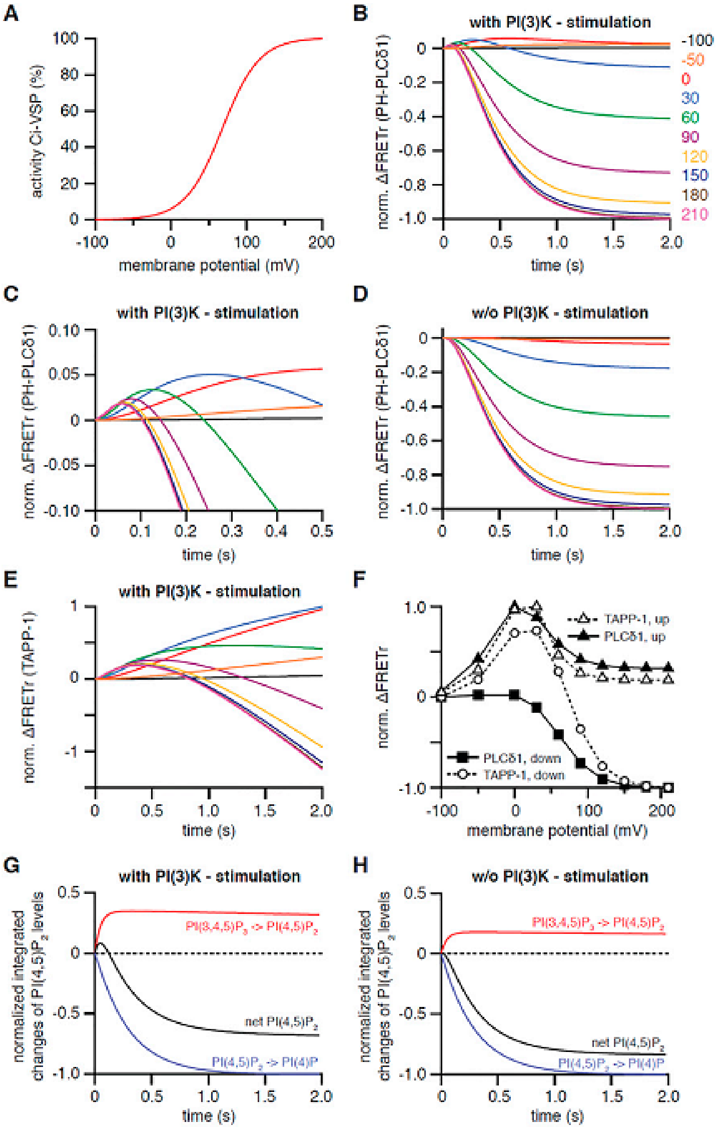

Figure 22. Simulation of FRETr responses to activation of Ci-VSP in oocytes of *X. laevis*

These simulations are meant to imitate figures 2C and 3 A and B of Grimm & Isacoff (2016). *(A)* Voltage dependence of simulated wild-type Ci-VSP activity. *(B)* Simulated FRETr response of PH-PLCδ1 domains to activation of Ci-VSP by a 2-s-long voltage step to various potentials as indicated. *(C)* Same simulation as for B, but enlarged and showing only the first 0.5 s of the voltage steps. (D) Same calculations as for B, but without insulin stimulation of PI(3)K. (E) Modeled FRETr response of PH-TAPP1 domains to activation of Ci-VSP with PI(3)K stimulated. Voltage steps areas in *B*. *(F)* Normalized ΔFRETr at the end of a 2-s depolarization for simulations shown in Band *E* for PH-PLCδ1 and TAPP-1 domains (“down”) as well as peak ΔFRETr for both reporters (“up”). (*G* and *H*) Dissection of the underlying subreactions as normalized integrals of the indicated fluxes during activation of Ci-VSP by a 2-s-long depolarization to 60 mV from a holding potential of −100 mV. Traces show production of PI(4,5)P_2 by dephosphorylation of PI(3,4,5)P_3 *(red)*, reduction of PI(4,5)P_2 levels due to dephosphorylation of PI(4,5)P*2* to PI(4)P *(blue)*, and the net change in PI(4,5)P_2 *(black)* upon stimulation of PI(3)K *(G)* or without stimulation of PI(3)K *(H)*. Note that increased PI(3,4,5)P_3 levels in the simulation with PI(3)K stimulation in *G* allow for observation of the transient net PI(4,5)P_2 production at the beginning of the depolarizing voltage step, whereas such an increase in PI(4,5)P_2 is lacking in *H* due to the absence of PI(3)K stimulation.

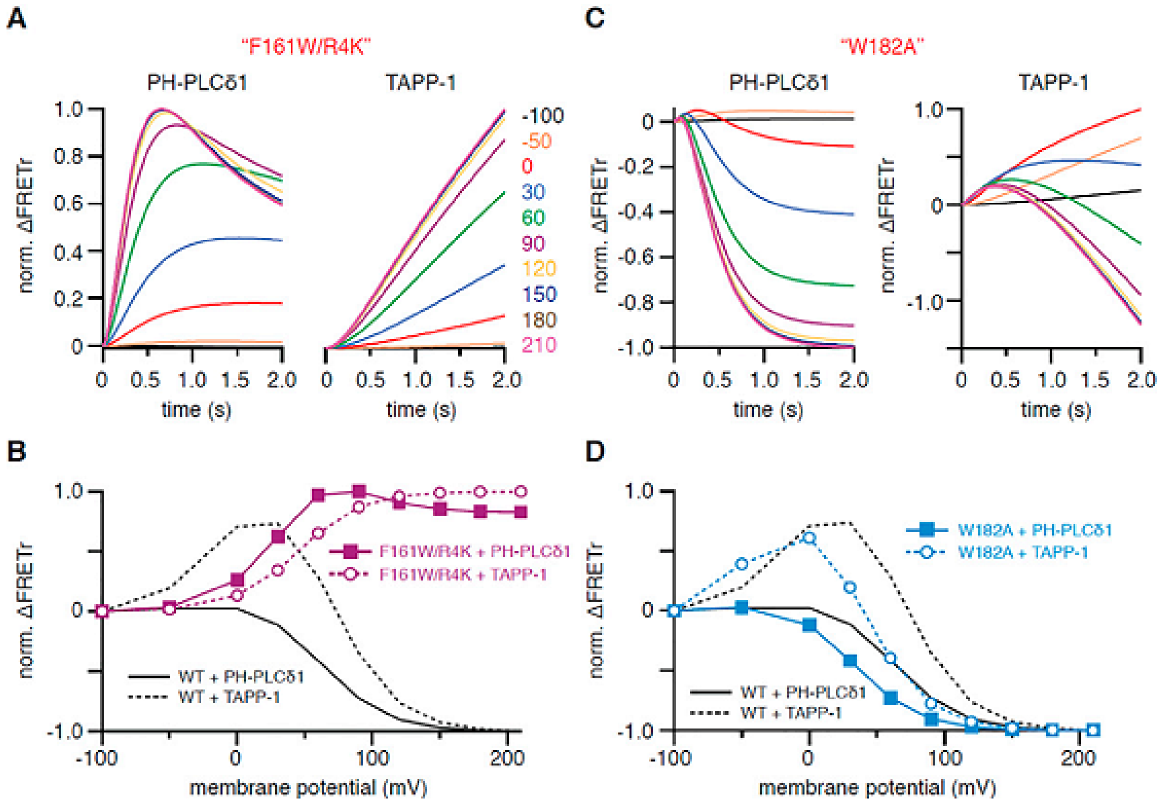

Figure 23. Simulation of activation of mutant variants of Ci-VSP

These simulations are meant to imitate figure 5 of Grimm and Isacoff (2016). *(A)* Simulated FRETr responses of PH-PLCδ1 *(Left)* and PH-TAPP1 *(Right)* domains to a 2-s-long activation of Ci-VSP-F161W/R4K by various voltage steps as indicated. The activity of Ci-VSP-F161W/R4K was modeled by reducing all V_{max} values of wild-type (WT) Ci-VSP by a factor of 20 (Table 5). *(B)* Normalized ΔFRETr at the end of a 2-s depolarization in simulations shown in *A* for PH-PLCδ1 and PH-TAPP1 domains (down) as well as peak ΔFRETr for both reporters (up). *(C)* Same as in A, but for Ci-VSP-W182A. For simulation of Ci-VSP-W182A, the voltage dependence of WT Ci-VSP was shifted by −30 mV. *(D)* Same type of display as in *B*, but for data plotted in *C*.

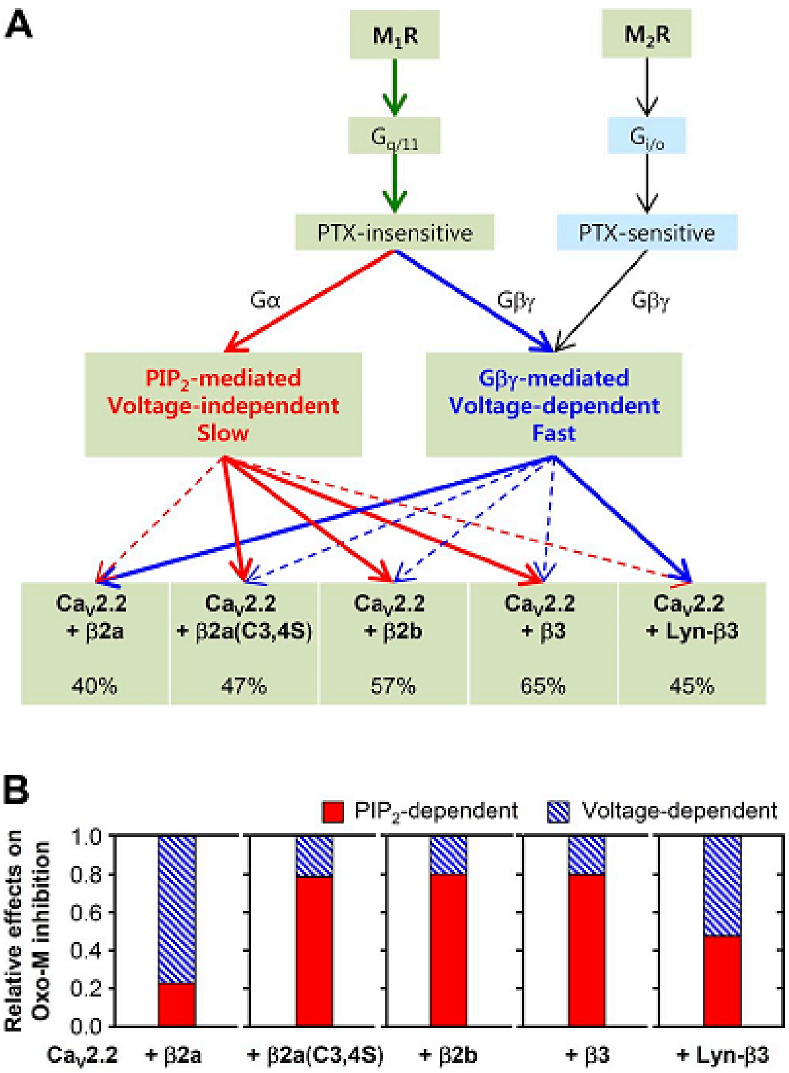

Figure 24. M$_1$R suppresses Ca$_V$2.2 currents through two separate pathways

(A) Diagram shows two separate signaling pathways independently modulating Ca$_V$2.2 channels. The predominance of each type of modulation is controlled by the β subunit. Solid lines indicate major inhibitory pathways. Dashed lines indicate minor or weak inhibitory pathways. *(B)* Relative effects of PIP$_2$- and Gβγ-dependent pathways on the Oxo-M regulation of Ca$_V$2.2 channels with different β subunits. Membrane localization of β subunits decreases the PIP$_2$-dependent regulation, whereas it enhances the effects of Gβγ subunit–mediated, voltage-dependent regulation.

VI. REFERENCES

Agler, H.L., J. Evans, L.H. Tay, M.J. Anderson, H.M. Colecraft, and D.T. Yue. 2005. G protein-gated inhibitory module of N-type (Cav2.2) Ca^{2+} channels. *Neuron*. 46:891–904. doi:10.1016/j.neuron.2005.05.011.

Bates, R.C., C.P. Fees, W.L. Holland, C.C. Winger, K. Batbayar, R. Ancar, T. Bergren, D. Petcoff, and B.J. Stith. 2014. Activation of Src and release of intracellular calcium by phosphatidic acid during *Xenopus laevis* fertilization. *Dev. Biol.* 386:165–180. doi:10.1016/j.ydbio.2013.11.006.

Bean, B.P. 1989. Neurotransmitter inhibition of neuronal calcium currents by changes in channel voltage dependence. *Nature*. 340:153–156. doi:10.1038/340153a0.

Beech, D.J., L. Bernheim, and B. Hille. 1992. Pertussis toxin and voltage dependence distinguish multiple pathways modulating calcium channels of rat sympathetic neurons. *Neuron*. 8:97–106.

Beuckmann, C.T., C.M. Sinton, N. Miyamoto, M. Ino, and M. Yanagisawa. 2003. N-type calcium channel α1B subunit (Cav2.2) knock-out mice display hyperactivity and vigilance state differences. *J. Neurosci.* 23:6793–6797.

Bezanilla, F., and C.A. Villalba-Galea. 2013. The gating charge should not be estimated by fitting a two-state model to a Q-V curve. *J. Gen. Physiol.* 142:575–578. doi:10.1085/jgp.201311056.

Boland, L.M., and B.P. Bean. 1993. Modulation of N-type calcium channels in bullfrog sympathetic neurons by luteinizing hormone-releasing hormone: kinetics and voltage dependence. *J. Neurosci. Off. J. Soc. Neurosci.* 13:516–533.

Cahill, A.L., J.H. Hurley, and A.P. Fox. 2000. Coexpression of cloned α1B, β2a, and α2/δ subunits produces non-inactivating calcium currents similar to those found in bovine chromaffin cells. *J. Neurosci. Off. J. Soc. Neurosci.* 20:1685–1693.

Campbell, R.B., F. Liu, and A.H. Ross. 2003. Allosteric activation of PTEN phosphatase by phosphatidylinositol 4,5-bisphosphate. *J. Biol. Chem.* 278:33617–33620. doi:10.1074/jbc.C300296200.

Cantley, L.C., and B.G. Neel. 1999. New insights into tumor suppression: PTEN suppresses tumor formation by restraining the phosphoinositide 3-kinase/AKT pathway. *Proc. Natl. Acad. Sci. U. S. A.* 96:4240–4245. doi:10.1073/pnas.96.8.4240.

Castle, P.M., K.D. Zolman, and S.C. Kohout. 2015. Voltage-sensing phosphatase modulation by a C2 domain. *Front. Pharmacol.* 6:63. doi:10.3389/fphar.2015.00063.

Catterall, W.A. 2000. Structure and regulation of voltage-gated Ca^{2+} channels. *Annu. Rev. Cell Dev. Biol.* 16:521–555. doi:10.1146/annurev.cellbio.16.1.521.

Chang, F., and N. Minc. 2014. Electrochemical control of cell and tissue polarity. *Annu. Rev. Cell Dev. Biol.* 30:317–336. doi:10.1146/annurev-cellbio-100913-013357.

Chien, A.J., K.M. Carr, R.E. Shirokov, E. Rios, and M.M. Hosey. 1996. Identification of palmitoylation sites within the L-type calcium channel β2a subunit and effects on channel function. *J. Biol. Chem.* 271:26465–26468.

Chien, A.J., X. Zhao, R.E. Shirokov, T.S. Puri, C.F. Chang, D. Sun, E. Rios, and M.M. Hosey. 1995. Roles of a membrane-localized beta subunit in the formation and targeting of functional L-type Ca^{2+} channels. *J. Biol. Chem.* 270:30036–30044.

Ciapa, B., B. Borg, and M. Whitaker. 1992. Polyphosphoinositide metabolism during the fertilization wave in sea urchin eggs. *Development*. 115:187–195.

Collingridge, G.L., S. Peineau, J.G. Howland, and Y.T. Wang. 2010. Long-term depression in the CNS. *Nat. Rev. Neurosci.* 11:459–473. doi:10.1038/nrn2867.

Comer, F.I., and C.A. Parent. 2007. Phosphoinositides specify polarity during epithelial organ development. *Cell*. 128:239–240. doi:10.1016/j.cell.2007.01.010.

Dickson, E.J., B.H. Falkenburger, and B. Hille. 2013. Quantitative properties and receptor reserve of the IP_3 and calcium branch of G_q-coupled receptor signaling. *J. Gen. Physiol.* 141:521–535. doi:10.1085/jgp.201210886.

Dickson, E.J., J.B. Jensen, and B. Hille. 2014. Golgi and plasma membrane pools of PI(4)P contribute to plasma membrane $PI(4,5)P_2$ and maintenance of KCNQ2/3 ion channel current. *Proc. Natl. Acad. Sci. U. S. A.* 111:E2281-2290. doi:10.1073/pnas.1407133111.

Dickson, E.J., J.B. Jensen, O. Vivas, M. Kruse, A.E. Traynor-Kaplan, and B. Hille. 2016. Dynamic formation of ER–PM junctions presents a lipid phosphatase to regulate phosphoinositides. *J. Cell Biol.* jcb.201508106. doi:10.1083/jcb.201508106.

Elmslie, K.S., W. Zhou, and S.W. Jones. 1990. LHRH and GTP-gamma-S modify calcium current activation in bullfrog sympathetic neurons. *Neuron*. 5:75–80.

Fabian, L., H.-C. Wei, J. Rollins, T. Noguchi, J.T. Blankenship, K. Bellamkonda, G. Polevoy, L. Gervais, A. Guichet, M.T. Fuller, and J.A. Brill. 2010. Phosphatidylinositol 4,5-bisphosphate directs spermatid cell polarity and exocyst localization in drosophila. *Mol. Biol. Cell.* 21:1546–1555. doi:10.1091/mbc.E09-07-0582.

Falkenburger, B.H., E.J. Dickson, and B. Hille. 2013. Quantitative properties and receptor reserve of the DAG and PKC branch of G_q-coupled receptor signaling. *J. Gen. Physiol.* 141:537–555. doi:10.1085/jgp.201210887.

Falkenburger, B.H., J.B. Jensen, and B. Hille. 2010. Kinetics of PIP_2 metabolism and KCNQ2/3 channel regulation studied with a voltage-sensitive phosphatase in living cells. *J. Gen.*

Physiol. 135:99–114. doi:10.1085/jgp.200910345.

Feng, Z.P., M.I. Arnot, C.J. Doering, and G.W. Zamponi. 2001. Calcium channel β subunits differentially regulate the inhibition of N-type channels by individual Gβ isoforms. *J. Biol. Chem.* 276:45051–45058. doi:10.1074/jbc.M107784200.

Ferreira, L.M.R., E.M. Floriddia, G. Quadrato, and S.D. Giovanni. 2012. Neural regeneration: lessons from regenerating and non-regenerating Systems. *Mol. Neurobiol.* 46:227–241. doi:10.1007/s12035-012-8290-9.

Frech, M., M. Andjelkovic, E. Ingley, K.K. Reddy, J.R. Falck, and B.A. Hemmings. 1997. High affinity binding of inositol phosphates and phosphoinositides to the Pleckstrin homology domain of RAC/protein kinase B and their influence on kinase activity. *J. Biol. Chem.* 272:8474–8481. doi:10.1074/jbc.272.13.8474.

Gamper, N., V. Reznikov, Y. Yamada, J. Yang, and M.S. Shapiro. 2004. Phosphatidylinositol 4,5-bisphosphate signals underlie receptor-specific $G_{q/11}$-mediated modulation of N-type Ca^{2+} channels. *J. Neurosci.* 24:10980–10992. doi:10.1523/JNEUROSCI.3869-04.2004.

Grimm, S.S., and E.Y. Isacoff. 2016. Allosteric substrate switching in a voltage-sensing lipid phosphatase. *Nat. Chem. Biol.* 12:261–267. doi:10.1038/nchembio.2022.

Halaszovich, C.R., M.G. Leitner, A. Mavrantoni, A. Le, L. Frezza, A. Feuer, D.N. Schreiber, C.A. Villalba-Galea, and D. Oliver. 2012. A human phospholipid phosphatase activated by a transmembrane control module. *J. Lipid Res.* 53:2266–2274. doi:10.1194/jlr.M026021.

Halaszovich, C.R., D.N. Schreiber, and D. Oliver. 2009. Ci-VSP is a depolarization-activated phosphatidylinositol-4,5-bisphosphate and phosphatidylinositol-3,4,5-trisphosphate 5′-phosphatase. *J. Biol. Chem.* 284:2106–2113. doi:10.1074/jbc.M803543200.

Halet, G., R. Tunwell, T. Balla, K. Swann, and J. Carroll. 2002. The dynamics of plasma membrane PtdIns(4,5)P_2 at fertilization of mouse eggs. *J. Cell Sci.* 115:2139–2149.

Halstead, J.R., M. Roefs, C.D. Ellson, S. D'Andrea, C. Chen, C.S. D'Santos, and N. Divecha. 2001. A novel pathway of cellular phosphatidylinositol(3,4,5)-trisphosphate synthesis is regulated by oxidative stress. *Curr. Biol. CB*. 11:386–395.

Hamid, J., D. Nelson, R. Spaetgens, S.J. Dubel, T.P. Snutch, and G.W. Zamponi. 1999. Identification of an integration center for cross-talk between protein kinase C and G protein modulation of N-type calcium channels. *J. Biol. Chem.* 274:6195–6202.

Heneghan, J.F., T. Mitra-Ganguli, L.F. Stanish, L. Liu, R. Zhao, and A.R. Rittenhouse. 2009. The Ca^{2+} channel β subunit determines whether stimulation of G_q-coupled receptors enhances or inhibits N current. *J. Gen. Physiol.* 134:369–384. doi:10.1085/jgp.200910203.

Hille, B. 1994. Modulation of ion-channel function by G-protein-coupled receptors. *Trends*

Neurosci. 17:531–536. doi:10.1016/0166-2236(94)90157-0.

Hobiger, K., T. Utesch, M.A. Mroginski, and T. Friedrich. 2012. Coupling of Ci-VSP modules requires a combination of structure and electrostatics within the linker. *Biophys. J.* 102:1313–1322. doi:10.1016/j.bpj.2012.02.027.

Hofmann, F., L. Lacinová, and N. Klugbauer. 1999. Voltage-dependent calcium channels: From structure to function. *In* Reviews of Physiology, Biochemistry and Pharmacology, Volume 139. Springer Berlin Heidelberg. 33–87.

Hossain, M.I., H. Iwasaki, Y. Okochi, M. Chahine, S. Higashijima, K. Nagayama, and Y. Okamura. 2008. Enzyme domain affects the movement of the voltage sensor in ascidian and zebrafish voltage-sensing phosphatases. *J. Biol. Chem.* 283:18248–18259. doi:10.1074/jbc.M706184200.

Hullin, R., D. Singer-Lahat, M. Freichel, M. Biel, N. Dascal, F. Hofmann, and V. Flockerzi. 1992. Calcium channel β subunit heterogeneity: functional expression of cloned cDNA from heart, aorta and brain. *EMBO J.* 11:885–890.

Hurley, J.H., A.L. Cahill, K.P. Currie, and A.P. Fox. 2000. The role of dynamic palmitoylation in Ca^{2+} channel inactivation. *Proc. Natl. Acad. Sci. U. S. A.* 97:9293–9298. doi:10.1073/pnas.160589697.

Iijima, M., Y.E. Huang, H.R. Luo, F. Vazquez, and P.N. Devreotes. 2004. Novel mechanism of PTEN regulation by its phosphatidylinositol 4,5-bisphosphate binding motif is critical for chemotaxis. *J. Biol. Chem.* 279:16606–16613. doi:10.1074/jbc.M312098200.

Itsuki, K., Y. Imai, H. Hase, Y. Okamura, R. Inoue, and M.X. Mori. 2014. PLC-mediated PI(4,5)P_2 hydrolysis regulates activation and inactivation of TRPC6/7 channels. *J. Gen. Physiol.* 143:183–201. doi:10.1085/jgp.201311033.

Iwasaki, H., Y. Murata, Y. Kim, M.I. Hossain, C.A. Worby, J.E. Dixon, T. McCormack, T. Sasaki, and Y. Okamura. 2008. A voltage-sensing phosphatase, Ci-VSP, which shares sequence identity with PTEN, dephosphorylates phosphatidylinositol 4,5-bisphosphate. *Proc. Natl. Acad. Sci. U. S. A.* 105:7970–7975. doi:10.1073/pnas.0803936105.

Jaffe, L.A. 1976. Fast block to polyspermy in sea urchin eggs is electrically mediated. *Nature.* 261:68–71. doi:10.1038/261068a0.

James, S.R., C.P. Downes, R. Gigg, S.J. Grove, A.B. Holmes, and D.R. Alessi. 1996. Specific binding of the Akt-1 protein kinase to phosphatidylinositol 3,4,5-trisphosphate without subsequent activation. *Biochem. J.* 315:709–713.

Jarquin-Pardo, M., A. Fitzpatrick, F.J. Galiano, E.A. First, and J.N. Davis. 2007. Phosphatidic acid regulates the affinity of the murine phosphatidylinositol 4-phosphate 5-kinase-Iβ for phosphatidylinositol-4-phosphate. *J. Cell. Biochem.* 100:112–128. doi:10.1002/jcb.21027.

Jensen, J.B., J.S. Lyssand, C. Hague, and B. Hille. 2009. Fluorescence changes reveal kinetic steps of muscarinic receptor–mediated modulation of phosphoinositides and Kv7.2/7.3 K^+ channels. *J. Gen. Physiol.* 133:347–359. doi:10.1085/jgp.200810075.

Kamel, L.C., J. Bailey, L. Schoenbaum, and W. Kinsey. 1985. Phosphatidylinositol metabolism during fertilization in the sea urchin egg. *Lipids*. 20:350–356.

Kammermeier, P.J., V. Ruiz-Velasco, and S.R. Ikeda. 2000. A voltage-independent calcium current inhibitory pathway activated by muscarinic agonists in rat sympathetic neurons requires both $G\alpha_{q/11}$ and $G\beta\gamma$. *J. Neurosci. Off. J. Soc. Neurosci.* 20:5623–5629.

Kamsler, A., T.J. McHugh, D. Gerber, S.Y. Huang, and S. Tonegawa. 2010. Presynaptic M_1 muscarinic receptors are necessary for mGluR long-term depression in the hippocampus. *Proc. Natl. Acad. Sci. U. S. A.* 107:1618–1623. doi:10.1073/pnas.0912540107.

Keum, D., C. Baek, D.I. Kim, H.J. Kweon, and B.C. Suh. 2014. Voltage-dependent regulation of Cav2.2 channels by G_q-coupled receptor is facilitated by membrane-localized β subunit. *J. Gen. Physiol.* 144:297–309. doi:10.1085/jgp.201411245.

Kim, C., D. Jeon, Y.-H. Kim, C.J. Lee, H. Kim, and H.S. Shin. 2009. Deletion of N-type Ca^{2+} channel Cav2.2 results in hyperaggressive behaviors in mice. *J. Biol. Chem.* 284:2738–2745. doi:10.1074/jbc.M807179200.

Kim, D.I., M. Kang, S. Kim, J. Lee, Y. Park, I. Chang, and B.C. Suh. 2015. Molecular basis of the membrane interaction of the β2e subunit of voltage-gated Ca^{2+} channels. *Biophys. J.* 109:922–935. doi:10.1016/j.bpj.2015.07.040.

Koch, W.J., B.E. Hawes, L.F. Allen, and R.J. Lefkowitz. 1994. Direct evidence that G_i-coupled receptor stimulation of mitogen-activated protein kinase is mediated by $G\beta\gamma$ activation of p21ras. *Proc. Natl. Acad. Sci. U. S. A.* 91:12706–12710.

Kubista, H., K. Kosenburger, P. Mahlknecht, H. Drobny, and S. Boehm. 2009. Inhibition of transmitter release from rat sympathetic neurons via presynaptic M_1 muscarinic acetylcholine receptors. *Br. J. Pharmacol.* 156:1342–1352. doi:10.1111/j.1476-5381.2009.00136.x.

Kuemmel, A., P. Simon, A. Breitkreuz, J. Röhlig, U. Luxemburger, A. Elsäßer, L.H. Schmidt, M. Sebastian, U. Sahin, Ö. Türeci, and R. Buhl. 2015. Humoral immune responses of lung cancer patients against the Transmembrane Phosphatase with TEnsin homology (TPTE). *Lung Cancer Amst. Neth.* 90:334–341. doi:10.1016/j.lungcan.2015.07.012.

Kumánovics, A., G. Levin, and P. Blount. 2002. Family ties of gated pores: evolution of the sensor module. *FASEB J.* 16:1623–1629. doi:10.1096/fj.02-0238hyp.

Kurokawa, T., S. Takasuga, S. Sakata, S. Yamaguchi, S. Horie, K.J. Homma, T. Sasaki, and Y. Okamura. 2012. 3′ Phosphatase activity toward phosphatidylinositol 3,4-bisphosphate [PI(3,4)P_2] by voltage-sensing phosphatase (VSP). *Proc. Natl. Acad. Sci. U. S. A.* 109:10089–10094. doi:10.1073/pnas.1203799109.

Lachyankar, M.B., N. Sultana, C.M. Schonhoff, P. Mitra, W. Poluha, S. Lambert, P.J. Quesenberry, N.S. Litofsky, L.D. Recht, R. Nabi, S.J. Miller, S. Ohta, B.G. Neel, and A.H. Ross. 2000. A role for nuclear PTEN in neuronal differentiation. *J. Neurosci. Off. J. Soc. Neurosci.* 20:1404–1413.

Lacroix, J., C.R. Halaszovich, D.N. Schreiber, M.G. Leitner, F. Bezanilla, D. Oliver, and C.A. Villalba-Galea. 2011. Controlling the activity of a phosphatase and tensin homolog (PTEN) by membrane potential. *J. Biol. Chem.* 286:17945–17953. doi:10.1074/jbc.M110.201749.

Leslie, N.R., I.H. Batty, H. Maccario, L. Davidson, and C.P. Downes. 2008. Understanding PTEN regulation: PIP_2, polarity and protein stability. *Oncogene*. 27:5464–5476. doi:10.1038/onc.2008.243.

Liu, K., Y. Lu, J.K. Lee, R. Samara, R. Willenberg, I. Sears-Kraxberger, A. Tedeschi, K.K. Park, D. Jin, B. Cai, B. Xu, L. Connolly, O. Steward, B. Zheng, and Z. He. 2010. PTEN deletion enhances the regenerative ability of adult corticospinal neurons. *Nat. Neurosci.* 13:1075–1081. doi:10.1038/nn.2603.

Liu, L., S.C. Kohout, Q. Xu, S. Müller, C.R. Kimberlin, E.Y. Isacoff, and D.L.J. Minor. 2012. A glutamate switch controls voltage-sensitive phosphatase function. *Nat. Struct. Mol. Biol.* 19:633–641. doi:10.1038/nsmb.2289.

Liu, L., and A.R. Rittenhouse. 2003. Arachidonic acid mediates muscarinic inhibition and enhancement of N-type Ca^{2+} current in sympathetic neurons. *Proc. Natl. Acad. Sci. U. S. A.* 100:295–300. doi:10.1073/pnas.0136826100.

Liu, X.J., A. Sorisky, L. Zhu, and T. Pawson. 1995. Molecular cloning of an amphibian insulin receptor substrate 1-like cDNA and involvement of phosphatidylinositol 3-kinase in insulin-induced *Xenopus* oocyte maturation. *Mol. Cell. Biol.* 15:3563–3570.

Luo, J., B.D. Manning, and L.C. Cantley. 2003. Targeting the PI3K-Akt pathway in human cancer: Rationale and promise. *Cancer Cell*. 4:257–262. doi:10.1016/S1535-6108(03)00248-4.

Magga, J.M., S.E. Jarvis, M.I. Arnot, G.W. Zamponi, and J.E. Braun. 2000. Cysteine string protein regulates G protein modulation of N-type calcium channels. *Neuron*. 28:195–204.

Matsuda, M., K. Takeshita, T. Kurokawa, S. Sakata, M. Suzuki, E. Yamashita, Y. Okamura, and A. Nakagawa. 2011. Crystal structure of the cytoplasmic phosphatase and tensin homolog (PTEN)-like region of *Ciona intestinalis* voltage-sensing phosphatase provides insight into substrate specificity and redox regulation of the phosphoinositide phosphatase activity. *J. Biol. Chem.* 286:23368–23377. doi:10.1074/jbc.M110.214361.

Mavrantoni, A., V. Thallmair, M.G. Leitner, D.N. Schreiber, D. Oliver, and C.R. Halaszovich. 2015. A method to control phosphoinositides and to analyze PTEN function in living cells using voltage sensitive phosphatases. *Front. Pharmacol.* 6:68. doi:10.3389/fphar.2015.00068.

McCrea, H.J., and P.D. Camilli. 2009. Mutations in phosphoinositide metabolizing enzymes and human disease. *Physiology*. 24:8–16. doi:10.1152/physiol.00035.2008.

Melliti, K., U. Meza, and B.A. Adams. 2001. RGS2 blocks slow muscarinic inhibition of N-type Ca^{2+} channels reconstituted in a human cell line. *J. Physiol.* 532:337–347.

Mitra-Ganguli, T., I. Vitko, E. Perez-Reyes, and A.R. Rittenhouse. 2009. Orientation of palmitoylated Cav β2a relative to Cav2.2 is critical for slow pathway modulation of N-type Ca^{2+} current by tachykinin receptor activation. *J. Gen. Physiol.* 134:385–396. doi:10.1085/jgp.200910204.

Mori, Y., M. Nishida, S. Shimizu, M. Ishii, T. Yoshinaga, M. Ino, K. Sawada, and T. Niidome. 2002. Ca^{2+} channel α1B subunit (Cav 2.2) knockout mouse reveals a predominant role of N-type channels in the sympathetic regulation of the circulatory system. *Trends Cardiovasc. Med.* 12:270–275. doi:10.1016/S1050-1738(02)00173-1.

Murata, Y., H. Iwasaki, M. Sasaki, K. Inaba, and Y. Okamura. 2005. Phosphoinositide phosphatase activity coupled to an intrinsic voltage sensor. *Nature*. 435:1239–1243. doi:10.1038/nature03650.

Murata, Y., and Y. Okamura. 2007. Depolarization activates the phosphoinositide phosphatase Ci-VSP, as detected in *Xenopus* oocytes coexpressing sensors of PIP_2. *J. Physiol.* 583:875–889. doi:10.1113/jphysiol.2007.134775.

Mutua, J., Y. Jinno, S. Sakata, Y. Okochi, S. Ueno, H. Tsutsui, T. Kawai, Y. Iwao, and Y. Okamura. 2014. Functional diversity of voltage-sensing phosphatases in two urodele amphibians. *Physiol. Rep.* 2:e12061. doi:10.14814/phy2.12061.

Newton, P.M., C.J. Orr, M.J. Wallace, C. Kim, H.-S. Shin, and R.O. Messing. 2004. Deletion of N-type calcium channels alters ethanol reward and reduces ethanol consumption in mice. *J. Neurosci.* 24:9862–9869. doi:10.1523/JNEUROSCI.3446-04.2004.

Normann, C., D. Peckys, C.H. Schulze, J. Walden, P. Jonas, and J. Bischofberger. 2000. Associative long-term depression in the hippocampus is dependent on postsynaptic N-type Ca^{2+} channels. *J. Neurosci.* 20:8290–8297.

Okamura, Y. 2007. Biodiversity of voltage sensor domain proteins. *Pflüg. Arch. - Eur. J. Physiol.* 454:361–371. doi:10.1007/s00424-007-0222-6.

Okamura, Y., and J.E. Dixon. 2011. Voltage-sensing phosphatase: its molecular relationship with PTEN. *Physiology*. 26:6–13. doi:10.1152/physiol.00035.2010.

Okamura, Y., Y. Murata, and H. Iwasaki. 2009. Voltage-sensing phosphatase: actions and potentials. *J. Physiol.* 587:513–520. doi:10.1113/jphysiol.2008.163097.

Park, K.K., K. Liu, Y. Hu, P.D. Smith, C. Wang, B. Cai, B. Xu, L. Connolly, I. Kramvis, M. Sahin, and Z. He. 2008. Promoting axon regeneration in the adult CNS by modulation of the PTEN/mTOR pathway. *Science*. 322:963–966. doi:10.1126/science.1161566.

Pichler, M., T.N. Cassidy, D. Reimer, H. Haase, R. Kraus, D. Ostler, and J. Striessnig. 1997. β subunit heterogeneity in neuronal L-type Ca^{2+} channels. *J. Biol. Chem.* 272:13877–13882.

Rameh, L.E., A. Arvidsson, K.L. Carraway, A.D. Couvillon, G. Rathbun, A. Crompton, B. VanRenterghem, M.P. Czech, K.S. Ravichandran, S.J. Burakoff, D.S. Wang, C.S. Chen, and L.C. Cantley. 1997. A comparative analysis of the phosphoinositide binding specificity of Pleckstrin homology domains. *J. Biol. Chem.* 272:22059–22066. doi:10.1074/jbc.272.35.22059.

Ratzan, W.J., A.V. Evsikov, Y. Okamura, and L.A. Jaffe. 2011. Voltage sensitive phosphoinositide phosphatases of *Xenopus*: their tissue distribution and voltage dependence. *J. Cell. Physiol.* 226:2740–2746. doi:10.1002/jcp.22854.

Rosasco, M.G., S.E. Gordon, and S.M. Bajjalieh. 2015. Characterization of the functional domains of a mammalian voltage-sensitive phosphatase. *Biophys. J.* 109:2480–2491. doi:10.1016/j.bpj.2015.11.004.

Rudge, S.A., and M.J.O. Wakelam. 2013. SnapShot: lipid kinases and phosphatases. *Cell*. 155:1654.e1. doi:10.1016/j.cell.2013.12.005.

Scott, V.E., M. De Waard, H. Liu, C.A. Gurnett, D.P. Venzke, V.A. Lennon, and K.P. Campbell. 1996. β subunit heterogeneity in N-type Ca^{2+} channels. *J. Biol. Chem.* 271:3207–3212.

Sharma, D., and W.H. Kinsey. 2006. Fertilization triggers localized activation of Src-family protein kinases in the zebrafish egg. *Dev. Biol.* 295:604–614. doi:10.1016/j.ydbio.2006.03.041.

Stith, B.J. 2015. Phospholipase C and D regulation of Src, calcium release and membrane fusion during *Xenopus laevis* development. *Dev. Biol.* 401:188–205. doi:10.1016/j.ydbio.2015.02.020.

Suh, B.C., T. Inoue, T. Meyer, and B. Hille. 2006. Rapid chemically induced changes of PtdIns(4,5)P_2 gate KCNQ ion channels. *Science*. 314:1454–1457. doi:10.1126/science.1131163.

Suh, B.C., D.I. Kim, B.H. Falkenburger, and B. Hille. 2012. Membrane-localized β-subunits alter the PIP_2 regulation of high-voltage activated Ca^{2+} channels. *Proc. Natl. Acad. Sci. U. S. A.* 109:3161–3166. doi:10.1073/pnas.1121434109.

Suh, B.C., K. Leal, and B. Hille. 2010. Modulation of high-voltage activated Ca^{2+} channels by membrane phosphatidylinositol 4,5-bisphosphate. *Neuron*. 67:224–238. doi:10.1016/j.neuron.2010.07.001.

Sundelacruz, S., M. Levin, and D.L. Kaplan. 2008. Membrane potential controls adipogenic and osteogenic differentiation of mesenchymal stem cells. *PLoS ONE*. 3:e3737. doi:10.1371/journal.pone.0003737.

Swartz, K.J. 1993. Modulation of Ca^{2+} channels by protein kinase C in rat central and peripheral neurons: disruption of G protein-mediated inhibition. *Neuron*. 11:305–320.

Turner, P.R., M.P. Sheetz, and L.A. Jaffe. 1984. Fertilization increases the polyphosphoinositide content of sea urchin eggs. *Nature*. 310:414–415. doi:10.1038/310414a0.

Vance, C.L., C.M. Begg, W.L. Lee, H. Haase, T.D. Copeland, and M.W. McEnery. 1998. Differential expression and association of calcium channel α1B and β subunits during rat brain ontogeny. *J. Biol. Chem.* 273:14495–14502.

Villalba-Galea, C.A. 2012. New insights in the activity of voltage sensitive phosphatases. *Cell. Signal.* 24:1541–1547. doi:10.1016/j.cellsig.2012.03.013.

Villalba-Galea, C.A., W. Sandtner, D.M. Starace, and F. Bezanilla. 2008. S4-based voltage sensors have three major conformations. *Proc. Natl. Acad. Sci. U. S. A.* 105:17600–17607. doi:10.1073/pnas.0807387105.

Vivas, O., H. Castro, I. Arenas, D. Elías-Viñas, and D.E. García. 2013. PIP_2 hydrolysis is responsible for voltage independent inhibition of $Ca_V2.2$ channels in sympathetic neurons. *Biochem. Biophys. Res. Commun.* 432:275–280. doi:10.1016/j.bbrc.2013.01.117.

van der Wal, J., R. Habets, P. Várnai, T. Balla, and K. Jalink. 2001. Monitoring agonist-induced phospholipase C activation in live cells by fluorescence resonance energy transfer. *J. Biol. Chem.* 276:15337–15344. doi:10.1074/jbc.M007194200.

Walker, S.M., C.P. Downes, and N.R. Leslie. 2001. TPIP: a novel phosphoinositide 3-phosphatase. *Biochem. J.* 360:277–283.

Wenk, M.R., L. Pellegrini, V.A. Klenchin, G. Di Paolo, S. Chang, L. Daniell, M. Arioka, T.F. Martin, and P. De Camilli. 2001. PIP kinase Iγ is the major $PI(4,5)P_2$ synthesizing enzyme at the synapse. *Neuron*. 32:79–88. doi:10.1016/S0896-6273(01)00456-1.

Westenbroek, R.E., J.W. Hell, C. Warner, S.J. Dubel, T.P. Snutch, and W.A. Catterall. 1992. Biochemical properties and subcellular distribution of an N-type calcium channel α1 subunit. *Neuron*. 9:1099–1115. doi:10.1016/0896-6273(92)90069-P.

Westenbroek, R.E., L. Hoskins, and W.A. Catterall. 1998. Localization of Ca^{2+} channel subtypes on rat spinal motor neurons, interneurons, and nerve terminals. *J. Neurosci.* 18:6319–6330.

Wheeler, D.G., R.D. Groth, H. Ma, C.F. Barrett, S.F. Owen, P. Safa, and R.W. Tsien. 2012. Cav1 and Cav2 channels engage distinct modes of Ca^{2+} signaling to control CREB-dependent gene expression. *Cell*. 149:1112–1124. doi:10.1016/j.cell.2012.03.041.

Wilson, D.B., T.E. Bross, S.L. Hofmann, and P.W. Majerus. 1984. Hydrolysis of polyphosphoinositides by purified sheep seminal vesicle phospholipase C enzymes. *J. Biol. Chem.* 259:11718–11724.

Wittemann, S., M.D. Mark, J. Rettig, and S. Herlitze. 2000. Synaptic localization and presynaptic function of calcium channel β 4-subunits in cultured hippocampal neurons. *J. Biol. Chem.* 275:37807–37814. doi:10.1074/jbc.M004653200.

Wu, L., C.S. Bauer, X. Zhen, C. Xie, and J. Yang. 2002. Dual regulation of voltage-gated calcium channels by PtdIns(4,5)P_2. *Nature*. 419:947–952. doi:10.1038/nature01118.

Wu, Y., D. Dowbenko, M.T. Pisabarro, L. Dillard-Telm, H. Koeppen, and L.A. Lasky. 2001. PTEN 2, a Golgi-associated testis-specific homologue of the PTEN tumor suppressor lipid phosphatase. *J. Biol. Chem.* 276:21745–21753. doi:10.1074/jbc.M101480200.

Xu, C., J. Watras, and L.M. Loew. 2003. Kinetic analysis of receptor-activated phosphoinositide turnover. *J. Cell Biol.* 161:779–791. doi:10.1083/jcb.200301070.

Yamaguchi, S., T. Kurokawa, I. Taira, N. Aoki, S. Sakata, Y. Okamura, and K.J. Homma. 2014. Potential role of voltage-sensing phosphatases in regulation of cell structure through the production of PI(3,4)P_2. *J. Cell. Physiol.* 229:422–433. doi:10.1002/jcp.24463.

Yasuda, T., L. Chen, W. Barr, J.E. McRory, R.J. Lewis, D.J. Adams, and G.W. Zamponi. 2004. Auxiliary subunit regulation of high-voltage activated calcium channels expressed in mammalian cells. *Eur. J. Neurosci.* 20:1–13. doi:10.1111/j.1460-9568.2004.03434.x.

Zamponi, G.W., E. Bourinet, D. Nelson, J. Nargeot, and T.P. Snutch. 1997. Crosstalk between G proteins and protein kinase C mediated by the calcium channel α1 subunit. *Nature*. 385:442–446. doi:10.1038/385442a0.

Zamponi, G.W., and K.P.M. Currie. 2013. Regulation of Cav2 calcium channels by G protein coupled receptors. *Biochim. Biophys. Acta*. 1828:1629–1643. doi:10.1016/j.bbamem.2012.10.004.

Zhang, J., J.C. Grindley, T. Yin, S. Jayasinghe, X.C. He, J.T. Ross, J.S. Haug, D. Rupp, K.S. Porter-Westpfahl, L.M. Wiedemann, H. Wu, and L. Li. 2006. PTEN maintains haematopoietic stem cells and acts in lineage choice and leukaemia prevention. *Nature*. 441:518–522. doi:10.1038/nature04747.

요약문

이노시톨 인지질과 전압개폐 칼슘채널에 대한 전압감응 탈인산화효소의 조절작용의 특징 파악

이 논문은 비교적 최근 발견된 전압감응 탈인산화효소(voltage-sensing phosphatase, VSP)가 세포막 인지질의 일종인 이노시톨인지질을 탈인산화 하는 생물물리학적 특징에 관한 내용을 다루고 있다. VSP 는 종양억제 효소로 알려진 PTEN 의 상동체이다. PTEN 이 PI(3,4)P$_2$ 와 PI(3,4,5)P$_3$ 의 3 번 인산기를 탈인산화 시키는 것과는 달리 VSP 는 PI(3,4)P$_2$, PI(4,5)P$_2$ 및 PI(3,4,5)P$_3$ 의 3 번과 5 번 인산기를 탈인산화 하는 것으로 알려져 있으나 PIP$_3$ 의 3 번 인산기에 대한 탈인산화 작용에 대해서는 이견이 있었다. 또한, 최근 연구에서는 VSP 가 여러 기질에 대해 각각 다른 전압의존성을 가지고 있다는 결과를 발표했다.

본 연구에서 우리는 여러 종류의 이노시톨인지질에 대한 Förster Resonance Energy Transfer(FRET) 표지를 이용해 살아있는 세포에서 전압 변화에 따른 각각의 기질에 대한 VSP의 3번과 5번 포스파타아제 작용의 특성을 측정했다. 먼저, PI 4 monophosphate 5-kinase type Iγ (PIPKIγ)가 VSP의 5번 포스파타아제 작용에 대해 선택적으로 길항작용을 한다는 것을 발견했고, 이 현상을 이용해 VSP가 PI(3,4,5)P$_3$의 3번 인산기를 탈인산화 시켜 PI(4,5)P$_2$를 생성함을 실험적으로 증명했다. 또한, VSP의 작용으로 알려진 PI(3,4,5)P$_3$→PI(4,5)P$_2$, PI(3,4,5)P$_3$→PI(3,4)P$_2$, PI(4,5)P$_2$→PI(4)P, PI(3,4)P$_2$→PI(4)P 반응들에 대한 전압의존성을 정량화하고 모델링 하는 데에 성공했다.

이 반응들은 VSP의 기질선호도와 이노시톨 인지질들의 내생적인 농도로 인하여 각각 다른 막전위에서 반응이 시작되는 것처럼 보였으나, 명백하게 하나의 전압의존성을 가지고 있는 것으로 판명됐다. 우리가 수립한 모델에 의하면 zebrafish VSP에서 PI(4,5)P$_2$의 5번 인산기에 대한 탈인산화 효과가 PI(3,4,5)P$_3$의 3번 인산기에 대한 탈인산화 효과에 비해 55배 크기 때문에 VSP에 의해 PI(3,4,5)P$_3$의 3번 인산기가 탈인산화 되어 PI(4,5)P$_2$가 생성되더라도 PI(4)P로 바로 바뀌기 때문에 지금까지 살아있는 세포에서 VSP의 PI(3,4,5)P$_3$에 대한 3번 인산기의 탈인산화를 관찰하지 못한 것으로 드러났다.

또한 이러한 VSP 의 특성을 실험적으로 응용하여 q 타입의 G 단백질 연결 수용체 (G$_q$PCR)이 이노시톨인지질 중 하나인 PI(4,5)P$_2$ 의 고갈과 G 단백질 연결 수용체의 βγ 아단위체의 직접적인 부착의 두 가지 경로를 통하여 전압감응 칼슘채널 (Ca$_V$ channel)의 활성화를 억제하는 것과 이러한 양 갈래 억제의 비율이 Ca$_V$ 채널의 β 아단위체의 세포 내 위치에 의해 조절됨을 보여주었다.